



University of Southern Denmark

## Emergence of MXene–olymer hybrid nanocomposites as high-performance next-generation chemiresistors for efficient air quality monitoring

Chaudhary, Vishal; Ashraf, Naveed; Khalid, Mohammad; Walvekar, Rashmi; Yang, Ya; Kaushik, Ajeet; Mishra, Yogendra Kumar

*Published in:*  
Advanced Functional Materials

*DOI:*  
10.1002/adfm.202112913

*Publication date:*  
2022

*Document version:*  
Final published version

*Document license:*  
CC BY

### *Citation for pulished version (APA):*

Chaudhary, V., Ashraf, N., Khalid, M., Walvekar, R., Yang, Y., Kaushik, A., & Mishra, Y. K. (2022). Emergence of MXene–olymer hybrid nanocomposites as high-performance next-generation chemiresistors for efficient air quality monitoring. *Advanced Functional Materials*, 32(33), [2112913]. <https://doi.org/10.1002/adfm.202112913>

Go to publication entry in University of Southern Denmark's Research Portal

### **Terms of use**

This work is brought to you by the University of Southern Denmark.  
Unless otherwise specified it has been shared according to the terms for self-archiving.  
If no other license is stated, these terms apply:

- You may download this work for personal use only.
- You may not further distribute the material or use it for any profit-making activity or commercial gain
- You may freely distribute the URL identifying this open access version

If you believe that this document breaches copyright please contact us providing details and we will investigate your claim.  
Please direct all enquiries to [puresupport@bib.sdu.dk](mailto:puresupport@bib.sdu.dk)

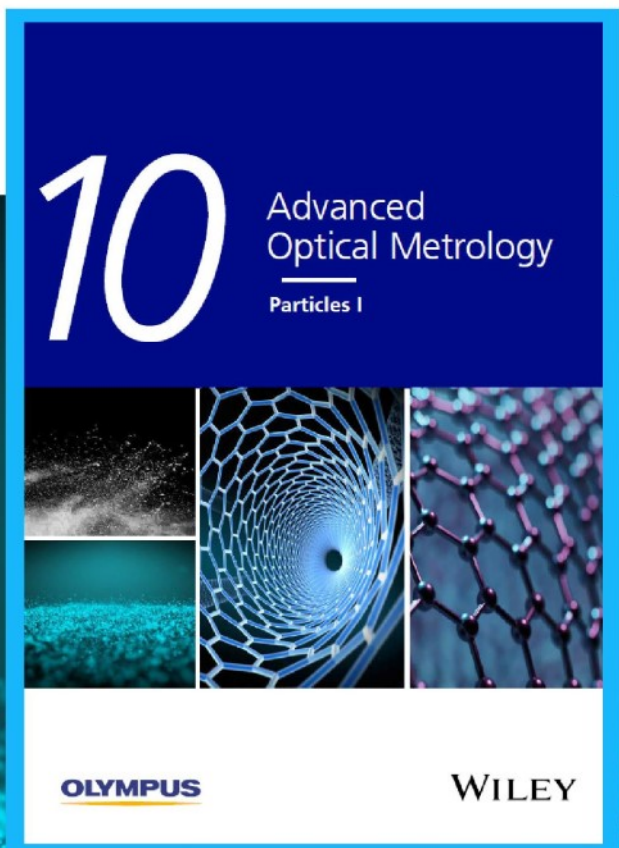


# Particles I

Access the latest eBook →

Particles: Unique Properties,  
Uncountable Applications

**Read the latest eBook and  
better your knowledge with  
highlights from the recent  
studies on the design and  
characterization of micro-  
and nanoparticles for  
different application areas.**



**Access Now**

This eBook is sponsored by

**OLYMPUS**

**WILEY**

# Emergence of MXene–Polymer Hybrid Nanocomposites as High-Performance Next-Generation Chemiresistors for Efficient Air Quality Monitoring

Vishal Chaudhary,\* Naveed Ashraf, Mohammad Khalid,\* Rashmi Walvekar, Ya Yang, Ajeet Kaushik,\* and Yogendra Kumar Mishra\*


Air contamination is one of the foremost concerns of environmentalists worldwide, which has elevated global public health concerns for monitoring air contaminants and implementing appropriate safety policies. These facts have generated nascent global demand for exploring sustainable and translational strategies required to engineer affordable, intelligent, and miniaturized sensors because commercially available sensors lack lower detection limits, room temperature operation, and poor selectivity. The state-of-the-art sensors are concerned with architecting advanced nanomaterials to achieve desired sensing performance. Recent studies demonstrate that neither pristine metal carbides/nitrides (MXenes) nor polymers (P) can address these practical challenges. However, synergistic combinations of various precursors as hybrid-nanocomposites (MXP-HNCs) have emerged as superior sensing materials to develop next-generation intelligent environmental, industrial, and biomedical sensors. The expected outcomes could be manipulative due to optimizing physicochemical and morphological attributes like tunable interlayer-distance, optimum porosity, enlarged effective surface area, rich surface functionalities, mechanical flexibility, and tunable conductivity. This review intends to detail a comprehensive summary of the advancements in state-of-the-art MXP-HNCs chemiresistors. Moreover, the underlying sensing phenomenon, chemiresistor architecture, and their monitoring performance are highlighted. Besides, an overview of challenges, potential solutions, and prospects of MXP-HNCs as next-generation intelligent field-deployable sensors with the integration of IoT and AI are outlined.

## 1. Introduction

One of the most significant challenges before humans in this era of technological advancements and industrialization is meeting growing population demand without causing irrevocable damage to the environment. However, these technological advancements have led to various global concerns such as global warming, climate change, forest fires, ozone depletion, acid rain, water scarcity, and energy crisis due to increasing contamination in the air, water, and soil. The degradation of the eminence of air due to release of various contaminants into the environment is the foremost global ecological concern, and seeking solutions urgently. These contaminants are released into the environment in the gaseous phase (ammonia ( $\text{NH}_3$ ), nitrous oxides ( $\text{NO}_x$ ), sulfur oxides ( $\text{SO}_x$ ), carbon oxides ( $\text{CO}_x$ ), vapor phase (alcohols, ketones, toluene( $\text{C}_7\text{H}_8$ )), and solid phase (particulate matter) through numerous human activities, including industries, automobiles, urbanization, households, and farming.<sup>[1–3]</sup> Both outdoor ( $\text{CO}_x$ ,  $\text{NO}_x$ ,  $\text{SO}_x$ , and  $\text{NH}_3$ , ground-level ozone) and indoor (volatile organic compounds

V. Chaudhary  
Research Cell & Department of Physics  
Bhagini Nivedita College  
University of Delhi  
New Delhi 110043, India  
E-mail: drvishal@bn.du.ac.in, chaudhary00vishal@gmail.com

N. Ashraf  
Department of Physics, Informatics and Mathematics  
University of Modena and Reggio Emilia  
Reggio Emilia, 42121 Modena, Italy

 The ORCID identification number(s) for the author(s) of this article can be found under <https://doi.org/10.1002/adfm.202112913>.

© 2022 The Authors. Advanced Functional Materials published by Wiley-VCH GmbH. This is an open access article under the terms of the Creative Commons Attribution License, which permits use, distribution and reproduction in any medium, provided the original work is properly cited.

DOI: 10.1002/adfm.202112913

M. Khalid  
Graphene & Advanced 2D Materials Research Group (GAMRG)  
School of Engineering and Technology  
Sunway University  
No. 5, Jalan Universiti, Bandar Sunway, Petaling Jaya, Selangor  
47500, Malaysia  
E-mail: khalids@sunway.edu.my

M. Khalid  
Sunway Materials Smart Science & Engineering (SMS2E)  
Research Cluster  
Sunway University  
No. 5, Jalan Universiti, Bandar Sunway, Petaling Jaya, Selangor 47500,  
Malaysia

R. Walvekar  
Department of Chemical Engineering  
School of New Energy and Chemical Engineering  
Xiamen University Malaysia  
Jalan Sunsuria, Bandar Sunsuria, Sepang, Selangor 43900, Malaysia

**Table 1.** Various air contaminants, including gaseous pollutants and VOCs: Major sources and adverse effects on humans and the environment with lowest exposure limit for humans.

Air contaminant	Major sources	Effect on environment	Effect on human	Lowest exposure range for human
Ammonia (NH <sub>3</sub> ) <sup>[10,11]</sup>	Fertilizers Industries Agriculture Livestock Forest fires Human waste	Soil acidification, eutrophication, particulate matter formation, favorable to virus transmission	Affects human nervous and respiratory system	25 ppm up to 8 h and 35 ppm up to 10 min
Oxides of nitrogen (NO <sub>x</sub> ) <sup>[1,9]</sup>	Transport and industries	Damage to agriculture, affects visibility, formation of particulate matter	Respiratory and cardiovascular weakness	100–150 ppm for 30–60 min
Carbon monoxide (CO) <sup>[16]</sup>	Household appliances, transport, tobacco smoke, generators	Green house effect, climate shift, and global warming	Weakness, dizziness, nausea or vomiting, shortness of breath, confusion	50 ppm for 8 h
Carbon dioxide (CO <sub>2</sub> ) <sup>[12]</sup>	Cement production, deforestation, transport, burning of fuels, respiration	Green house effect	Headaches, dizziness, difficulty in breathing, sweating, tiredness, increased heart rate, elevated blood pressure	5000 ppm for 8 h
Sulfur dioxide (SO <sub>2</sub> ) <sup>[13–15]</sup>	Winemaking, volcanic activities, metal smelting, petrochemical industries	Acid rain, acidification of water bodies	Nervous system, skin, and respiratory system	5 ppm
Particulate matter (PM) <sup>[1,9]</sup>	Volcanic eruption, construction, sea salt, marine transport	Change in weather patterns, cause drought, contribute to global warming, affect visibility, and cause the ocean to acidify, virus transmission	Affects immune system, respiratory system, nervous system, cardiovascular effects such as heart attack	35 mg per cubic meter of air for 24 h
Ethanol (C <sub>2</sub> H <sub>5</sub> OH) <sup>[4,5]</sup>	VOC, industries,	Formation of ground level ozone and smog	Headache, drowsiness, nausea and vomiting, and unconsciousness	3300 ppm
Methanol (CH <sub>3</sub> OH) <sup>[1,6]</sup>	VOC, industrial uses and naturally from volcanic gases, vegetation, and microbes	Fertility of biota	Headache, dizziness, agitation, acute mania, amnesia, decreased level of consciousness	10 mg kg <sup>-1</sup>
Acetone (C <sub>3</sub> H <sub>6</sub> O) <sup>[7,8]</sup>	VOC, automobiles, petroleum production	Contamination of water bodies and affects aquatic life	Headaches, dizziness, confusion, a faster pulse, vomiting, a shorter menstrual cycle in women	750 ppm for 15 min and 500 ppm for 8 h

(VOCs) like benzene (C<sub>6</sub>H<sub>6</sub>), alcohols, ketones, C<sub>7</sub>H<sub>8</sub>) contribute to air eminence degradation<sup>[1,2,4–16]</sup> as listed in **Table 1**.

Y. Yang  
CAS Center for Excellence in Nanoscience  
Beijing Key Laboratory of Micro-Nano Energy and Sensor  
Beijing Institute of Nanoenergy and Nanosystems  
Chinese Academy of Sciences  
Beijing 101400, P. R. China

A. Kaushik  
NanoBioTech Laboratory  
Health System Engineering  
Department of Environmental Engineering  
Florida Polytechnic University  
Lakeland, FL 33805, USA  
E-mail: akaushik@floridapoly.edu

A. Kaushik  
School of Engineering  
University of Petroleum and Energy Studies (UPES)  
Dehradun, Uttarakhand, India

Y. K. Mishra  
Mads Clausen Institute  
NanoSYD  
University of Southern Denmark  
Alison 2, Sønderborg 6400, Denmark  
E-mail: mishra@mci.sdu.dk

The presence of these contaminants in the surroundings is hazardous to the environment and humans (Table 1). Air pollution, for example, is estimated to be responsible for 20% of cardiovascular and stroke-related mortalities.<sup>[17]</sup> It has led to an estimation that 3.8 million people every year suffer from severe fatal diseases due to air contamination. Besides, World Health Organization (WHO) reports that these contaminants cause damage to the human respiratory, immune and nervous system, turning humans more prone to high-risk diseases such as coronavirus disease (COVID-19).<sup>[2,3,16,18,19]</sup> Accordingly, it has raised global demand for intelligent monitoring and control strategies such as gas/vapor sensors for air contaminants. The application of gas/vapor sensors is not limited to air quality monitoring but also resides in intelligent farming, military, smart cities, public security, food safety, workplace safety, and therapeutic diagnosis.<sup>[9,16,20–25]</sup> For instance, airborne NH<sub>3</sub> acts as a biomarker for diagnosing renal and gastric disorders due to *Helicobacter pylori* contagion, and lately for COVID-19.<sup>[10,11]</sup> The exhaled breath of a patient with renal disorder contains NH<sub>3</sub>'s concentration in the range around 0.82–14.7 ppm. The real-time detection of NH<sub>3</sub> in this low-trace concentration range through gas/vapor sensors can replace conventional expensive and time-consuming diagnostic techniques.<sup>[10,11]</sup> This diversified demand

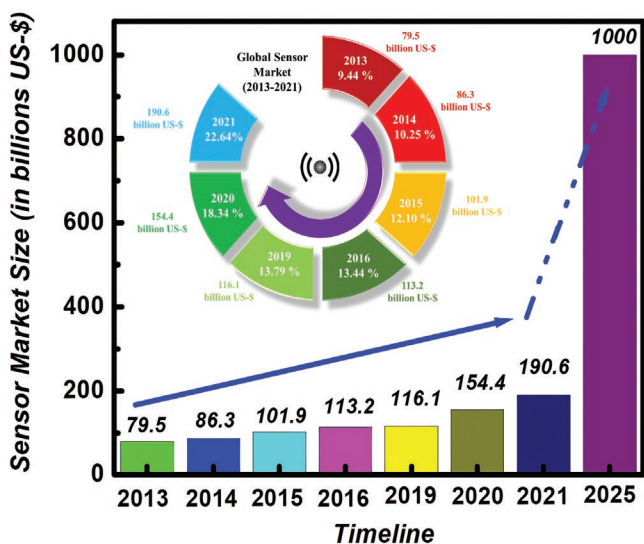


**Figure 1.** Statistics of the global sensor market with total percentage share and value (in US dollars) worldwide from 2013–2021 with projection up to 2025 illustrates the expanding high demand for sensors in diverse sectors.

has resulted in the expansion of the global sensor market with a worldwide value of 190 billion \$ in 2021, which is expected to reach 1 trillion \$ by 2025 (Figure 1).<sup>[9]</sup>

The research and development dedicated to these sensors are concerned with designing wearable, self-operating, and wireless technologies supported by internet of things (IoT) and artificial intelligence (AI).<sup>[26–28]</sup> Apart from intelligent functioning,

the development of these sensors requires the integration of advanced features, including rapid and low trace detection, stability, easy processability, compact and portable design, cost-effectiveness, energy efficiency, and reusability,<sup>[10,29]</sup> which is the hot topic of on-going research.

In the past few decades, numerous strategies have been developed to cater to these advanced sensing features grounded on various underlying signal transduction mechanisms, including optical, electrical, electrochemical, calorimetric, gravimetric, thermoelectric, chromatographic, and acoustic (Figure 2).<sup>[9,10,22,23,25,30–34]</sup> However, most investigated sensing strategies suffer disadvantages such as complex and sophisticated architecture, expensive, time-consuming, lack of portability, large size, and complex operation.<sup>[10,35]</sup> On the contrary, electrical transducers, especially chemiresistors, have gained inordinate interest owing to their ease of processing and operation, energy efficiency, flexibility, ability to monitor real-time signal, compact and portable design, compatibility with non-line-of-sight monitoring, cost-effectiveness, and environmentally friendly.<sup>[30,36]</sup>

A chemiresistor sensor comprises an optimized sensing material layer deposited over a substrate (working or sensing electrode), further connected to appropriate detecting circuitry selected according to the transduction method.<sup>[10,37]</sup> Such fabricated electrode detects alternation in electrical properties such as resistivity of sensing layer in the specific analyte (air contaminant) environment. The sensing performance of a chemiresistor with reference to targeted air contaminants analysis in terms of basic and advanced sensing features, including mainly 3-S's (sensitivity, stability, selectivity) and 5-R's (room temperature operability, detection range, reproducibility, recovery, and response

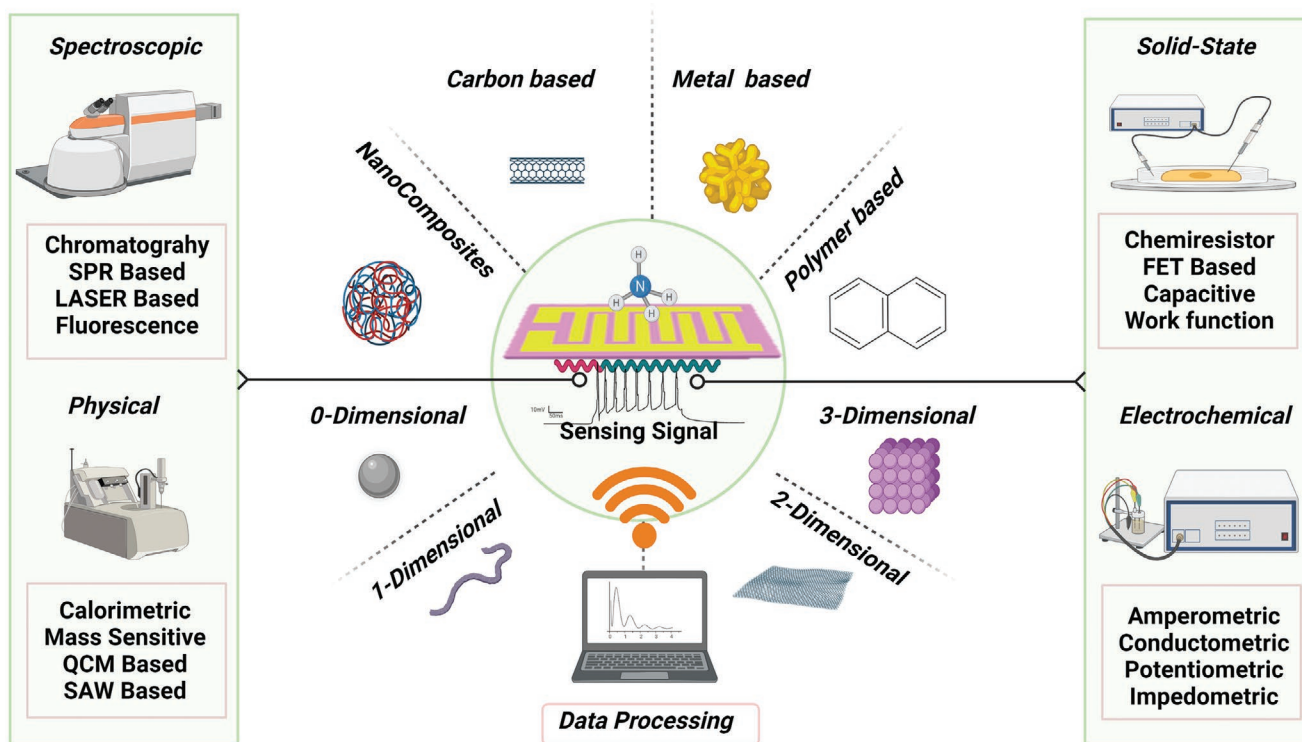


**Figure 2.** Schematic illustration of various air contaminant sensing strategies depending upon the nature of transducing signals and diversified sensing materials with different dimensions for air monitoring and detection [Created with BioRender.com].

time). Besides these essential basic features, the advanced sensing features comprise flexibility, intelligent operation, automation, pattern recognition, self-operation, and array design.<sup>[9,10,16,38]</sup>

The state-of-art chemiresistors are to engineer sensing materials and flexible substrates, optimize layer thickness, architect electrode design, and material, and improvise the design of detecting circuitry. However, the most active sensors research is dedicated to developing advanced sensing materials to cater to all essential sensing features.

Since the interaction of analyte and surface sensing material is a surface phenomenon, researchers' quest is dedicated to engineering low dimensional materials with high specific surface area. Various low-dimensional materials such as metal-based nanomaterials, conducting polymers, carbon nanomaterials, and solid electrolytes have been investigated to design an efficient chemiresistor.<sup>[9,34,39–42]</sup> Among them, metal oxides and their hybrids nanocomposites are widely used for commercial gas/vapor monitoring due to their high sensitivity and low detection limit (LDL).<sup>[43–45]</sup> However, their high-temperature operation, which produces suitable oxygen adsorbents ( $O^{2-}$ ,  $O^-$ , and  $O_2^-$ ) on the sensor surface, results in significant power consumption, complex design due to the requirement of micro heaters, and low stability due to degradation of sensing nanostructures at high temperature. On the other hand, carbon nanomaterials based chemiresistors operate at room temperature and efficiently detect a low trace of analytes. But such sensing systems exhibited low selectivity and also possess a delayed recovery rate due to greater affinity towards analyte molecules. It has escalated the quest for novel sensing structures/materials which can enhance and advance sensing features, especially room temperature operation, significant recovery, and mechanical flexibility.

Nowadays, 2D nanomaterials like graphene and its derivatives, borophene, 2D organic frameworks, and polymers, metal carbides/nitrides (MXenes), metal dichalcogenides, black phosphorus (BP), molybdenum disulfide ( $MoS_2$ ), and phosphorene are emerging as promising sensing materials.<sup>[35,43,46–50]</sup> Their superior surface area, exceptional electrical properties, and tunable surface chemistries are credited to their enhanced sensing performance. As the main feature, conventional 2D nanomaterials like graphene, graphene oxide, reduced graphene oxide (rGO),  $MoS_2$ , and metal dichalcogenides have been evaluated for air contaminant monitoring. However, associated complex synthesis techniques, low selectivity, and rugged surface functionalization restrict the utilization of the materials for developing sensings for the commercial level. Among the 2D sensing materials family, MXenes is one recently class of sensing material showing promising sensing features according to 3-S and 5-R aspects.<sup>[51–54]</sup> MXenes, as a surface-engineered platform, are popular in designing chemiresistors due to their excellent conductivity, enlarged effective surface area, abundant surface functionalities, excellent hydrophilicity, biocompatibility, and significant tribological characteristics.<sup>[55]</sup> However, the application of MXenes is limited to detecting reducing analytes such as  $NH_3$  due to their excellent conductivity.<sup>[10,56]</sup> The high adsorption energy of MXenes towards analytes like  $NH_3$  prolongs their recovery and constrains them from achieving their initial state. MXenes are also prone to oxidation in the environment, which costs a low lifetime for MXene-chemiresistors.<sup>[46,53]</sup> Their conductivity requires to be optimized for detecting

oxidizing analytes through MXenes efficiently. From a commercial sensor development point of view, high flexibility with significant mechanical endurance is also required during machine processability. Hence, despite such remarkable characteristics, the real-world applications of MXenes chemiresistors are limited due to the simultaneous need to optimize flexibility, conductivity, and mechanical strength.

Contrary to this, the nanostructured polymers (NPs) and copolymers such as polypyrrole (PPy), polyaniline (PAN), polystyrene (PS), poly (aniline co-pyrrole) (PAP), poly 3,4-ethylene dioxythiophene (PEDOT), polyvinyl alcohol (PVA), and cationic polyacrylamide (CPAM), etc., have widely investigated for air contaminant monitoring at room temperature.<sup>[30,36,57]</sup> The NP-based chemiresistors are getting attention due to the abundance of polymers, ease of functionalization, user and environmentally friendly, miniature and portable design, room temperature operation, energy and cost-effectiveness, easy processability, operation, and flexibility. However, the large affinity of NPs toward VOCs and humid environments causes an issue of cross-sensitivity and low stability, which limits their commercial development.

Consequently, to back up each other's limitations, applying two significant classes of sensing materials (MXenes and NPs), the form of hybrids, nanocomposites, or both, is limited for their versatile utilization in air contaminant detection. The associated processing difficulties and poor selectivity of MXenes, and cross-sensitivity along with poor stability of NPs are the most pressing challenges for designing these sensors for real-world applications. However, these challenges can possibly be overcome using hybrid nanocomposites (HNCs) of these two classes of materials to develop high-performance chemiresistors. It is anticipated that host-guest interactions and chemistry between MXene and NP precursors in HNCs collectively eliminate their drawbacks due to synergetic effects, leading to high-performance chemiresistors. MXene-polymer hybrid nanocomposite (MXP HNCs) based chemiresistors have recently stimulated extensive interest in air contaminant monitoring.<sup>[10,58,59]</sup> Though there are dedicated literature on using various organic-inorganic HNCs for air contaminant monitoring,<sup>[60–62]</sup> most reports attribute their high sensing performances to forming heterojunctions among the precursors.

Nevertheless, the presence of MXene as one of the precursors in HNCs turns it more unique and more efficient for air contaminant detection compared to reported hybrids.<sup>[52,58]</sup> The presence of rich surface functionalities (due to surface terminals like  $-O$ ,  $-OH$ , or  $-F$ ) over MXenes makes them more prone to forming enhanced HNCs with polymers. The addition of polymer precursors into MXene protects its oxidation through the environment if they exhibit a more substantial affinity towards MXene, which is already established for energy storage applications.<sup>[63,64]</sup>

Although MXenes are emerging as a promising sensing material for air contaminant detection,<sup>[6,51,53,65,66]</sup> MXP HNCs based chemiresistors for air contaminant monitoring are not well explored. To the best of our knowledge, there is no specific review dedicated to MXP HNCs based chemiresistors to detect air contaminants in the literature. As a motivation to fill this knowledge gap, the review aims to provide a fundamental work structure on MXP HNCs-based chemiresistors to lead future research in the field of air contaminant monitoring. This review comprises state-of-the-art MXP HNCs based chemiresistors,

their synthesis, and properties favorable to detecting air contaminants. Moreover, efforts are dedicated to summarizing MXP HNCs' sensing performances toward various gaseous and vapor phase contaminants with their precursors in detail. This report provides a comprehensive overview of air contaminants detection sensing mechanisms through MXP HNCs based chemiresistors. Besides, the challenges associated with MXP HNCs based chemiresistors for practical application, possible solutions, and prospects to design next-generation intelligent field-deployable sensors are also discussed critically and carefully in this report.

## 2. Emerging Class of Advanced MXenes and MXP HNCs for Air Contaminant Monitoring

The MXP HNCs are an emerging class of advanced functional nanomaterials suitable for various technological applications.<sup>[10,59,67–69]</sup> These HNCs are nanodimensional composites of polymer and MXene counterparts, with unique physical and chemical characteristics arising from multi-interactions at the molecular level. MXene is a new family in the class of 2-D inorganic materials, which is obtained via selective elimination of “A”: 13 or 14 group elements from its precursor MAX phase (with “M” representing an early transition material, and “X” can be nitrogen, carbon or both).<sup>[70]</sup> Typically, MAX phases are composed of hexagonally layered early transition metal nitrides and carbides with a stoichiometry described by the formula  $M_{n+1}AX_n$  ( $n = 1, 2, \text{ or } 3$ ). Around 70 MAX phases and more than 30 MXenes have been theoretically analyzed to date (Figure 3).<sup>[71]</sup> The universal formula representing MXene is  $M_{n+1}X_nT_x$ , along with “(n+1)” number of layers comprising “M” integrated with “n” number of layers comprising “X” and with “T” representing different surface terminals (–OH, –F, –O, and –Cl).<sup>[72]</sup>

Owing to their unique physicochemical characteristics, including excellent hydrophilicity, metallic conductivity, large specific surface area, and rich surface chemistries, MXenes have emerged as a promising sensing layer for architecting chemiresistors.<sup>[6,51–53,65,74,75]</sup> Among them,  $M_3X_2T_x$  MXenes, especially titanium carbide ( $Ti_3C_2T_x$ ), are mainly utilized for air contaminant detection due to their ease of processing and stability. First, Lee et al.<sup>[76]</sup> reported the air contaminant sensing using  $Ti_3C_2T_x$  MXene fabricated using drop-casting  $Ti_3C_2T_x$  MXene over PI substrate with Pt- interdigitated electrodes under ambient conditions. The sensor exhibited p-type semiconducting behavior (due to increased resistance) on  $NH_3$ ,  $CH_3OH$ ,  $C_2H_5OH$ , and  $C_3H_6O$  adsorption. It was due to the charge transfer from contaminant molecules to MXene, increasing its resistance by reducing the number of majority charge carriers. Kim et al.<sup>[77]</sup> further fabricated a metallic sensor based on  $Ti_3C_2T_x$  MXene possessing a remarkable signal-to-noise ratio for detecting various air contaminants, including  $NH_3$ ,  $SO_2$ ,  $C_2H_5OH$ ,  $C_3H_6O$ , nitrogen dioxide ( $NO_2$ ), and  $CO_2$  at room temperature. Moreover, Shuck et al.<sup>[78]</sup> explored the effect of precursors ( $Ti_3AlC_2$ ) over air contaminant sensing performance of  $Ti_3C_2T_x$  MXene. It was found that MXene derived from the MAX phase possesses higher sensitivity than that derived from carbon black (Figure 4).

Further, the  $M_2X_2T_x$ -MXenes (like vanadium carbide ( $V_2CT_x$ ) and niobium carbide:  $Nb_2CT_x$ ) possessed a larger effective surface area due to lesser atomic layers than  $M_3X_2T_x$ -MXenes, and

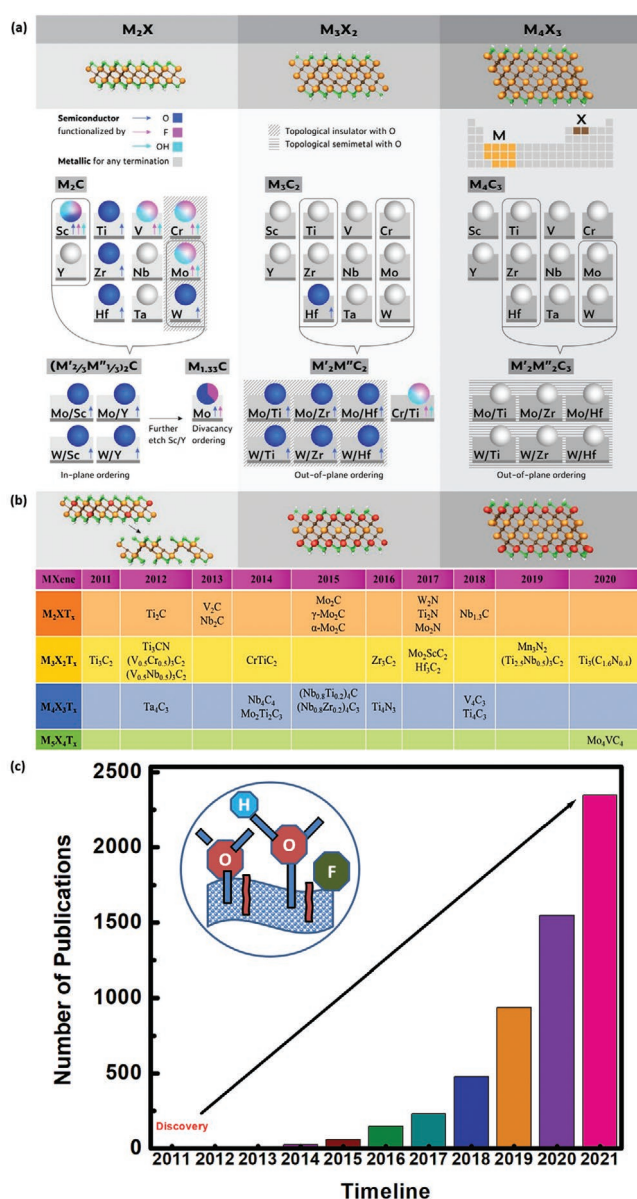


**Figure 3.** a) Schematic depiction of the MXene family classification based upon the number of layers with their structures, stoichiometry, type of surface functionalities, electronic properties. MXene surface groups are highlighted using different colors with violet, blue and sky-blue colors signifying oxygen, hydroxyl group, and fluorine, respectively. The gray color represents the metallic terminated-MXenes. Reproduced with permission.<sup>[73]</sup> Copyright 2019, Elsevier. b) Timeline illustrating discoveries of different types of MXenes classified based on number of layers in 2-D lamellar structure. c) Expanding number of publications on MXenes since its discovery till date searched on web of science with keyword MXenes (with inset: Surface terminals of MXenes turning them unique for diversified applications).

are found promising for air contaminant monitoring through chemiresistive mode.<sup>[79,80]</sup> Lee et al.<sup>[81]</sup> reported using  $V_2CT_x$  to monitor polar and non-polar air contaminants. The fabricated sensor was more selective towards hydrogen ( $H_2$ ) due to manifestation of “V,” anticipating that by choice of transition metal in MXene, the desired selectivity for specific contaminant

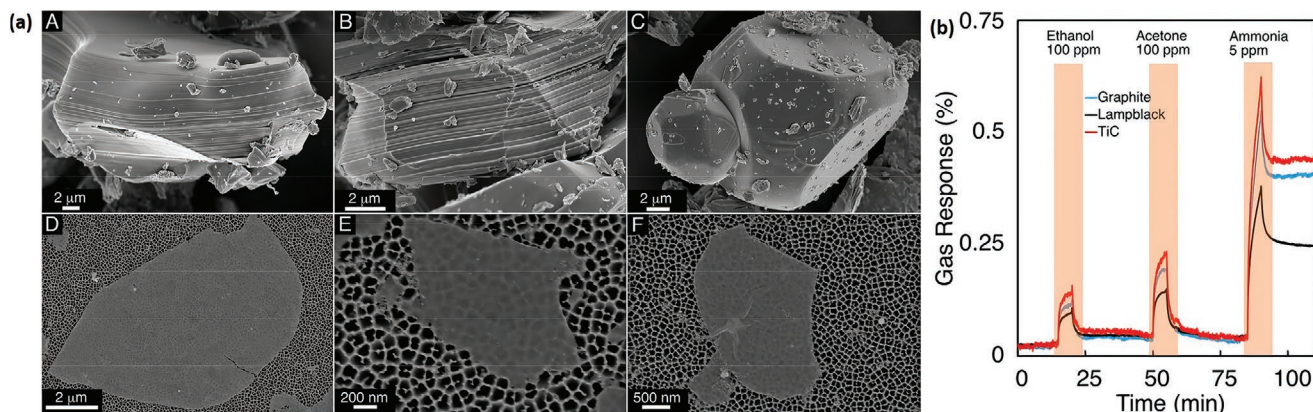


**Figure 4.** a) Morphological analysis of  $\text{Ti}_3\text{AlC}_2$  fabricated using precursors including (A) graphite, (B) TiC, and (C) carbon lampblack source of carbon;  $\text{Ti}_3\text{C}_2\text{T}_x$ -MXene fabricated utilizing a MILD-like strategy from (D) graphite, (E) TiC, and (F) carbon lampblack derived MAX phases. b) VOC monitoring ( $\text{C}_2\text{H}_5\text{OH}$ ,  $\text{C}_3\text{H}_6\text{O}$ , and  $\text{NH}_3$ ) characteristics of the  $\text{Ti}_3\text{C}_2\text{T}_x$ -MXene fabricated from MAX phases derived from different precursors. Reproduced with permission.<sup>[78]</sup> Copyright 2019, American Chemical Society.

detection can be achieved. However, the recovery time was relatively large (7 min for  $\text{H}_2$ , 5.5 min for methane:  $\text{CH}_4$ ), limiting its practical viability. Guo et al.<sup>[65]</sup> evaluated molybdenum carbide ( $\text{Mo}_2\text{CT}_x$ ) based chemiresistor for monitoring various VOCs; however, no recovery was reported.

These experiments are also complimented through numerous theoretical simulations based on molecular dynamics (MD) and density functional theory (DFT). Yu et al.<sup>[82]</sup> evaluated simulative interaction among semiconducting  $\text{Ti}_2\text{CO}_2$  and the gases like  $\text{CO}$ ,  $\text{N}_2$ ,  $\text{CH}_4$ , and  $\text{NO}_2$ . It was predicted that  $\text{NH}_3$  possesses lesser adsorption energy towards  $\text{Ti}_2\text{CO}_2$  ( $-0.37$  eV) compared to  $\text{V}_2\text{CO}_2$  ( $-0.81$  eV) and  $\text{Ti}_2\text{C}(\text{OH})_2$  ( $-0.48$  eV). Further, Ma et al.<sup>[83]</sup> reported the interaction of various VOCs with  $\text{M}_2\text{CO}_2$  ( $\text{M} = \text{Sc}$ ,  $\text{Hf}$ ,  $\text{Zr}$ , and  $\text{Ti}$ ) MXene. They found them more suitable for  $\text{NH}_3$  monitoring due to their lowest adsorption energy than other contaminants. In this study, these observations were further supported by Wang et al.,<sup>[84]</sup> via investigating  $\text{Hf}_2\text{CO}_2$  for monitoring multiple contaminants such as  $\text{CO}$ ,  $\text{CO}_2$ ,  $\text{NO}_2$ ,  $\text{SO}_2$ , hydrogen sulfide ( $\text{H}_2\text{S}$ ),  $\text{NH}_3$ , and  $\text{HCN}$  and found it best suitable for  $\text{NH}_3$  monitoring. On the contrary, Kim et al.<sup>[77]</sup> supported their experimental findings with DFT studies showing  $\text{Ti}_3\text{C}_2(\text{OH})_2$  possessed larger binding energy towards  $\text{C}_3\text{H}_6\text{O}$  than  $\text{Ti}_3\text{C}_2\text{O}_2$  and  $\text{Ti}_3\text{C}_2\text{F}_2$  MXenes, and other 2D nanomaterials like  $\text{MoS}_2$ , graphene, and BP. Theoretical modeling also predicted nitride MXene as a promising air contaminant monitoring material. For instance, Naqvi et al.<sup>[66]</sup> evaluated  $\text{M}_2\text{NS}_2$ -MXenes ( $\text{M} = \text{Ti}$ ,  $\text{V}$ ) to detect  $\text{SO}_2$ ,  $\text{H}_2\text{S}$ ,  $\text{CO}$ ,  $\text{NH}_3$ ,  $\text{CO}_2$ ,  $\text{CH}_4$ ,  $\text{NO}_2$ , and  $\text{NO}$ . They predicted  $\text{Ti}_2\text{NS}_2$  and  $\text{V}_2\text{NS}_2$  as promising materials for monitoring oxides of nitrogen. However, most theoretically reported MXenes are yet to be evaluated experimentally and are limited in practical production and applications.

However, the practical utilization of experimentally reported pristine MXene chemiresistors possessed common bottlenecks, including low flexibility, restacking of layers, oxidation, and slow recovery due to higher affinity toward polar contaminants. These drawbacks were catered through engineering the surface chemistry and structure by fabricating HNCs of MXenes with different materials.<sup>[58,75]</sup> There are several strategies to target specific

challenges; for example, surface functionalization can address oxidation issues, and intercalation can address restacking problems. However, fabricating HNCs can address all these issues, as secondary material inclusion like polymers prevents the MXene layers from restacking and increases flexibility while maintaining significant mechanical endurance. Furthermore, through multi-interactions, their interacting surface terminals can prevent oxidation and tune optical and electrical bandgap. The formation of interfacial heterojunctions among HNCs also contributes to improved sensitivity and recovery time.

Lee et al.<sup>[85]</sup> fabricated MXene/rGO HNC and evaluated it to monitor various air contaminants such as  $\text{NH}_3$ ,  $\text{H}_2\text{S}$ ,  $\text{SO}_2$ ,  $\text{C}_2\text{H}_5\text{OH}$ ,  $\text{C}_6\text{H}_6$ , and xylene. Although the response of HNC toward  $\text{NH}_3$  was enhanced compared to that of pristine precursor-based chemiresistors, the purification and functionalization are tedious. Further, Sun et al.<sup>[86]</sup> evaluated the air contaminant monitoring performance of the  $\text{W}_{18}\text{O}_{49}/\text{Ti}_3\text{C}_2\text{T}_x$  hybrid and found it to exhibit a significant selective response toward  $\text{C}_3\text{H}_6\text{O}$ . However, the response was limited at a high concentration of  $\text{W}_{18}\text{O}_{49}$  precursors due to  $-\text{F}$  functional group. Hermawan et al.<sup>[87]</sup> further evaluated copper oxide ( $\text{CuO}$ )/  $\text{Ti}_3\text{C}_2\text{T}_x$  HNC to detect a low trace of  $\text{C}_7\text{H}_8$ . However, the operation temperature for  $\text{CuO}/\text{Ti}_3\text{C}_2\text{T}_x$  HNC to detect  $\text{C}_7\text{H}_8$  was optimized as  $250^\circ\text{C}$ , which increases its cost and energy requirement limiting its practical application. Thus, several bottlenecks of high-temperature operation, complex processing, toxicity, and low flexibility limit the practical application of the inorganic-MXene HNCs and open prospects for forming HNCs with abundant macromolecules.

Various DFT and MD studies have confirmed that MXenes possess a greater affinity for polymers to form HNCs due to their unique surface functionalities.<sup>[59]</sup> These surface functionalities result in multi-interactions such as electrostatic, covalent, or hydrogen bonding among polymers and MXenes, which results in stable HNCs. Moreover, taking advantage of polymers such as abundance, ease of processing, low toxicity, mechanical flexibility, tunable conductivity, and solution processability, the HNCs of MXene and polymers can further result in superior air contaminant monitoring performance.



The fabrication of MXP HNC<sup>[88]</sup> was first reported in 2014 when the HNC of  $Ti_3C_2T_x$  was prepared using PVA and PDDA. Since then, various aspects of origin, fundamentals, developments, and prospects of MXP NCs have been demonstrated for multidisciplinary applications. Despite extensive dedicated research on MXP HNCs, the research performed in this direction is much smaller than precursor MXene (Figures 4c and 5a).

There are various reports focused on fabricating MXP HNCs using different hydrophilic (PI, PS, PVA, PE, silicones) and conducting (PPy, PVP, PSS, PEDOT, PAP, PAN) polymers.<sup>[59,68,69,89]</sup> The research has been devoted to optimizing and enhancing the physicochemical properties emerging from organic–inorganic interfaces in MXP HNCs through molecular and supramolecular dynamics.

Studies revealed that the formation of MXP HNCs can be based on multi-interactions such as covalent interaction, van der Waal interaction, and electrostatic interaction among polymer and surface functionalities of MXenes.<sup>[69]</sup> The involved interactions depend solely on the NP types and the MXene surface functionality. Various small macromolecules are found to be associated with MXene through covalent bonding due to strong affinity of MXene toward electron donors. Macromolecules with an electron-donating group are reported to replace the “T” group from MXene, resulting in the formation of HNCs.<sup>[67]</sup> For instance, Tran et al.<sup>[90]</sup> reported the persistence of covalent bonding in HNCs of silane-modified polymers such as poly(2-(dimethylamino)ethyl methacrylate) (PDMAEMA). The electrostatic interactions between negatively charged MXene surface with polymer precursor also play a crucial role in architecting MXP HNCs. However, these interactions can be various electrostatic interactions depending upon the nature of the precursor polymer.<sup>[91,92]</sup> For instance, aniline monomers are suspected of adsorbing on the MXene surface and between the MXene layers electrostatically.<sup>[93]</sup>

Fu et al.<sup>[94]</sup> reported similar observation information of graphene encapsulated  $Ti_2CT_x$ /PAN hybrid through cetyltrimethylammonium bromide (CTAB) assistance for supercapacitor applications. On the other hand, Chen et al.<sup>[95]</sup> fabricated the PEDOT/ $Ti_3C_2T_x$  HNC by charge transfer induced polymerization of EDOT monomer over MXene surface. Apart from organic–inorganic solid interactions such as covalent bonding and electrostatic interaction, supermolecular interactions also play a vital role in forming MXP HNCs. For instance, Zhu et al.<sup>[96]</sup> fabricated the  $Ti_3C_2T_x$ /PPy hybrid film through electrodeposition technique due to hydrogen bonding among its precursors. Further, Zhang et al.<sup>[97]</sup> reported HNC formation of  $Ti_3C_2T_x$  and PAM through cross-linking of PAM over MXene surface. The cross-linking in HNC was attributed to the hydrogen bond among the –OH and –F (hydrophilic terminals) of the  $Ti_3C_2T_x$ -MXene and the –CONH<sub>2</sub> terminals from PAM precursor. The typical interactions among various polymers and MXene surface functionalities are summarized in Figure 5b.

Various experimental outcomes have shown that incorporating polymer precursor into MXenes or vice-versa results in MXP HNCs possessing optimum physicochemical characteristics.<sup>[68]</sup> These enhanced diversified properties make MXP HNCs a unique sensing material compared to their precursors and other hybrids. These properties include tunable conductivity (metallic to semiconducting), flexibility and mechanical

strength owing to multi interactions, and stability in the oxygen environment. Further, it has been revealed that the addition of polymer results in the exfoliation of MXene layers, increasing the interlayer separation,<sup>[69,98]</sup> which inhibits the MXene stacking. It results in the hierarchal lamellar structured MXene and prevents them from oxidation in ambient conditions. It enhances the specific surface area of MXP HNCs to interact with environmental stimuli. Hence, MXP NCs have been suspected to be promising in diversified sectors, including energy storage and generation, sensors, actuators, electromagnetic shielding, biomedical sector, and optical sensors.<sup>[59]</sup>

Various DFT and MD outcomes further revealed that MXP HNCs possess a special affinity toward various air contaminants such as NH<sub>3</sub> due to their lower adsorption energies.<sup>[53,99]</sup> High effective surface area and optimum porosity obtained due to intercalation of polymer among MXene layers in MXP HNCs further make them promising to detect various air contaminants. The presence of abundant surface functionalities and synergistic effects due to creation of heterojunctions at the precursor's interface and enhanced interfacial charge transport in MXP HNCs is suspected to improve their contaminant monitoring performances.<sup>[100,101]</sup> However, these synergistic effects can only be controlled through optimizing various HNC synthesis parameters such as synthesis technique, synthesis time, nature, and concentration of precursors. By optimizing various reaction parameters during synthesis, dedicated MXP HNCs can be engineered for specific air contaminants to achieve selectivity. Hence, MXP HNCs require dedicated attention to explore the prospect of this class of materials as a commercial sensing material. In the next sections, this review will discuss the various synthesis techniques, properties, contaminant sensing mechanisms, and the performance of different MXP NCs.

### 3. Engineering MXene–Polymer HNCs Based Chemiresistors

The current research and development in investigating MXP HNCs for air contaminant sensing are dedicated to efficiently optimizing their desired properties like morphology, porosity, topology, lattice structure, electrical, optical, thermal, and mechanical properties. These salient features were optimized at the fabrication stage via controlling different reaction parameters like precursors' nature, concentration, and reaction conditions. The current state-of-the-art MXP HNCs based chemiresistors are a three-stage procedure including engineering MXene architect, architecting MXP HNC hybrids, and chemiresistor fabrication.

#### 3.1. Engineering MXene Architect

The primary stage for developing an MXP NCs based chemiresistor is synthesizing MXene of desired features. The current strategies to architect MXenes can be summarized into two strategies: 1) selective etching technique (Molten state etching, wet etching), and 2) bottom-up routes (Salt template growth, chemical vapor deposition-CVD). Numerous developments

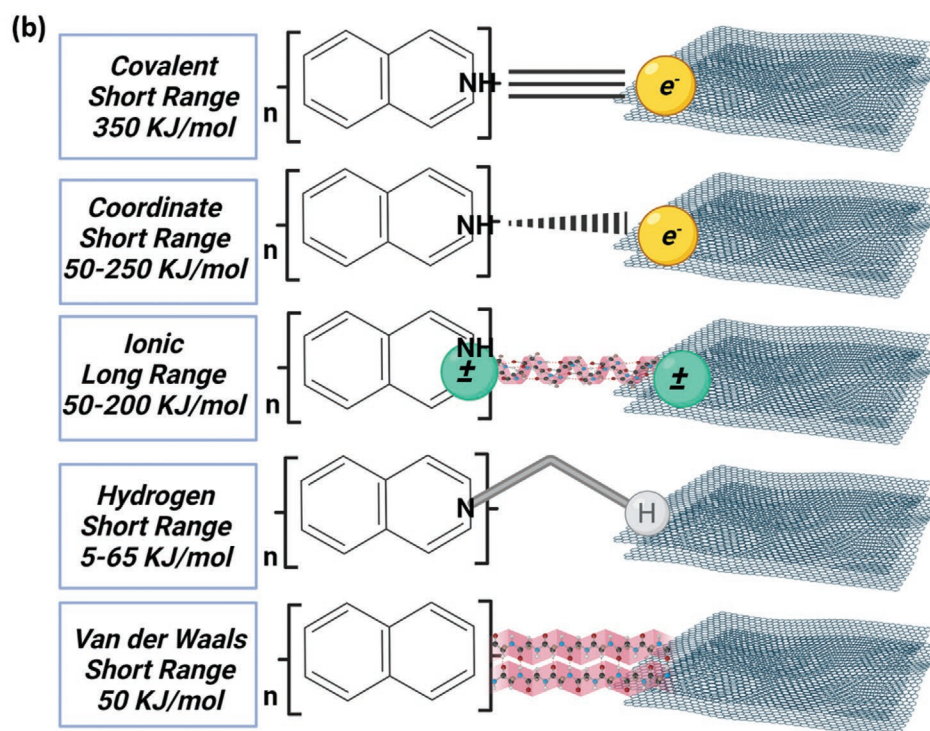
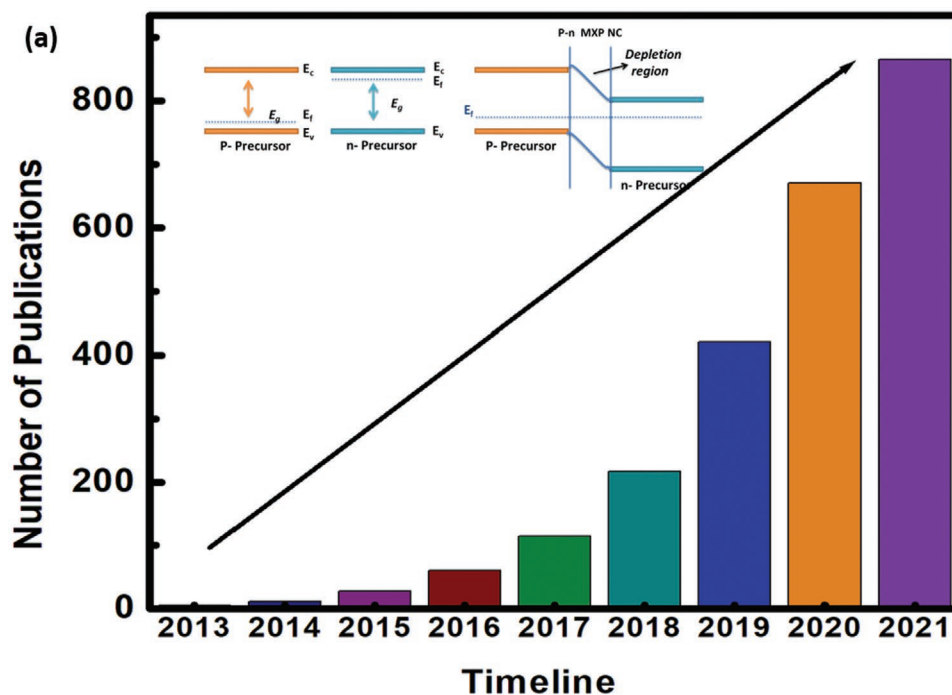


**Figure 5.** a) Growing interest of researchers in terms of number of publications on MXP HNCs till date searched on web of science with keywords MXene polymer hybrid nanocomposites. (with inset: depicting formation of p-n type MXP HNCs in light of band theory). b) Illustration of multiinteractions among MXenes surface functionalities and polymers to form MXP HNCs with approximate ranges in  $\text{KJ mol}^{-1}$  [Created with BioRender.com].

in these strategies have already been extensively discussed in various research and review articles<sup>[54,70–72,102]</sup> (Figure 6). Hence, the scope of this review is kept limited to the essentials and elementary concepts of stage-1 of fabrication route and dedicated to elaborated strategies used to architect MXP HNC chemiresistors.

### 3.1.1. Selective Etching Technique

A selective etching involves MAX and non-MAX phases as a precursor that induces functionalized terminations upon the etching process. A typical top-down etching technique involves eliminating the “A” element from MAX precursor

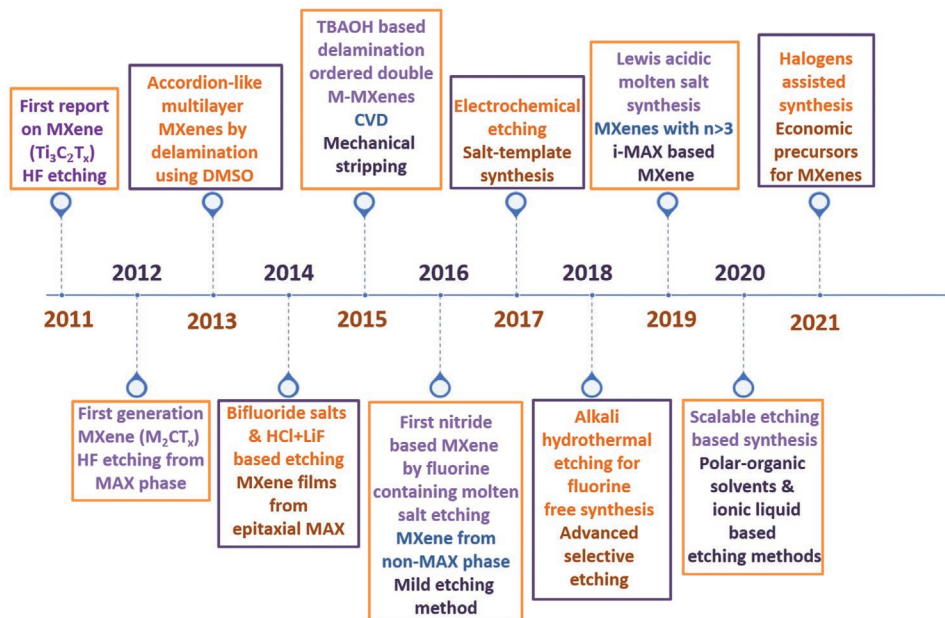


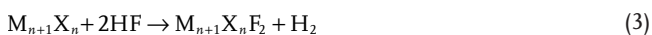
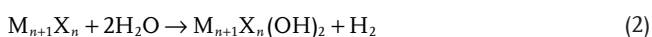
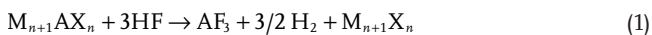
**Figure 6.** Timeline of development and advancement in various MXene fabrication strategies in past decade since its discovery in 2011 to 2021.

using different etchants and combinations.<sup>[71]</sup> There were several ways to exfoliate and etch “A” group elements from layers. Mechanical exfoliation seems complicated in this case due to strong metallic bonding between transition metal “M” and “A” group elements. Such a bond is chemically stable compared to the transition metal element “M” and “X” elements.

Naguib et al.<sup>[72,104]</sup> reported using hydrofluoric (HF) acid as an etching agent to delaminate the “A” group element layers for the first synthesis of MXenes. In a typical synthesis, the MAX phase, i.e., powder, is soaked in HF solution for 120 min with the follow-up protocol of stirring, centrifugation, filtration, and washing to get a pH value between 4 to 6 (**Figure 7**).

However, several alternative processes, including hydrothermal processes, molten salts, etc., have been discussed and are useful to understand the optimization of structural features and properties of MAX during chemical procedure<sup>[71,72]</sup> and surface modifications.<sup>[64,70,88,105]</sup> Some of the experimentally synthesized MXenes using various MAX phases have been summarized in **Table 2**.

The chemical Reaction to etch MXene from its MAX precursor with hydrofluoric acid that would take place in the following steps are presented in Equations (1–3).<sup>[72]</sup>



This chemical process weakens the “M–A” bond by producing the AF and freeing the H<sub>2</sub> gas, exfoliating the MXene layers, and replacing the atoms with surface termination group elements. Following this scheme, surfaces will be terminated with functional layers by which the whole surface becomes negatively charged. These types of MXenes are thermodynamically

more stable as compared to their pristine form. Moreover, HF etching agent has been widely used to attain more unusual MXenes like MO<sub>2</sub>C, Ti<sub>3</sub>SiC<sub>2</sub> and Ti<sub>2</sub>C etc.<sup>[71]</sup>

However, using a high concentration of HF during MXene synthesis is hazardous and highly corrosive.<sup>[114]</sup> Due to high toxicity of HF, various alternative mild etchants, including a mixture containing salts of lithium fluoride (LiF) and hydrochloric acid (HCl), ammonium bifluoride, and in situ HF methods are used. However, the etching with these mild etchants is slow in which intercalation of water molecule cations occurs, favoring the MXene with an enhanced gap between its layers and fewer crystal defects.<sup>[115–117]</sup>

### 3.1.2. Etching from the Non-MAX Precursors

A few studies in the past have shown that new MAX phases needed to be searched for all those MXenes that did not have any precursor for ternary metal carbides.<sup>[118,119]</sup> However, several transition metals such as Hf, Zr, and Sc are in practice to form unique layered compounds (MC)<sub>n</sub>[Al(A)]<sub>m</sub>C<sub>m-1</sub> instead of general MAX phases (where *n* is the same as discussed in previous MAX; but *m* is 3,4, and A is Si or Ge<sup>[118]</sup>). Some of these MXenes derived from non-MAX precursors are summarized in **Table 3**.

These materials are layered in a unique manner such that they have Al (A)–C sublayers. The M<sub>n+1</sub>AlC<sub>n</sub> phase has a strong M-bonding layer with intercalation of Al layer (**Figure 8**). On the other hand, carbon is shared with transition metal and Al (A) sub-layers at their boundaries in (MC)<sub>n</sub>[Al(A)]<sub>m</sub>C<sub>m-1</sub>. Zhou et al.<sup>[121]</sup> fabricated the Zr<sub>3</sub>C<sub>2</sub>T<sub>x</sub> from Zr<sub>3</sub>Al<sub>3</sub>C<sub>5</sub> (non-MAX precursor), that is synthesized using PES of Zr, Al and graphite powders.

It has been also reported that the etching of “A–C” results in a more conductive product and is easy compared to the

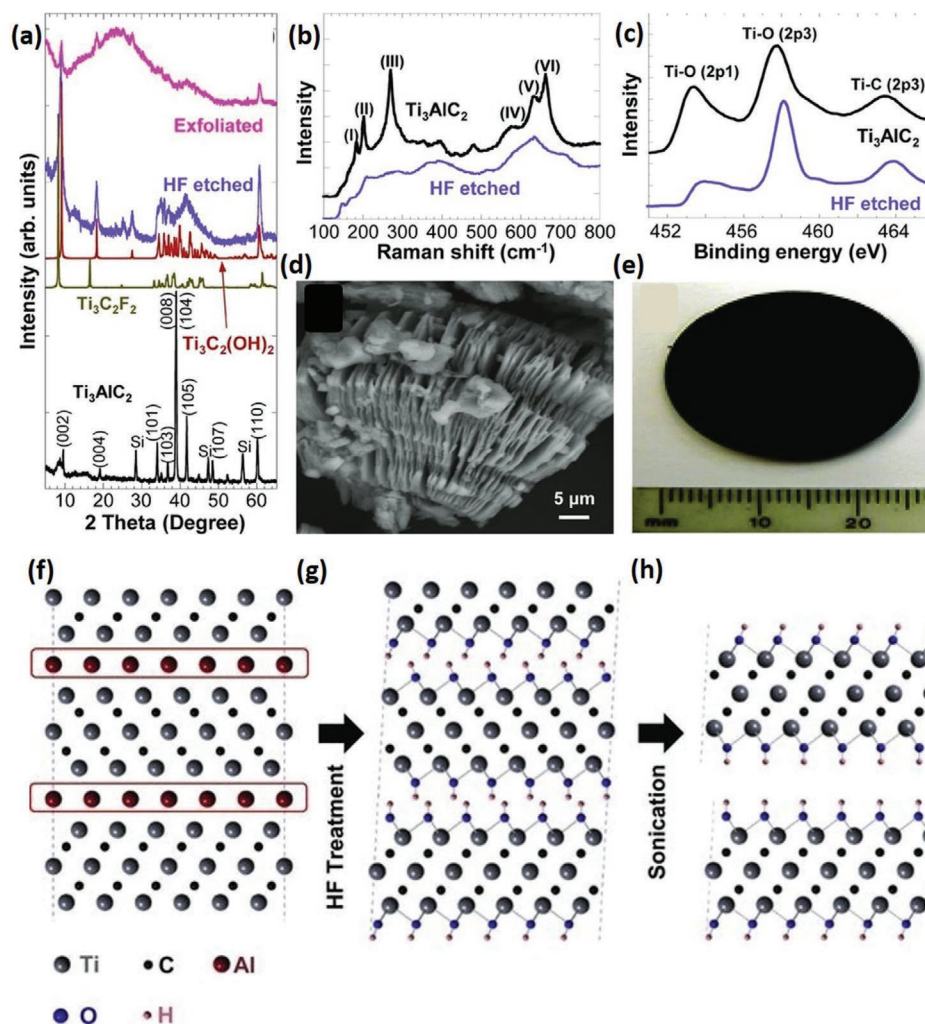


**Figure 7.** a) XRD Analysis of  $\text{Ti}_3\text{AlC}_2$ -MAX precursor prior to HF-treatment of  $\text{Ti}_3\text{C}_2(\text{OH})_2$  and  $\text{Ti}_3\text{C}_2\text{F}_2$  obtained by simulated XRD patterns; XRD spectra of  $\text{Ti}_3\text{AlC}_2$  subsequent to HF-treatment, and exfoliated MXenes resultant from sonication. b) Raman analysis of  $\text{Ti}_3\text{AlC}_2$  prior to and subsequent to HF-treatment. c) XPS outcomes of  $\text{Ti}_3\text{AlC}_2$  precursor prior to and subsequent to HF-treatment. d) SEM micrographs prior to HF treatment. e) Cold-pressed disk (25 mm) of etched and exfoliated sample subsequent to HF treatment. Schematic illustration of MAX ( $\text{Ti}_3\text{AlC}_2$ ). f) Structure of  $\text{Ti}_3\text{AlC}_2$ . g) Substitution of Al atoms by OH on reacting with HF-treatment. h) Separation of nanosheets on sonification with methanol due to breaking of hydrogen bonds; Reproduced with permission.<sup>[104]</sup> Copyright 2011, Wiley-VCH.

aforementioned etching of “A” element.<sup>[123]</sup> The “A – C” etching to form  $\text{U}_2\text{CT}_x$  MXene from  $\text{U}_2\text{Al}_3\text{C}_4$  has also been reported in the same study. This etching mode is possible with the help of chemical reaction between HCl and molten fluoride salt (LiF) that will successfully remove “A” group elemental layers in a much safer way with fewer defects. It produces large flakes and develops extended spacing between its layers with cations like  $\text{Li}^+$  and it will further modify the surface chemistry.<sup>[124]</sup> However, the toxic nature of etchants used for these strategies has motivated the researchers to find alternative techniques which are environmental and user friendly.

### 3.1.3. Bottom-Up Method

The mechanical vibration produces more defects that affect many structural properties, and chemical exfoliation is known

to be hazardous.<sup>[72]</sup> Therefore, it is required to progress novel fabrication routes to advance the expansion of MXenes.<sup>[71]</sup> Various bottom-up synthesis strategies, including chemical vapor deposition (CVD), atomic layer deposition (ALD), and plasma-enhanced pulsed laser deposition (PEPLD), are adequate routes to achieve the desired architecture and address these issues.<sup>[69,71,72]</sup> For instance, Gogotsi et al.<sup>[125]</sup> reported a molybdenum carbide structure fabricated by CVD. They reported the use of a bilayer substrate of copper on molybdenum foil of size larger than 100  $\mu\text{m}$ , which can be reduced to ultrathin  $\alpha$ - $\text{Mo}_2\text{C}$  crystal by keeping it at  $T \approx 1085^\circ\text{C}$  with a low concentration of  $\text{CH}_4$ . These strategies prevent environmental contamination by excluding the utilization of hazardous etchants. However, they are time-consuming, resulting in lower yield, complex and expensive. As well there are no reports in literature on fabrication of MXP HNC for air contaminant sensing applications using bottom-up strategies. For this purpose, the

**Table 2.** List of various experimentally synthesized MXenes derived from MAX phase using different etching agents.

No.	Etching agent	Phases	MAX phase	Derived MXenes
1	Hydrofluoric acid (HF) with 50 wt%	211	Ti <sub>2</sub> AlC <sup>[106]</sup>	Ti <sub>2</sub> AlC
			V <sub>2</sub> AlC <sup>[107]</sup>	V <sub>2</sub> C
			Nb <sub>2</sub> AlC <sup>[107]</sup>	Nb <sub>2</sub> C
			(Ti,V) <sub>2</sub> AlC <sup>[107]</sup>	(Ti,V) <sub>2</sub> C
			(W <sub>0.67</sub> Y <sub>0.33</sub> ) <sub>2</sub> AlC <sup>[108]</sup>	(W <sub>0.67</sub> ) <sub>2</sub> C
312	Ti <sub>3</sub> AlC <sub>2</sub> <sup>[104]</sup>	Ti <sub>3</sub> C <sub>2</sub>		
	(Mo <sub>2</sub> Ti)AlC <sub>2</sub> <sup>[109]</sup>	(Mo <sub>2</sub> Ti)C <sub>2</sub>		
413		Nb <sub>4</sub> AlC <sub>3</sub> <sup>[110]</sup>	Nb <sub>4</sub> C <sub>3</sub>	
		Ta <sub>4</sub> AlC <sub>3</sub> <sup>[72]</sup>	Ta <sub>4</sub> C <sub>3</sub>	
2	Molten salts like (Li/Na/K)F	413	Ti <sub>4</sub> AlN <sub>3</sub> <sup>[111]</sup>	Ti <sub>4</sub> N <sub>3</sub>
3	LiF in HCl	312	Ti <sub>3</sub> AlC <sub>2</sub> <sup>[112]</sup>	Ti <sub>3</sub> C <sub>2</sub>
4	NH <sub>4</sub> HF <sub>2</sub>	312	Ti <sub>3</sub> AlC <sub>2</sub> <sup>[113]</sup>	Ti <sub>3</sub> C <sub>2</sub>

scope of this report is oriented to physical top down etching based techniques. It is evident that the synthesis of MXene is challenging, still growing and requires extensive advancements to optimize desired properties favorable to sensing applications.

### 3.2. Engineering MXene–Polymer HNC Architect

Various MXP HNCs are typically filled composites (random distribution of precursors) and complexes (ordered or homogeneous dispersion of precursors). The state-of-the-art MXP HNC fabrication can be broadly categorized into two strategies, including in situ and ex situ techniques. Ex situ routes generally result in the formation of random dispersion of precursors in MXP HNC. However, in situ techniques are used to synthesize MXP HNC with homogeneously distributed precursors. The other reported novel strategies include roller mill

assisted synthesis, RIRMAPLE deposition, and emulsion-based routes. However, these routes require substantial attention for realistic prospects. Each route has its own merits and demerits and requires ordinate advancements for numerous practical applications.

#### 3.2.1. Ex Situ Strategies to Architect MXP HNCs

Ex situ routes are promising due to their easy optimization of composition and properties of MXP HNCs. It involves dispersing presynthesized precursors through various techniques like blending, alternate deposition and melt processing, and solvent removal using vacuum filtration, precipitation, and evaporation. The formation of HNCs using ex situ routes is based on weak multi-interactions, including van der Waals attraction, electrostatic interaction, and hydrogen bonding forces.<sup>[126]</sup> Blending techniques like solution processing and wet spinning are majorly used to fabricate MXP HNCs from hydrophilic precursors. In a typical wet spinning, the blending of an aqueous solution of pre-synthesized precursors (polymer and MXene) through centrifugation results in the formation of MXP HNC. For instance, Zhao et al.<sup>[100]</sup> adopted stirring of an aqueous solution of Ti<sub>3</sub>C<sub>2</sub>T<sub>x</sub> and CPAM to obtain Ti<sub>3</sub>C<sub>2</sub>T<sub>x</sub>/CPAM HNC. On the contrary, solution processing involves blending two different mutually soluble precursor solutions. Naguib et al.<sup>[127]</sup> fabricated Ti<sub>3</sub>C<sub>2</sub>T<sub>x</sub>/PAM NC through blending the dispersion of MXene in aqueous PAM and dimethylsulfoxide (DMSO). The blending of precursors is reported to insert the polymer chains in the interlayer space of MXenes, resulting in a 3D continual hierarchy-type network of conductive layers/sheets. These lamellar structures with the continuously linked conductive network are crucial to architect a state-of-the-art chemiresistor. Hence, the desired properties and composition of HNCs can easily be achieved via optimizing the precursor's concentration using blending techniques. However, only protic and aprotic polar solvents/polymers can be processed through

**Table 3.** List of zirconium and hafnium based non-MAX precursors with derived 2D carbides and nitrides.

S. no.	Non-MAX precursors with formula (MC) <sub>n</sub> [Al(A)] <sub>m</sub> C <sub>m-1</sub> where M = transition metal, "A" is group (13–16) elements	Derived 2D C's/N's or CN's (MC) <sub>n</sub> C <sub>m-1</sub> With M as a transition metal, A as a group (13–16) elements		
1.	Zirconium based <sup>[72,118,120,121]</sup>	Al contained	Zr <sub>2</sub> Al <sub>3</sub> C <sub>4</sub>	Zr <sub>2</sub> C <sub>4</sub>
		Zr <sub>3</sub> Al <sub>3</sub> C <sub>5</sub>	Zr <sub>3</sub> C <sub>5</sub>	
		ZrAl <sub>8</sub> C <sub>7</sub>	ZrC <sub>7</sub>	
		ZrAl <sub>4</sub> C <sub>4</sub>	ZrC <sub>4</sub>	
		Zr <sub>2</sub> Al <sub>4</sub> C <sub>5</sub>	Zr <sub>2</sub> C <sub>5</sub>	
		Zr <sub>3</sub> Al <sub>4</sub> C <sub>6</sub>	Zr <sub>3</sub> C <sub>6</sub>	
	Al(A) contained	Zr <sub>2</sub> [Al(Si)] <sub>4</sub> C <sub>5</sub>	Zr <sub>2</sub> C <sub>5</sub>	
		Zr <sub>3</sub> [Al(Si)] <sub>4</sub> C <sub>6</sub> [ZrY] <sub>2</sub> Al <sub>4</sub> C <sub>5</sub>	Zr <sub>3</sub> C <sub>6</sub>	
		Zr <sub>2</sub> [Al(Ge)] <sub>4</sub> C <sub>5</sub>	[ZrY] <sub>2</sub> C <sub>5</sub>	
		Zr <sub>3</sub> [Al(Ge)] <sub>4</sub> C <sub>6</sub> Zr[Al(Si)] <sub>8</sub> C <sub>7</sub>	Zr <sub>2</sub> C <sub>5</sub>	
		Zr[Al(Si)] <sub>4</sub> C <sub>4</sub>	Zr <sub>3</sub> C <sub>6</sub>	
			ZrC <sub>7</sub>	
2.	Hafnium based <sup>[72,118,122]</sup>	Al contained	Hf <sub>2</sub> Al <sub>4</sub> C <sub>5</sub>	Hf <sub>2</sub> C <sub>5</sub>
		Hf <sub>3</sub> Al <sub>4</sub> C <sub>6</sub>	Hf <sub>3</sub> C <sub>6</sub>	
		HfAl <sub>4</sub>	HfC <sub>4</sub>	
		Hf <sub>2</sub> Al <sub>3</sub> C <sub>4</sub>	Hf <sub>2</sub> C <sub>4</sub>	
			ZrC	

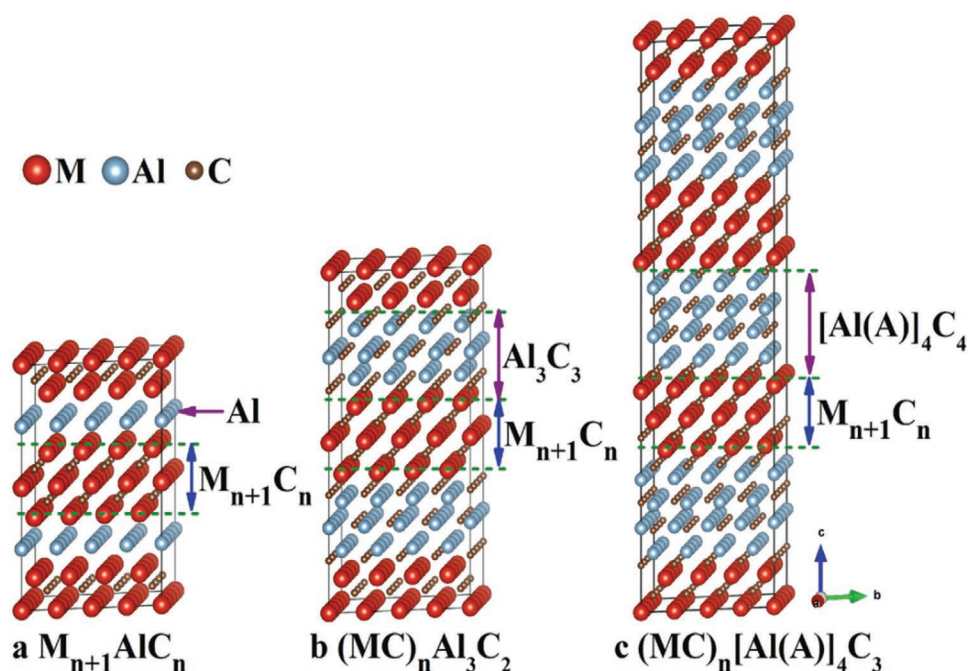


**Figure 8.** Schematic stepwise depiction of selective etching fabrication of  $M_3X_2MXene$  from a  $M_3AX_2$  layered phase. Reproduced with permission.<sup>[118]</sup> Copyright 2019, Springer.

a blending route owing to their intrinsic compatibility with MXenes.<sup>[10,128]</sup> On the contrary, nonpolar/weakly polar polymers require surface modification before blend processing. For instance, Yu et al.<sup>[129]</sup> enhanced the dispersion of  $Ti_3C_2T_x$ -MXene into thermoplastic polyurethane (TPU) using CTAB pre-treatment. The melt-processing strategies include thermal strategies like extrusion, hot pressing, and injection molding beyond precursor polymer's melting point.<sup>[128]</sup> For instance, Sheng et al.<sup>[98]</sup> reported a melt-processing technique to fabricate  $Ti_3C_2T_x$ /polyethylene glycol (PEG) HNC. This technique is highly advantageous in achieving a high yield of HNCs and their large-scale processing. However, it is restricted to the polymer precursors, which can be melt-processed, resulting in the degradation of precursors affecting the intrinsic characteristics of fabricated HNCs.

Recently, Wang et al.<sup>[79,80]</sup> reported an ex situ route to directly architect chemiresistor devices. It includes alternate deposition of presynthesized precursors over substrate followed by solvent removal through thermal/vacuum methods. Before sequential deposition, authors fabricated polymer precursors using an in situ polymerization approach and MXene precursors using selective etching. In a typical process, they spray-coated layer of  $Nb_2CT_x$  over the substrate with PAN layer to obtain  $Nb_2CT_x$ /PAN HNC (Figure 9).

This synthesis strategy is simple and advantageous to optimize the thickness and composition of HNC. Thus, the ex situ techniques are extensively used to architect MXP HNCs. However, their practical applications are limited due to challenge of complexity in evaporation of the solvent, contamination of environment because of evaporated solvent, deficiency of intrinsic interaction/bonding among precursors, poor flatness, lesser mechanical endurance, and nonhomogenous distribution of precursors.

### 3.2.2. In Situ Strategies to Architect MXP HNC

In situ approaches include fabricating one of the precursors in the presence of another or one-pot synthesis of both the precursors. Typically, a monomer is polymerized in the presence of presynthesized MXenes using in situ polymerization.<sup>[59]</sup> These strategies can be broadly categorized as solvent-assisted route and thermally assisted ring-opening polymerization.<sup>[10]</sup> In a typical solvent-assisted route, a desired amount of monomer is polymerized in the presence of MXene through reaction agents like dopant, surfactant, and oxidant for a fixed interval. The HNC fabrication is established through visible indicators like color change (green or pale yellow for PAN).<sup>[37]</sup> These strategies include dip coating, spin coating, drop-casting, spray coating, and inkjet printing. In this direction, Jin et al.<sup>[130]</sup> fabricated the MXP HNC of PEDOT:PSS and  $Ti_3C_2T_x$  using chemical-based polymerization of EDOT monomer over  $Ti_3C_2T_x$ -MXene to manifest PSS (Figure 10a). In contrast, Qin et al.<sup>[131]</sup> adopted an in situ electrodeposition route for architecting MXene/PPy HNC possessing a 3D porous morphology. Furthermore, Carey et al.<sup>[132]</sup> reported heat-activated ring-opening polymerization to architect polyamide (PA)-6-based MXene HNC. In a typical process, the mixing of precursors (amide and MXene) is processed at high temperatures (beyond the melting point of monomer) in ambient surroundings.

It has been reported that the adoption of in situ strategies results in improved characteristics of MXP HNCs such as dispersity, electrical, mechanical, and thermal properties.<sup>[79,80]</sup> It is due to the homogenous dispersion of precursors during in situ synthesis resulting in the formation of hetero-interface junctions among the precursors.<sup>[69,101]</sup> The inclusion of polymer chains in interlayer sites of MXenes results in

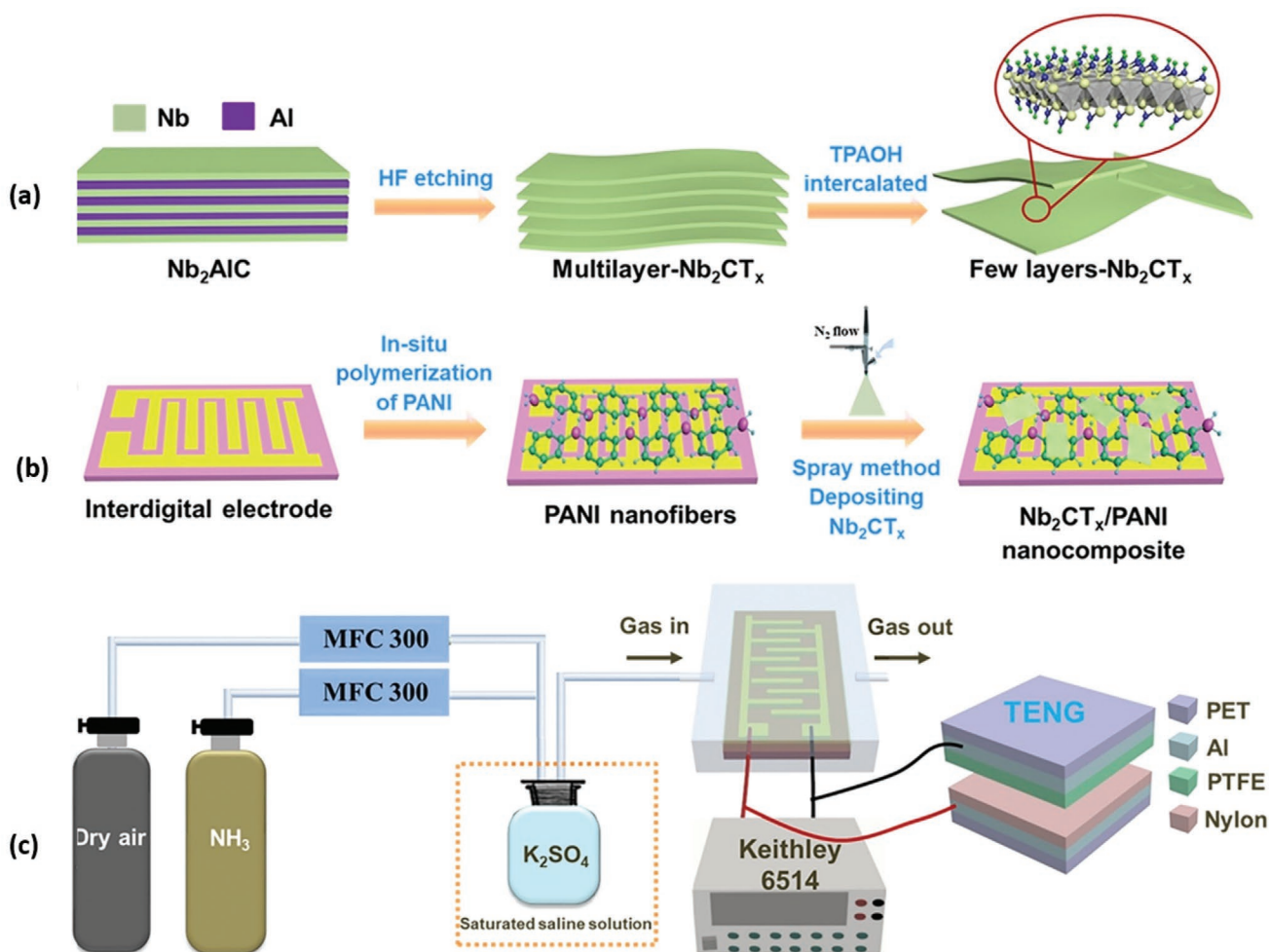


**Figure 9.** Illustration of fabrication of MXP HNC. a) Fabrication of multilayered Nb<sub>2</sub>CT<sub>x</sub> MXene from Nb<sub>2</sub>AlC MAX phase through HF etching method followed by intercalation using TPAOH to segregate its different layers. b) Ex situ alternative deposition technique to fabricate MXP HNCs chemiresistor involving alternate deposition of PANI and Nb<sub>2</sub>CT<sub>x</sub> MXene through spray coating over interdigitated electrodes to obtain working sensor. c) TENG driven air contaminant sensing apparatus; Reproduced with permission.<sup>[80]</sup> Copyright 2021, Elsevier.

exfoliation and expansion of its layer resulting in superior specific surface area and porosity.<sup>[69,129]</sup> These layered structures with higher surface-to-volume ratios and with the presence of heterointerfacial junctions are essential for state-of-the-art chemiresistors.

However, the bottlenecks restricting the practical applicability of in situ routes requires sufficient polymerization energy to grow over the MXene surface. As a result, only a few monomers can be polymerized over MXene layers, and the space between monomers, as well as the MXene layer itself, must be kept to a minimum to facilitate electron transport during polymerization. The in-situ strategies are assisted by two types of electron transfer processes among precursors during polymerization.<sup>[59,133]</sup> It includes either electron transfer from the highest occupied molecular orbitals (HOMO) of MXene to the lowest unoccupied molecular orbitals (LUMO) of monomer or vice-versa. Hence, the charge transfer-assisted synthesis process facilitates the creation of the heterointerfacial junctions throughout the HNC.

### 3.2.3. Other Novel Strategies to Architect MXP HNC

Besides the two widely used synthesis routes mentioned above, several novel techniques are also reported to form MXP HNCs. Zhi et al.<sup>[134]</sup> reported a novel emulsion-based route to fabricate MXP HNC, mixing PU emulsion with MXene. Furthermore, Ghidui et al.<sup>[135]</sup> utilized the conductive MXene clay to fabricate MXene HNCs, whereas a high-speed mechanical agitation route to fabricate Ti<sub>3</sub>C<sub>2</sub>/UHMWPE HNC was also reported.<sup>[72]</sup> Ajnsztajn et al.<sup>[136]</sup> reported a novel RIR-MAPLE synthesis technique to fabricate a transparent HNC electrode using poly(9,9-di-n-octylfluorenyl-2,7-diyl) (PFO) with Ti<sub>3</sub>C<sub>2</sub>T<sub>x</sub>. In a typical synthesis, a sequential deposition of an emulsion of PFO in trichlorobenzene and an aqueous suspension of colloidal Ti<sub>3</sub>C<sub>2</sub>T<sub>x</sub> was performed. It results in the formation of films with superior areal capacitances with an increase in MXene concentration. It is advantageous to overcome material constraints like solvent stability compared to conventional in situ routes like spin coating. However, the realistic prospects of these routes are limited due to low yield and complexity of processing.<sup>[68,71,72]</sup>

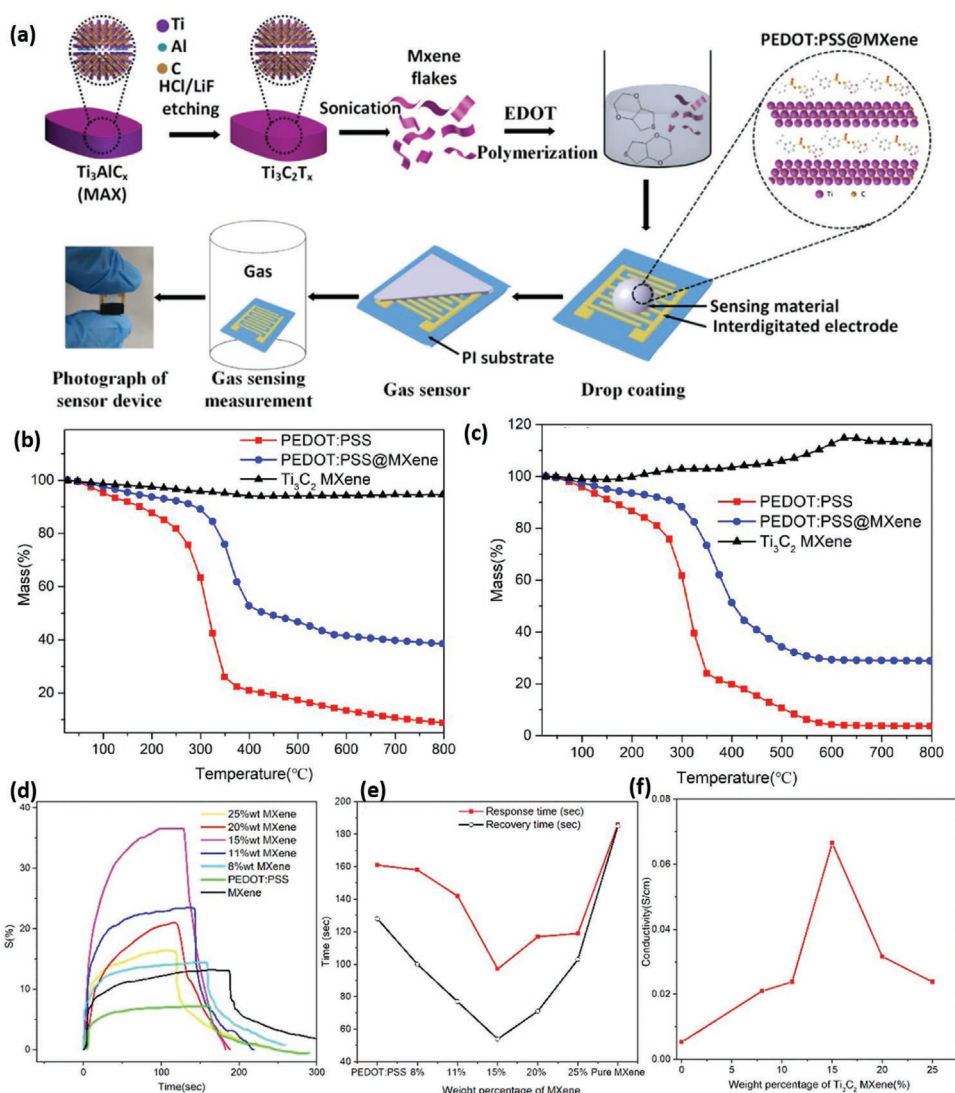


**Figure 10.** a) Illustration of in situ strategy for synthesis of MXP HNC based chemiresistor including synthesis of  $Ti_3C_2T_x$  MXene from  $Ti_3AlC_x$  MAX phase using HCl/LiF etching followed by polymerizing EDOT in presence of obtained MXene flakes. Chemiresistor was architected through drop-casting the prepared HNC over a flexible PI substrate possessing interdigitated electrodes. b, c) Enhancement in thermal characteristics of  $Ti_3C_2T_x$ /PEDOT:PSS compared to its pristine precursors shows better thermal stability of HNCs in harsh temperature conditions. Effect of concentration of  $Ti_3C_2T_x$  on d) sensitivity, e) recovery and response time, and f) conductivity of  $Ti_3C_2T_x$ /PEDOT:PSS HNC. Reproduced with permission.<sup>[130]</sup> Copyright 2020, American Chemical Society.

### 3.3. Chemiresistor Fabrication

Chemiresistors are architected in the last step by depositing the sensing film of MXP HNCs on an appropriate substrate, in general, possessing conducting electrodes. Numerous deposition methods include spin coating, dip coating, drop-casting, electrospinning, spray coating, and inkjet printing (Figure 11).<sup>[7,80,85,137,138]</sup> The deposition of MXP HNCs is performed over different flexible and nonflexible substrates like glass substrate, polyindole (PI), polyethylene terephthalate (PET), indium tin oxide (ITO), and fluorine-doped tin oxide (FTO) substrates.<sup>[50,54,139]</sup> These substrates consist of suitable conducting electrode configurations like interdigitated and parallel electrodes. Generally, gold (Au) electrodes are deposited

over these substrates to avoid probable noise due to the Schottky effect.<sup>[10]</sup> These electrodes are deposited using suitable masks coating, inkjet printing, dip coating, and thermal/vacuum evaporation.<sup>[71]</sup> For instance, Yang et al.<sup>[8]</sup> adopted a PET substrate with 27 interdigitated Au finger electrodes of 50  $\mu\text{m}$  width and 50  $\mu\text{m}$  spacing for chemiresistor fabrication. There are also reports in the literature on using glass substrates and silver or Au parallel electrode-based chemiresistor configuration.<sup>[62,140]</sup> However, their practical scope is limited, and current state-of-the-art chemiresistors are concerned with advancements in electrode configuration, composition, and thickness. Hence, the current development in chemiresistor engineering is dedicated to architecture, design, composition, materials used, and surface modifications.



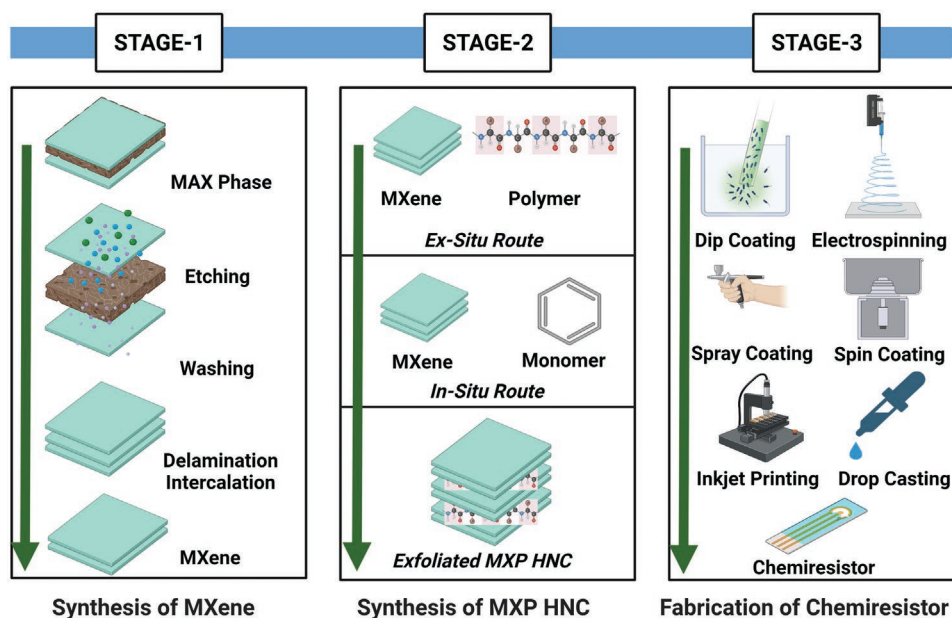


**Figure 11.** Various stages to fabricate MXP HNCs based chemiresistors for air contaminant monitoring, including Stage-1: Synthesis of MXene from various precursors, Stage-2: Fabricating MXP HNCs using ex situ/in situ strategies, Stage-3: Architecting MXP HNCs based chemiresistor through various deposition techniques such as spray coating, drop casting, spin coating, electrospinning, inkjet printing and dip coating [Created with BioRender.com].

## 4. Unique Properties of MXP HNCs for Air Contaminant Monitoring

The properties of MXene are tunable depending on functionalization, doping, and architecting hybrids with other materials, to achieve desired requirements as per the application field. For instance, the surface chemistries can be modified to target specific air contaminants for designing a selective sensor.<sup>[116]</sup> The MXP HNCs have recently been reported for high-performance contaminant detection and monitoring due to their optimized and enhanced properties.<sup>[10]</sup> The optimization is performed by controlling different reaction parameters during fabrication and improving the architecture of the detecting device. As discussed below, various enhancements in the properties of MXP HNCs found to be desired and supportive to their potential for detecting and monitoring contaminants (gases and VOCs).

### 4.1. Morphological and Topological Advancements for Sensing Applications

Morphology is the most crucial parameter governing the contaminant monitoring performance of sensing material.<sup>[44,50]</sup> Since gas/vapor detection is a surface phenomenon, the effective surface area, nature of pores, pore volume, surface roughness, and dimensionality of sensing material are vital factors in governing its sensing performance. The formation of HNCs using various precursors is rendered to enhance these governing factors resulting in superior sensing performance. The polymer insertion exfoliates the MXene layered structure resulting in superior effective surface area and porosity in MXP HNCs. Additionally, several studies have demonstrated enhancements in the specific surface area of

MXenes due to inclusion of NPs in MXP HNCs, required for several advanced applications such as energy (areal capacitance),<sup>[141,142]</sup> heavy metal removal in the context of adsorption efficiency<sup>[143]</sup> and gas/vapor sensor through a surge in interlayer layer distance.<sup>[80,130,144]</sup> These investigations were well-characterized using X-ray diffraction (XRD), Raman spectroscopy, scanning electron microscopy (SEM), tunneling electron microscopy (TEM), Brunauer-Emmett-Teller (BET) analysis. For instance, Li et al.<sup>[99]</sup> reported that the presence of dendrites on PAN NPs exfoliates the interlayer spacing of  $Ti_3C_2T_x$  nanosheets in HNCs using SEM outcomes. It significantly increases the effective surface area and porosity of  $Ti_3C_2T_x/PAN$ , turning it into a potential candidate for contaminant detection. Moreover, the architect of  $Ti_3C_2T_x/PAN$  was revealed to be core-shell type, which further enhances its stability.

Chen et al.<sup>[142]</sup> reported enhancement in specific surface area of DL-tartaric acid (DLTA) assembled  $Ti_3C_2T_x$ -MXene due to inclusion of PAN using BET analysis. The BET specific surface area of  $Ti_3C_2T_x/PAN/DLTA$  HNCs ( $20\text{--}23\text{ m}^2\text{ g}^{-1}$ ) was superior to that of pristine  $Ti_3C_2T_x$  (less than  $5\text{ m}^2\text{ g}^{-1}$ ) and DLTA-PAN ( $14.51\text{ m}^2\text{ g}^{-1}$ ). Additionally, the MXP HNC was found to be mesoporous with broad pore size distributions ranging from 2 to 40 nm, which facilitates the rapid ion diffusion and is highly favorable to high adsorption of analyte molecules, electrical energy, and metal ions. Furthermore, Zhao et al.<sup>[100]</sup> reported the gluing action of CPAM to hold multilayer  $Ti_3C_2T_x$  structure using TEM analysis. Wang et al.<sup>[79,80]</sup> reported the formation of 3D porous HNC film owing to the growth of PAN nanofibers on 2D  $Nb_2CT_x$ -MXene using SEM/TEM outcomes. This is a result of multi-interactions caused by the MXene surface functionalities. Moreover, the formation of abundant irregular pores on the HNC surface considerably enhanced the contaminant's

adsorption and desorption, resulting in its superior detection performance. Yuan et al.<sup>[8]</sup> reported the formation of ternary 3D MXene-polymer-rGO framework using a self-assembly approach through electrostatic interactions with superior VOC monitoring performance. Zhao et al. revealed the increase in interlayer spacing due to deposition of PAN-NPs into the  $Ti_3C_2T_x$  MXene layers using XRD analysis. It is attributed to a slightly weak characteristic (002) peak that shifts from  $8.13^\circ$  ( $Ti_3C_2T_x$  MXenes) to  $7.64^\circ$  (HNC), which signifies an increase in interlayer spacing of MXene layers in fabricated MXP HNC (Figure 12). The advancements in state-of-the-art chemiresistors are dedicated to architect lamellar and porous morphologies with enhanced interlayer spacing. These hierarchal layers connected through polymers endorse prompt adsorption and desorption of contaminants owing to their larger effective surface area, high roughness, large pore volume, and improved topology.

## 4.2. Structural and Surface Advancements for Sensing Applications

The manifestation of surface and structural defects with abundant surface chemistries and molecular interactions considerably prompts the adsorption and desorption of air contaminants. Generally, various spectroscopic techniques are used to reveal the present molecular interactions and structural defects. For instance, Wang et al.<sup>[79]</sup> confirmed the presence of hydrogen bonding in PAN-Nb<sub>2</sub>CT<sub>x</sub> HNC in terms of a blue shift in its FTIR peaks compared to pure precursors. Similarly, Zhao et al. showed the existence of weak multi-interactions among precursors of PANI/ $Ti_3C_2T_x$  HNCs through observing a shift in peak positions of HNCs compared to pristine precursors. They further revealed the presence of ordered structure with (002) plane of an interplanar spacing 13.20 Å. These open-ordered layered structures create many mass transport pathways for faster

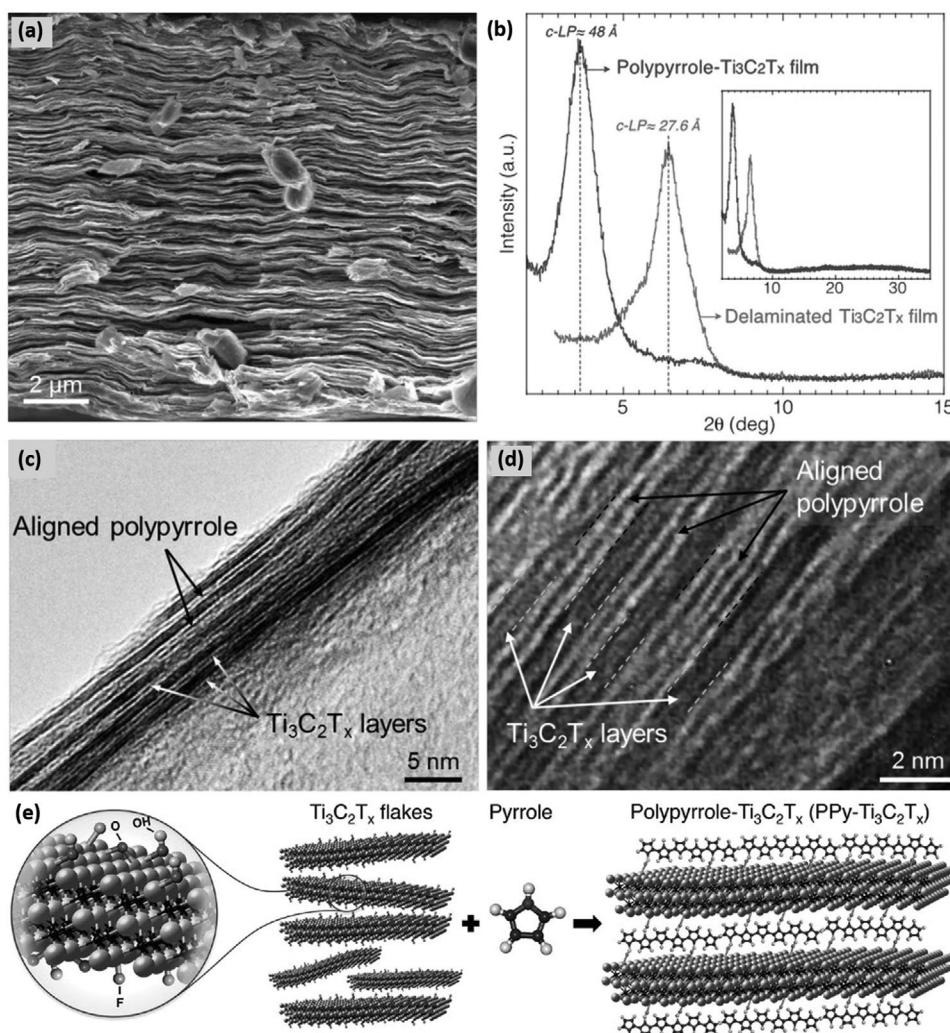


**Figure 12.** a) Cross-sectional SEM image of  $Ti_3C_2T_x$ /PPy HNC binder-free film fabricated using in situ fabrication strategy. b) XRD pattern of pristine  $Ti_3C_2T_x$  paper and  $Ti_3C_2T_x$ /PPy HNC exhibiting a reduction in (002) peak indicating increase in interlayer distance between  $Ti_3C_2T_x$  layers due to inclusion of PPy. c,d) Cross-sectional TEM micrograph reveals PPy chains intercalated and aligned among the  $Ti_3C_2T_x$  layer. e) Schematic of inclusion of PPy into  $Ti_3C_2T_x$  layers leading to exfoliation of layers in MXP HNC. Reproduced with permission.<sup>[145]</sup> Copyright 2016, Wiley-VCH.

contaminant diffusion, resulting in rapid response at room temperature.

Moreover, Zhao et al.<sup>[100]</sup> reported the existence of surface defects by Raman outcomes possessing an enhanced D-peak to G-peak intensity ratio ( $I_{(D)}/I_{(G)}$ ) in  $Ti_3C_2T_x$ /CPAM HNC than that of pure precursors. Jin et al.<sup>[130]</sup> reported the presence of electrostatic interaction and hydrogen bonding among the precursors of  $Ti_3C_2T_x$ /PAN HNC of superior  $I_{(D)}/I_{(G)}$  with a relative shift in G- and D- bands. Recently, Chaudhary et al.<sup>[15,146]</sup> revealed the crucial role of the ordering of molecules/polymer chains in governing the sensing performance of HNC. In general, polymers are amorphous, and the addition of MXene into the polymer matrix induces order to a certain extent. For instance, Li et al.<sup>[101]</sup> reported decreasing peak width and intensity at half height (FWHM) for polymer precursor in PAN/ $Ti_3C_2T_x$  HNC (Figure 13). These outcomes are analogous to those described in the literature for PAN, where a reduction in FWHM results in increased interlayer spacing.<sup>[146]</sup> It restricts interchain hopping of charge carriers and promotes intrachain hopping resulting in 1D movement of charge carriers during sensing phenomena. It provides a better conductive pathway for charge carrier movement resulting in superior sensing performance.<sup>[146]</sup> Hence, the molecular interactions, structural defects, ordering, and surface functionalities are reported to felicitate the contaminant adsorption and desorption through the HNC surface. The current efforts are dedicated to understanding the physiochemical properties and morphology of HNCs, which is crucial to architect the advanced sensing materials with superior monitoring performances.

### 4.3. Advancements in Electrical Properties for Sensing Applications

MXene has excellent electric conductivity, which can be tuned from metallic to semiconducting by projecting MXP HNCs as

prominent candidates for sensing applications. Additionally, MXenes-based electrodes are widely used as transducers for sensing of property for biological receptors due to their direct electron transfer between enzymes and protein.<sup>[147,148]</sup> Various computational and theoretical analyses have shown that the pristine MXene has metallic nature, and its electronic bands lie near the Fermi level.<sup>[70,72]</sup> It has been revealed that the MXenes have excellent electric conductivity with ( $9880 \text{ S cm}^{-1}$ ) near to that of graphene.<sup>[149,150]</sup>

The typical metallic behavior of non-terminated MXenes is attributed to the outer layer of “M” elements.<sup>[70,151]</sup> The existence of a high density of states (DOS) near their Fermi surface is governed by the “d-electrons” of “M,” and “p-electrons” of “X” contribute to the formation of energy bands (around  $-3$  to  $-5$  eV) below Fermi surface.<sup>[56,152]</sup> Moreover, the outer layer of “M-atoms” dominates the governing of electronic properties of MXenes compared to inner layers.<sup>[64,70]</sup> Furthermore, the surface terminations generated during the fabrication of MXenes bond with the outer “M” layers and alter their electronic behavior in a range of metallic to semiconducting characteristics. Thus, the electronic configuration of “M” elements plays a vital role in governing the electronic nature as well as the resulting semiconducting behavior in terminated MXenes. For instance, the “Ti” is a group IV element, and “Nb” is a group V element, and their bonding with the C atoms and surface terminations governs the electronic nature of respective MXene.<sup>[151]</sup> Moreover, the existence of extra electron results in a shift from metallic behavior to variable-range hopping type semiconducting behavior. These extra electrons from outer “M” layers result in formation of a new energy band below the Fermi surface.<sup>[70,151]</sup> Thus, the type of surface termination ( $-\text{OH}$  and  $-\text{F}$  receive a single electron, and  $-\text{O}$  accepts two) and the nature “M” ( $d^1$ ,  $d^2$  or other) cumulatively decide the semiconducting characteristic

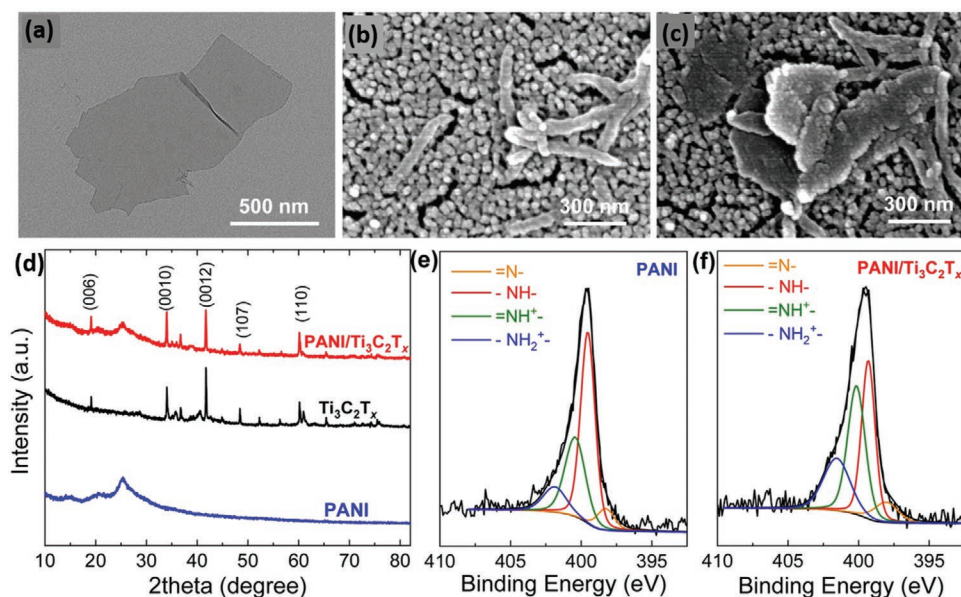


**Figure 13.** Spectroscopic studies illustrating structural and surface defects induced in MXP HNCs. a) TEM image of exfoliated  $Ti_3C_2T_x$  sheet. b,c) SEM images of pristine PAN and  $Ti_3C_2T_x$ /PAN HNC films, respectively. d) XRD Pattern of  $Ti_3C_2T_x$ /PAN, pristine  $Ti_3C_2T_x$  and PAN films showing reduction in FWHM of PAN in HNC compared to pristine PAN. e,f) XPS N1 spectra of pristine PAN and  $Ti_3C_2T_x$ /PAN HNC film showing higher degree of protonation of PAN in HNC compared to pristine PAN felicitating charge carrier transport. Reproduced with permission.<sup>[101]</sup> Copyright 2019, Elsevier.

in MXenes. However, the position of the formed Dirac cone, whether below the Fermi surface or above it, governs the self n-type and p-type doping characters, respectively, in the vicinity of any modification in the surroundings.<sup>[153–156]</sup> Several experimental outcomes have validated that the electronic property of metallic MXene can also be changed into semiconductors by the phenomena of surface functionalization.<sup>[133,157,158]</sup> The DOS and band structure calculations of the  $Ti_2CT_x$  at different terminations are shown in **Figure 14**.<sup>[56]</sup> It is obvious that the  $-OH$  and  $-F$  layout leads to an identical effect on the electronic properties of MXenes.

They both accept the single electron termination during the equilibrium condition, while O's oxidation state creates a different effect when it accepts two electrons. When the terminated group is oriented, it changes the electronic properties of MXenes, so during the postmodification techniques and synthetic approaches, the electronic properties of MXenes change. Various other factors, including doping, film thickness, intercalants, crystal lattice symmetry, strain, stoichiometric engineering, external electric field, etc., are also reported to govern the energy structure and semiconducting nature of MXenes.<sup>[70,151]</sup> In most cases, the semiconducting MXenes exhibit a direct bandgap in the range of 0.25–2.0 eV, excluding  $Sc_2C(OH)_2$ , which has an indirect bandgap.<sup>[159]</sup>

Most polymers are insulators, and their interface can increase their conductivity with MXenes.<sup>[59]</sup> Incorporating the polymer between the MXene layers provides the molecular-level coupling among them and delamination of the multilayer MXenes. It is studied that the electric conduction of  $Ti_3C_2/PVA$  was enhanced.<sup>[88]</sup> For instance, the electronic conductivity of  $Ti_3C_2T_x$  ( $210 \mu S cm^{-1}$ ) increases to 73.6% after the hosting of PEO.<sup>[160]</sup>

In addition, other examples have been studied to increase the electrical conductivity of MXP membranes, like  $Ti_3C_2T_x$ /cellulose ( $739 S m^{-1}$ ) and  $Ti_3C_2T_x/NR$  ( $1400 S m^{-1}$ ).<sup>[161,162]</sup> MXenes/polymers membranes' dielectric permittivity increased by hosting  $Ti_3C_2T_x$  sheets into matrix of poly(vinylidene fluoride-trifluoro-ethylene-chlorofluoroethylene) P(VDF-TrFE-CFE).<sup>[163]</sup> The increment of the dielectric permittivity is due to the accumulation of charges at the interface of  $Ti_3C_2T_x$  and P(VDF-TrFE-CFE). It is noted that the dielectric constant of

acrylic resin increased by 140 and 75 folds by the integration of 6.36 vol%  $Ti_3C_2T_x$  and 5.98 vol% PPy-modified  $Ti_3C_2T_x$ , respectively.<sup>[164]</sup> The tuning of the electrical nature of MXP HNCs is essential for versatility in detecting a wide range of oxidizing and reducing contaminants. However, optimizing the electrical conductivity of HNC is crucial for sensing prospects.<sup>[10]</sup> It is demonstrated by optimizing the precursor's HNC concentration to attain the desired conductivity regime. Jin et al.<sup>[130]</sup> analytically examined the change in electrical conductivity of pure PEDOT:PSS (about  $0.01 S cm^{-1}$ ) on a surge in weight percentage (wt%) of  $Ti_3C_2T_x$  in HNC. The electrical conductivity initially improved ( $\approx 0.02 S cm^{-1}$  at 8%,  $0.07 S cm^{-1}$  at 15%) and then reduced ( $\approx 0.03$  at 20% and  $\approx 0.02$  at 25%) with the increase in wt% of  $Ti_3C_2T_x$  precursor. The 15 wt%  $Ti_3C_2T_x$  exhibited the highest electrical conductivity, ascribed to the equilibrium among the percolation threshold and confinement of  $Ti_3C_2T_x$ . The small addition of  $Ti_3C_2T_x$  enhances the charge carrier transport, while the larger  $Ti_3C_2T_x$  content decreases it to a rigidly confined pathway.

Furthermore, Li et al.<sup>[101]</sup> reported the improved protonation in PAN due to the addition of  $Ti_3C_2T_x$ , promoting charge carrier transfer in HNC, leading to superior sensing performance. They reported the protonation degree for  $Ti_3C_2T_x/PAN$  conforming to the percentage of  $=NH^+$  and  $-NH_2^+$  (58.2%) as observed through X-ray photoelectron spectra (XPS) was superior to that of pristine PAN precursor (41.4%). Hence, incorporating MXene into polymer improves its conductivity and promotes charge carrier transport via forming conductive pathways, which facilitate selective analyte detection performances.

#### 4.4. Advancements in Thermal Characteristics

The thermal properties of a material, such as thermal stability, thermal expansion, and thermal conductivity, are dependent upon HNC processing and closely related to its practical applications. Thermal stability is crucial for state-of-the-art chemiresistors to determine their viability in different environmental conditions. First principle DFT and MD studies have revealed that MXene has superior thermal stability than most conducting and semiconducting 2D materials.<sup>[68,70]</sup> However, the

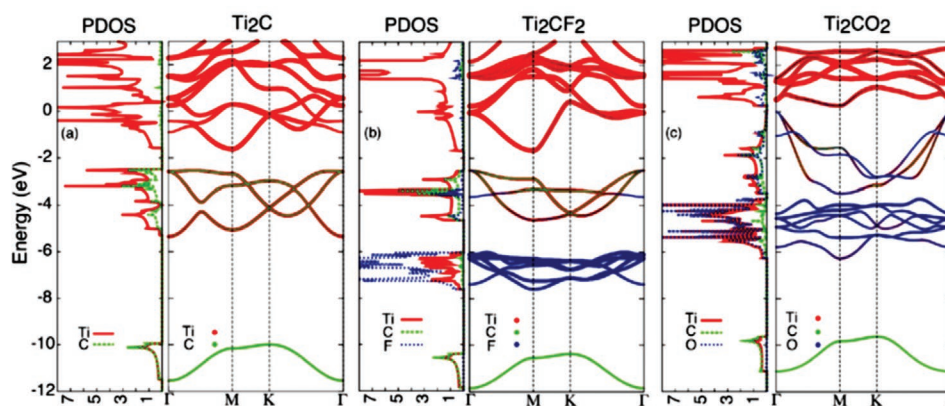


**Figure 14.** Density of state and band diagram of DFT study  $Ti_2CT_x$  at different terminations layouting the similarities and differences among the electronic characteristics due to specific termination on MXene, Reproduced with permission.<sup>[56]</sup> Copyright 2017, Royal Society of Chemistry.

thermal stability of NPs is comparatively lower, which can be augmented via mixing with MXenes. For instance, a team of the Chinese Academy of Sciences reported that the thermal conductivity of SCF<sub>2</sub> increased to 472 W m<sup>-1</sup> K<sup>-1</sup>, which is higher than traditionally used Ag.<sup>[165]</sup> The NCs of MXene/PVDF are prepared using solution mixing. The conductivity and diffusivity thermal value of the HNCs with an only ratio of 5 wt% of the MXene increase up to 0.363 m<sup>-1</sup> K<sup>-1</sup> and 0.167 mm<sup>2</sup> s<sup>-1</sup>, respectively. The reported thermal conductivity of MXene/polymer is twofold greater than the pristine PVDF.<sup>[166]</sup> The researchers believe that the layered MXene forms a bridge-like structure interacting with polymer in HNC, suggesting the creation of hydrogen and chemical bonds with the polymers. These phenomena make heat transfer between the chains of polymers. MXene's distinctive thermal feature is that it reduces the random arrangement of polymers, which diminishes the dispersion of photons and thermal vibrations and increases the thermal conduction of polymer materials.<sup>[167]</sup> Moreover, MXene/low-density polyethylene (LDPE) HNCs are reported to possess excellent thermal stability, with the average values of  $T_{20\%}$ ,  $T_{40\%}$ , and  $T_{max}$  of a sample at glass temperature increased.<sup>[168]</sup>

Furthermore, Jin et al.<sup>[130]</sup> reported that the rate of weight loss as a function of temperature (in the range of 27 °C to 300 °C) for HNC is slower than that of pure precursor polymer (Figure 10b,c). It is believed to be the result of multielectron interactions among its precursors. Moreover, it has been reported that the proliferation in thermal conductivity of MXP HNC leads to superior heat-dissipation capability of HNC, enhancing its thermal stability. The improved thermal stability in MXP HNCs provides a steady sensing performance under variable temperatures, especially in punitive surroundings. Nevertheless, the evaluation of the direct role of the thermal properties of MXP HNCs in air contaminant sensing phenomena still requires special attention.

#### 4.5. Advancements in Mechanical Properties for Sensing Applications

MXenes are known to exhibit excellent flexural property and good rigidity. Polymers with a polar group are closely linked with the MXenes due to their interaction with surface terminal groups. It improves the mechanical property of polymers, such as hardness, young modulus, yield, and ultimate tensile strength and index of toughness.<sup>[106,169]</sup> It has been reported that Ti<sub>3</sub>C<sub>2</sub>T<sub>x</sub> improves the mechanical properties of ultrahigh molecular weight polyethylene (UHMWPE) and that the tensile strength of the polymer increases nonlinearly with the addition of MXene. In addition, 0.75 wt% of Ti<sub>3</sub>C<sub>2</sub>T<sub>x</sub> increases the strength of UHMWPE from 36.61 to 39.65 MPa. The increase in the hardness is due to the excellent strength MXene Ti<sub>3</sub>C<sub>2</sub>T<sub>x</sub> nanosheet of UHMWPE nanocomposite (Figure 15a,b).<sup>[89]</sup> The associated phenomenon for enhancement in the mechanical attributes of MXenes is explained in the context of interface formation between precursors (Figure 15c).

Ling et al. reported the mechanical strength of PVA increased from 30 to 91 MPa, which is threefold superior to pure PVA.<sup>[88]</sup> The composite of MXenes with polymers does not enhance the rigidity but also increases the toughness of

NCs. Similarly, another study found that adding the 0.5 wt% of MXene increased the mechanical stiffness of TPU from 14 to 20 MPa (47%), which is a significant improvement in stiffness.<sup>[98]</sup> For better mechanical properties, another study was performed by interfacing the Ti<sub>3</sub>C<sub>2</sub>T<sub>x</sub> surface group on the surface of cellulose nanofiber (CNF) to prepare a composite paper of Ti<sub>3</sub>C<sub>2</sub>T<sub>x</sub>/CNF. It was reported that mechanical strength increased from 49.3 to 135 MPa, and fraction strain enhanced from 10% to 16.7%, which is higher than pristine CNF with 50 wt% of Ti<sub>3</sub>C<sub>2</sub>T<sub>x</sub>.<sup>[162]</sup> The critical factors to increasing the mechanical toughness and strength of interfacial MXene/polymer composite NCs are excellent chemical interaction and good interfacial adhesion with uniform dispersion.<sup>[98]</sup>

Mechanical flexibility characterizes a portable, bendable, foldable, compact, and stable chemiresistor for commercial development.<sup>[54]</sup> This feature makes it easier to install a chemiresistor at every emission site of air contaminant. It can be achieved by either designing self-standing flexible films or using a flexible substrate. For instance, Tong et al.<sup>[170]</sup> reported a flexible freestanding array film of iron-doped titanium dioxide (TiO<sub>2</sub>) to detect H<sub>2</sub>S. Moreover, Li et al.<sup>[101]</sup> and Wang et al.<sup>[79,80]</sup> adopted flexible PI substrates to attain mechanical flexibility in architected MXP HNC-based NH<sub>3</sub> chemiresistors. Contrary, Zhao et al.<sup>[100]</sup> reported VOC monitoring performance of flexible Ti<sub>3</sub>C<sub>2</sub>T<sub>x</sub>-PAN film deposited over PET substrate. It was confirmed that Ti<sub>3</sub>C<sub>2</sub>T<sub>x</sub>/CPAM HNC is flexible and robust due to binding function of CPAM between the Ti<sub>3</sub>C<sub>2</sub>T<sub>x</sub> layers. It is attributed to the forces due to H-bonds existing among the CPAM chains and Ti<sub>3</sub>C<sub>2</sub>T<sub>x</sub>'s surface amide group. Nevertheless, maintaining flexibility along with mechanical strength with machine processing is very challenging. It is done by optimizing the concentration of precursors during material processing. Hence, the current studies illustrate promising techniques for the commercial processing of MXP HNCs-based chemiresistors possessing enhanced reinforced mechanical characteristics. Nonetheless, numerous unanswered tribological apprehensions persist due to the uneven distribution of precursors, stress transfer mechanism, and size effects due to precursors.

## 5. Sensing Mechanism in MXP HNCs for Detecting Air Contaminants

Air contaminant's monitoring using MXene-polymer HNC-based chemiresistors has been achieved and evaluated via a time-dependent change in surface resistance as a function of contaminant concentration.<sup>[10,46,50,57]</sup> During sensing, the interaction of HNC surface with reducing or oxidizing contaminant molecules causes a change in sensing material's resistance. Concurrently, the contaminant is replaced by ambient atmosphere/inert gas resulting in restoration of the initial resistance magnitude. The recorded variation in surface resistance of HNC is due to either chemisorption or physisorption of contaminant molecules on its surface. The types of interaction among HNC and contaminant molecules depend on the nature of both precursors of HNC and contaminants. Hence, it is critical to analyze the interaction of contaminants with pristine

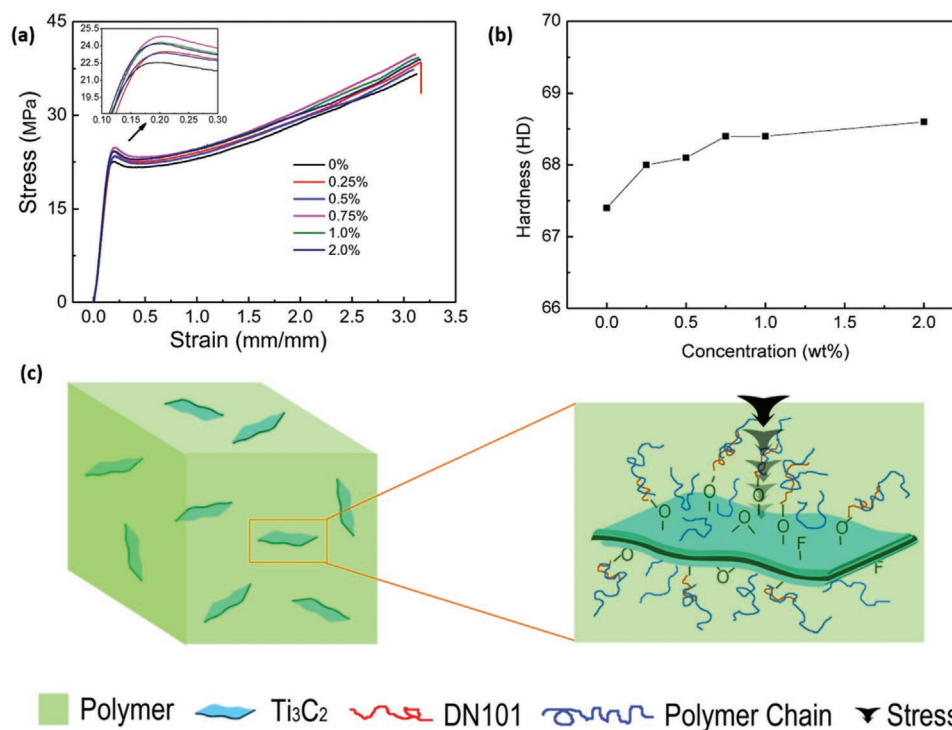


**Figure 15.** Advancement in mechanical characteristics of MXP HNC. a) Stress and strain curves of  $\text{Ti}_3\text{C}_2\text{T}_x/\text{UHMWPE}$  nanocomposite. b) Variation in hardness of the HNC with variation in concentration of  $\text{Ti}_3\text{C}_2\text{T}_x$ . c) Schematic illustration of mechanism behind improvement in mechanical characteristics of MXP HNCs due to presence of both the precursors. Reproduced with permission.<sup>[89]</sup> Copyright 2016, Elsevier.

precursors for the fundamental understanding of sensing phenomenon associated with HNCs.

### 5.1. Sensing Mechanism in Conducting Polymers

The sensing mechanism of conducting polymers due to change in resistance due to adsorption of oxidizing or reducing contaminant is accounted for mobility and production or neutralization of charge carriers (polarons and bipolarons) in polymers.<sup>[36,57,137]</sup> The motion of these charge carriers in the presence of various contaminants changes morphological and structural characteristics such as variation in the height of the potential barrier ( $V_{\text{air}}$ ), swelling due to absorption of contaminant molecules, interaction with dopant molecules, and variation in bond angle or bond length.<sup>[14,137,139,171]</sup> Hence, resulting in electrical resistance changes due to a change in charge carrier number density ( $N$ ) on interaction with contaminant molecules. Consequently, the electrical resistance of the NPs is governed by the factors in Equation (4):<sup>[137,171]</sup>

$$R_A = R_0 \exp\left(\frac{eV_A}{k_B N_A T}\right) \quad (4)$$

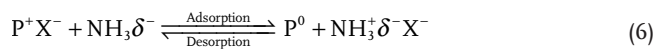
with  $R_0$  as a constant,  $e$  as the elementary charge with magnitude  $1.6 \times 10^{-19}$  C,  $k_B$  represents the Boltzmann constant, and  $T$  symbolizes the absolute temperature.

The interaction of NPs with oxidizing contaminants such as  $\text{SO}_2$  results in electron transfer from p-type NP to electron-accepting contaminants, increasing the majority charge carrier

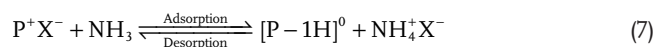
(hole) density and decreasing the barrier height<sup>[13,14,137,140,171]</sup> It increases the net conductivity and decreases the net resistance of NPs, and the interaction is Equation (5):



However, the interaction of reducing contaminants such as  $\text{NH}_3$  with p-type NPs leads to the compensation of charge carriers through transferring the protons or electrons from polymer ring to adsorbed contaminant molecules, which is given by Equations 6 and 7:<sup>[37,62,137,139,171]</sup>



and



with  $\text{X}^-$  is any dopant radical like  $\text{NO}_3^-$ ,  $\text{Cl}^-$ ,  $\text{SO}_4^-$ ,  $\text{ClO}_4^-$ .

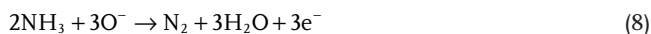
It results in a decrease in the number density of majority charge carriers and an increase in the height of the potential barrier, increasing the electrical resistance of NP in reducing contaminant environment. Thus, the resistance variation as a function of time in the contaminant environment is evaluated for sensitivity.<sup>[10]</sup> It depends upon the rate of adsorption/desorption of contaminant molecules, which is further influenced by various factors, including operational temperature, exposure time, charge carrier transport, the number density

of charge carriers, or the concentration of the contaminant molecules.

## 5.2. Sensing Mechanism in MXenes

The sensing phenomenon in MXenes majorly depends upon its electrical properties. Using DFT calculations, it has been demonstrated that MXenes can be transformed from metallic into semiconducting nature with a narrow electrical bandgap ranging from 0.05 to 1.8 eV by the surface functionalization.<sup>[53,56,70,159]</sup> Thus, the sensing behavior in MXene with reference to specific contaminants depends upon the nature of semiconducting functionalized MXene. For instance, Li et al.<sup>[101]</sup> reported p-type sensing response of  $Ti_3C_2T_x$  MXene towards reducing contaminants such as  $NH_3$ . This research demonstrated an increase in resistance of  $Ti_3C_2T_x$  MXene on interaction with  $NH_3$  molecules. Similar observations were validated by Lee et al.<sup>[76,81]</sup> for monitoring various electron-donating/reducing gases such as  $C_2H_5OH$ ,  $NH_3$ ,  $C_3H_6O$ , and  $CH_3OH$  through p-type  $Ti_3C_2T_x$  MXene (Figure 16a). The p-type nature of  $Ti_3C_2T_x$  MXene is due to adsorbed species such as oxygen and water molecules in the etching stage, resulting in acting as a p-type dopant for  $Ti_3C_2T_x$ -MXene. On interaction, the contaminant molecules are either adsorbed at active defect sites of  $Ti_3C_2T_x$  MXene or interact with surface terminals. The interaction of polar molecules with surface functional groups is due to dispersion forces like electrostatic forces resulting in slight resistance variation due to its weaker intermolecular force. Contrary, the adsorption of contaminant molecules at the surface has been anticipated to arise by replacing surface functional groups with contaminant molecules. This results in charge transfer among adsorbent sensing surface and adsorbed contaminant molecules, which causes a substantial variation in the electrical resistance of  $Ti_3C_2T_x$  MXene. The underlying sensing mechanism in p-type MXenes can be explained in terms of electron transfer from adsorbed reducing gas molecule to  $Ti_3C_2T_x$  MXene, increasing its resistance.

The electron transfer is majorly governed by the type of surface termination and can be illustrated through Equations (8 and 9):



This phenomenon results in the generation of electrons resulting in hole-electron recombination, which causes an increase in electrical resistance of  $Ti_3C_2T_x$  MXene. Contrary, Wang et al.<sup>[79,80]</sup> explained the sensing behavior of  $Nb_2CT_x$  MXene with reference to  $NH_3$  to be of n-type nature. They reported a decrease in resistance of  $Nb_2CT_x$  MXene in an  $NH_3$  environment. The charge transfer from adsorbed contaminant molecules to  $Nb_2CT_x$  increases its majority charge carrier concentration, causing a reduction in the electrical resistance of  $Nb_2CT_x$ -MXene. Hence, the electrical nature of MXene determines its sensing mechanism towards specific air contaminants.

## 5.3. Sensing Mechanism in MXene–Polymer HNCs

The sensing mechanism in inorganic–organic nanocomposite systems, as discussed in various reports, is due to the formation of various heterointerfaces among the precursors.<sup>[10,13,37,48,172]</sup> The nature of newly formed heterointerfaces such as p–p type or p–n type junctions among the precursors determines the sensing characteristics of HNCs. The features of heterojunctions depend upon the nature of precursors involved in the making of HNC. It is observed that the electrical nature of MXenes can be varied from metallic to semiconducting range, contingent on the nature of “M” element, “X” type, and surface functional groups.<sup>[59,70,101]</sup> Moreover, the addition of polymers into MXene leads to the semiconducting nature of MXP HNCs.<sup>[68,131]</sup> Nevertheless, the shift in the magnitude of electrical response of MXP HNCs is governed by the properties and stoichiometry of precursors. As a result, the air contaminants sensing mechanism associated with MXP HNCs-based sensor primarily depends on the nature of heterointerface (p–n or p–p type) among its precursors and is secondarily governed by weak chemical interactions. These chemical interactions, including hydrogen bonding, chemisorption, and the formation of unique heterointerfaces, are typical in all kinds of MXP HNCs.<sup>[10]</sup> These four predominant interactions contribute to the net air contaminant sensing phenomenon in MXP HNCs.

### 5.3.1. Primary Sensing Phenomena in MXene–Polymer HNCs

The physisorption of gaseous molecules predominantly governs the sensing behavior of MXP HNCs over the HNCs surface.<sup>[10]</sup> However, the electrical nature of MXene and polymer plays a significant role in determining its sensing behavior with reference to specific air contaminants. The electrical resistance of MXP HNCs either increases or decreases depending upon the nature of the contaminant (oxidizing or reducing), the dominance of either of precursors (MXene or polymer), and the nature of heterojunctions (p–n or p–p type) formed between them. These three factors together determine the sensing phenomena in MXP HNCs. For instance, the electrical resistance of  $Ti_3C_2T_x$ /PEDOT:PSS HNC was observed to decrease in the presence of  $NH_3$ .<sup>[130]</sup> It has been linked to the incorporation of  $Ti_3C_2T_x$  in PEDOT:PSS resulting in improved  $\pi$ – $\pi$  interaction, enhanced effective absorption area, and enriched majority charge carriers. It results in a direct charge carrier transfer among HNC and  $NH_3$ , leading to a decrease in the net electrical resistance of HNC.<sup>[85,130]</sup> However, the available report lacks enough scientific support and requires well-planned experimentations to generate evidence-based knowledge.

Contrary, Li et al.<sup>[101]</sup> revealed an increment in PAN/ $Ti_3C_2T_x$  HNC’s electrical resistance in an  $NH_3$  environment that is attributed to the dominance of PAN over  $Ti_3C_2T_x$ , and the presence of Schottky-type heterojunctions among them. A p-type PAN’s work function was slightly larger compared to that of p-type  $Ti_3C_2T_x$  resulting in the creation of miniature Schottky junctions at the precursor’s interfaces. It leads to the formation of a hole depletion region in PAN. On the interaction with electron-donating  $NH_3$ , the hole depletion layer’s width decreases, resulting in narrower conducting channels for charge carriers

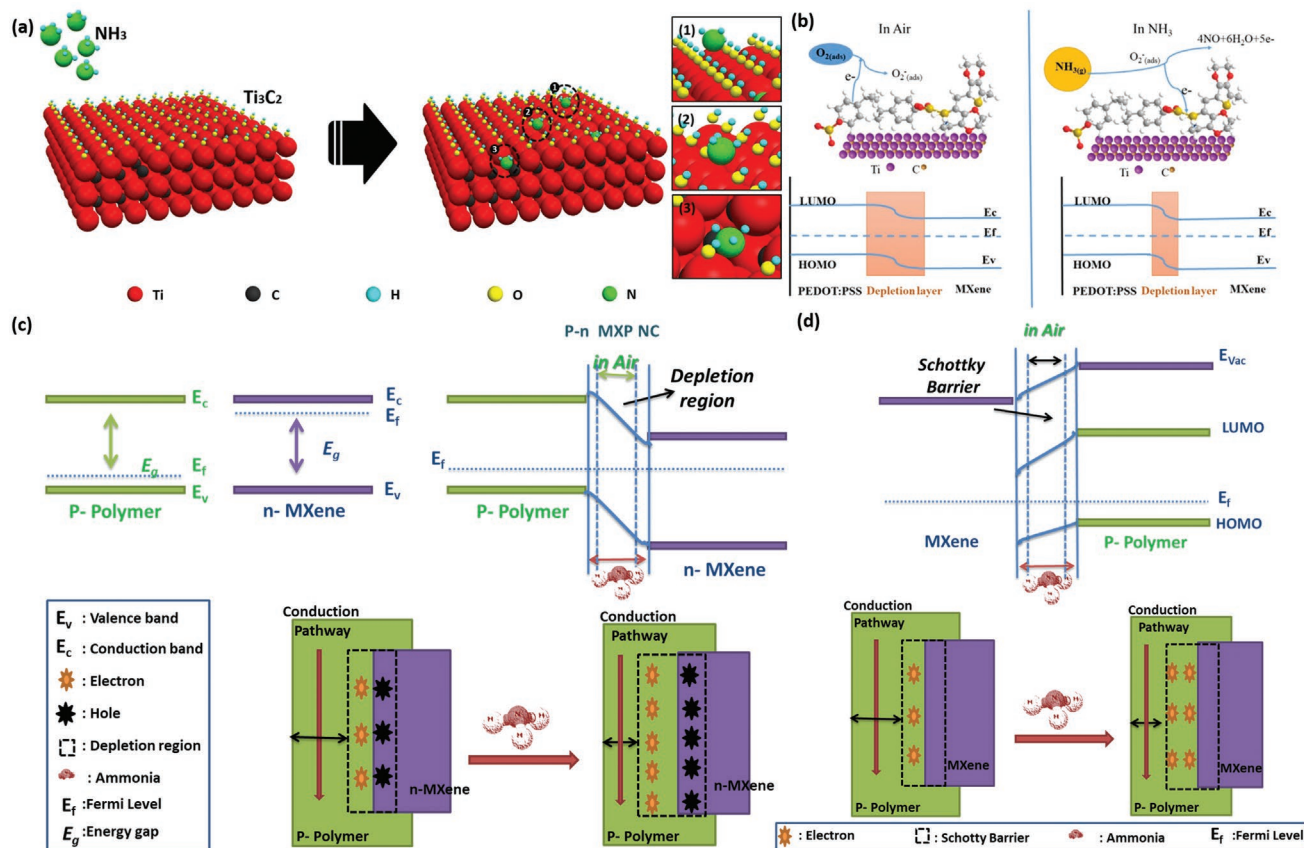


**Figure 16.** a) Various interactions among  $\text{Ti}_3\text{C}_2\text{Tx}$  MXene and reducing contaminants contributing to its gas sensing mechanism, Reproduced with permission.<sup>[76,81]</sup> Copyright 2017, American Chemical Society. b,c) Sensing mechanism in p-p type and p-n type semiconducting MXP NCs. Reproduced with permission.<sup>[10]</sup> Copyright 2021, Multidisciplinary Digital Publishing Institute. d) Chemisorption of  $\text{NH}_3$  over PEDOT:PSS-MXene HNC. Reproduced with permission.<sup>[130]</sup> Copyright 2020, American Chemical Society.

transport through PAN during sensing process. It surges the net electrical resistance of HNC on interaction with  $\text{NH}_3$  molecules. Zhao et al.<sup>[173]</sup> confirmed similar observations for  $\text{Ti}_3\text{C}_2\text{Tx}$ /CPAM-based  $\text{NH}_3$  chemiresistor. Hence, the associated sensing phenomenon for p-p type semiconducting MXP HNCs is determined via exploring synergistic effects due to creation of heterojunctions of Schottky type and predominance of either of precursors<sup>[174]</sup> (Figure 16c).

Similar observations were reported by Zhou et al.<sup>[175]</sup> for  $\text{CO}_2$  detection using a ternary HNC of polyethyleneimine (PEI), nitrogen-doped  $\text{Ti}_3\text{C}_2\text{Tx}$ -MXene (N-MXene), and rGO. All three precursors play a significant role during the sensing mechanism in such ternary HNC. However, the predominance of one of the precursors determines the exact nature of sensing phenomena. They reported that PEI dominates the sensing mechanism in their studies.<sup>[175]</sup> However, N-MXene and rGO played significant roles owing to their hydrophilic nature and excellent conductivity during the sensing process. Nevertheless, in detecting VOCs, MXene is observed to dominate in HNCs, which determines the nature of the sensing mechanism.

In contrast, Wang et al.<sup>[80]</sup> reported the dominance of p-type PAN precursor over n-type  $\text{Nb}_2\text{CT}_x$ -MXene during  $\text{NH}_3$  monitoring through p-n semiconducting MXP HNCs. The creation of p-n heterojunctions at the MXene-PAN interface was

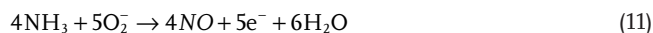
speculated, resulting in barrier layer formation among them. On interaction with  $\text{NH}_3$ , the hole concentration of PAN decreases, resulting in augmentation of the depletion region's width toward the PAN side, which increases the resistance of HNC in  $\text{NH}_3$  environment. There is a similar sensing mechanism for various p-n type semiconducting organic-inorganic HNCs<sup>[13,172,176]</sup> (Figure 16d). Hence, the predominance of either of the precursors in MXP, their concentration, and the nature of contaminant molecules determine its sensing mechanism.

### 5.3.2. Secondary Sensing Phenomenon in MXene-Polymer HNCs

**Chemisorption:** The most conventional sensing mechanism observed in various materials, such as metal oxides, is the adsorption of environmental oxygen molecules.<sup>[45]</sup> In the ambient environment, the p-type semiconducting MXP HNC surface adsorbs environmental oxygen molecules and transforms them into oxygen radicals by trapping the conduction band electrons of HNCs.<sup>[63]</sup> It results in the creation of an electron depletion region of large electrical resistance between precursors. On interaction with adsorbed reducing contaminant molecules such as  $\text{NH}_3$ , trapped electrons are released again to the HNC's conduction band.<sup>[37]</sup> It results in a variation of space



charge region in the HNC's conduction band that reduces its electrical resistance. Jin et al.<sup>[130]</sup> reported similar observations for Ti<sub>3</sub>C<sub>2</sub>T<sub>x</sub>/PEDOT: PSS HNC for monitoring NH<sub>3</sub> (Figure 16b) and summarized the entire chemisorption process through Equations (10 and 11):



Nevertheless, chemisorption is inadequate at room temperature due to significantly less transformation of oxygen molecules into oxygen radicals. As a result, the role of chemisorption in the net sensing phenomenon is minimal at room temperature.

*Formation of Hydrogen Bonds and Unique Heterointerfacial Functional Groups:* Numerous theoretical and experimental outcomes have predicted the formation of intermolecular hydrogen bonds and unique heterointerfacial functional groups among precursors during the synthesis of MXP NCs.<sup>[46,53]</sup> The existence of unique heterointerfacial functional terminals over the HNC surface transforms the electric nature of MXene from conducting to the semiconducting range.<sup>[70]</sup> These unique functionalities are further reported to felicitate interfacial charge transfer during interaction with contaminant molecules enhancing the monitoring performance of HNCs. Wang et al.<sup>[79,80]</sup> reported similar reasoning associated with enhanced NH<sub>3</sub> sensing performance of fabricated Nb<sub>2</sub>CT<sub>x</sub>/PAN and Nb<sub>2</sub>CT<sub>x</sub>/PAN-TENG-based chemiresistors. Similarly, the formation of intermolecular hydrogen bonds reduces the water adsorption sites on the HNC surface by occupying many hydrophilic surface functionalities. It felicitates the sensitive and selective monitoring of specific contaminants by reducing the impact of humidity on its sensing performance.

Kim et al.<sup>[77]</sup> explained the sensing mechanism in MXP HNCs for detecting various VOCs through its hydrogen bonding capabilities due to the presence of surface functionalities. Yuan et al.<sup>[8]</sup> reported that resistance of MXP HNC increases in the presence of all used VOCs regardless of their electrical nature. It is attributed to the dominance of MXene in MXP HNC due to its excellent conductivity. Yuan et al.<sup>[8]</sup> also suggested a selectivity mechanism in MXP NCs towards VOCs in terms of their hydrogen bonding capabilities with extra electronegative atoms like O<sub>2</sub> atoms and the electrostatic interactions with MXene. As a result, VOCs such as alcohols and ketones are easily detectable through MXP HNCs. However, monitoring polar and non-polar VOCs with very few or negligible hydrogen-bonding capacities becomes difficult using a similar sensing mechanism.

## 6. Air Contaminant Monitoring Performance of MXP HNCs

MXene is a growing family of metal nitrides/carbides layers arranged in 2-D architecture.<sup>[102]</sup> They are further classified based on the number of layers present in their 2-D lamellar layered structure. Various MXenes like Ti<sub>3</sub>C<sub>2</sub>T<sub>x</sub>, Ti<sub>2</sub>CT<sub>x</sub>, Ti<sub>4</sub>N<sub>3</sub>,

Nb<sub>4</sub>C<sub>3</sub>T<sub>x</sub>, Nb<sub>2</sub>CT<sub>x</sub>, V<sub>2</sub>CT<sub>x</sub>, Ta<sub>4</sub>C<sub>3</sub>T<sub>x</sub>, Mo<sub>2</sub>CT<sub>x</sub>, (Mo<sub>2</sub>Ti)C<sub>3</sub>, Zr<sub>3</sub>C<sub>2</sub>, and many others have been reported.<sup>[72]</sup> The interlayer space of MXenes can be tuned through various techniques such as intercalation, functionalization, or by inserting foreign material in between them.<sup>[177]</sup> It has been shown that the addition of a macromolecule, especially a polymer in MXP HNCs increases their interlayer separation.<sup>[10]</sup> It results in a large specific surface area with optimum porosity, favorable for air contaminant sensing applications. The MXP HNCs can be classified based on the number of layers in precursor MXene and can be denoted through expression: M<sub>n+1</sub>X<sub>n</sub>T<sub>x</sub>-P with "P" signifying precursor polymer/polymer combinations.<sup>[10]</sup> Majorly, M<sub>3</sub>X<sub>2</sub>T<sub>x</sub>-P and M<sub>2</sub>X<sub>2</sub>T<sub>x</sub>-P type MXP HNCs are reported for air contaminant detection applications to date.<sup>[46,51]</sup> It's because they're easier to make and more resistant to environmental degradation than other MXP HNC families.

The sensing performance of MXP HNC-based chemiresistors is estimated by recording a time-dependent change in their conductance (in terms of current, voltage, or resistance) in a contaminant environment at room temperature. Typically, these estimations are recorded through two strategies, including static and dynamic mode sensing.<sup>[146]</sup> In static mode, a definite concentration of a particular contaminant is added into a sensing chamber, possessing provisions to record the change in conductance and control temperature and humidity changes. The change in conductance is recorded as a function of time and function of a contaminant concentration until its saturation value. For instance, Jin et al.<sup>[130]</sup> evaluated NH<sub>3</sub> monitoring performance of Ti<sub>3</sub>C<sub>2</sub>T<sub>x</sub>/PEDOT:PSS HNC using static mode. Typically, they inserted a definite amount of NH<sub>3</sub> into the air-tight sensing chamber using a microsyringe and recorded the change in resistance of HNC using an automated digital multimeter.

In contrast, during dynamic-mode sensing, a constant flow of fixed concentration of the contaminant is sustained in the sensing chamber using a mass flow controller, and the resultant variation in conductance is recorded. For instance, Li et al.<sup>[101]</sup> estimated variation in Ti<sub>3</sub>C<sub>2</sub>T<sub>x</sub>/PAN HNC resistance in NH<sub>3</sub> environment using dynamic mode sensing. These sensing strategies are standard for estimating air contaminant monitoring performance. These estimations are typically evaluated in terms of 3S's (selectivity, stability, sensitivity). The degree of variation (S)/percentage (S%) variation in magnitude of resistance of a chemiresistor on interaction with contaminant molecules is termed as sensitivity and is represented by Equations (12 and 13):

$$S = \Delta R/R_0 \quad (12)$$

$$S\% = (\Delta R/R_0) \times 100 \quad (13)$$

here,  $\Delta R$  represents the variation in surface resistance of chemiresistor in the presence of a specific contaminant, estimated as  $(R_a - R_0)$ , where  $R_0$  represents the saturated magnitude of its resistance in the ambient environment, with  $R_a$  as the saturated magnitude of resistance on exposing to a specific air contaminant. It depends upon the nature of sensing material (morphology, topology, surface chemistries, conductivity,

bandgap, and structure), the interaction between contaminant and sensing material (affinity and multiinteractions like hydrogen bonding, physisorption, chemisorption), and the nature of contaminant (reducing and oxidizing).<sup>[43]</sup> For instance, by increasing the effective surface area of sensing material, the sensitivity of the chemiresistor can be increased due to a surge in the probability of interaction among material surface and contaminant molecules. Chaudhary et al.<sup>[14,15,140]</sup> reported a higher sensitivity value of PAN nanoneedles than other nanostructures towards SO<sub>2</sub> due to their larger surface area.

Further, a fabricated chemiresistor is expected to possess reliable and selective detection of a particular contaminant and distinguish it from other interfering contaminants. Selectivity is observed by either comparing the sensitivity of the designed chemiresistor with reference to a targeted contaminant against interfering contaminants or observing sensitivity toward specific contaminants in the manifestation of other interfering contaminants. The selectivity of chemiresistor depends upon the absorption energies, surface chemistries, and affinity of particular sensing material toward specific contaminants. For instance, Yu et al.<sup>[129]</sup> developed DFT-based theoretical calculations to reveal selective NH<sub>3</sub> detection through Ti<sub>2</sub>C-type MXene due to NH<sub>3</sub>'s high adsorption energy compared to other contaminants. Additionally, the selectivity can be achieved by distinguishing between reducing and oxidizing analytes using appropriate circuitry due to their contrary sensing mechanism.<sup>[13,62,141]</sup>

Moreover, stability is the most crucial parameter to developing commercial chemiresistor in terms of consistency and lifetime. The degradation of sensing layer material on interaction with sample gaseous molecules and environment highly affects the stability of chemiresistors.<sup>[10,15]</sup> It is measured by estimating the sensitivity of a chemiresistor as a function of time (in days or weeks) in ambient conditions. Alternatively, it is also evaluated by recording the sensitivity of the chemiresistor towards contaminant in variable relative humidity (RH). Abdulla et al.<sup>[178]</sup> showed that the water molecules present in humid surroundings on adsorption on polymer surface source the discharge of electrons. It leads to the generation of H<sub>3</sub>O<sup>+</sup> radicals, increasing the ionic conductivity of precursor polymer. While reacting with reducing contaminants like NH<sub>3</sub>, NH<sub>3</sub>·H<sub>2</sub>O, or NH<sub>4</sub>OH generation leads to proton capture from polymer, resulting in enhanced sensitivity.

It has been reported that polymer and inorganic materials like MXenes are relatively prone to degradation in a variable environment<sup>[30,58,68]</sup> Thus, the stability of pristine material-based chemiresistor is of concern and limits its practical application in terms of lifetime. However, the formation of polymer-inorganic HNCs like MXP HNCs, metal oxide-NP HNCs, and metal-NP HNCs overcomes this situation due to formation of heterojunctions among their precursors. Hence, the state-of-the-art air contaminant chemiresistors are concerned with advancing three essential "S" parameters by architecting advanced functional nanomaterials and HNCs. The subsequent sections emphasize various classes of MXP HNCs evaluated for air contaminant applications.

## 6.1. M<sub>3</sub>X<sub>2</sub>T<sub>x</sub>-P Based Chemiresistors for Air Contaminant Monitoring

### 6.1.1. Need for M<sub>3</sub>X<sub>2</sub>T<sub>x</sub>-P Based Chemiresistors

The first successfully synthesized M<sub>3</sub>X<sub>2</sub>T<sub>x</sub> MXene (Ti<sub>3</sub>C<sub>2</sub>T<sub>x</sub>) opened the enormous potential for various application sectors. However, the first theoretical contaminant sensing studies based on DFT and MD were performed on M<sub>2</sub>X<sub>2</sub>T<sub>x</sub> MXenes.<sup>[76]</sup> Conversely, the first breakthrough in contaminant monitoring through MXene was the successful practical evaluation of Ti<sub>3</sub>C<sub>2</sub>T<sub>x</sub>-based chemiresistor.<sup>[76]</sup> Such fabricated chemiresistor using drop-casting Ti<sub>3</sub>C<sub>2</sub>T<sub>x</sub> over a flexible PI substrate containing Pt-interdigitated electrodes. Recently, reported p-type semiconducting behavior of fabricated chemiresistor on adsorption of various contaminants, including NH<sub>3</sub>, C<sub>3</sub>H<sub>6</sub>O, CH<sub>3</sub>OH, and C<sub>2</sub>H<sub>5</sub>OH molecules, have been investigated and discussed well. The electron transfer from contaminant molecules to the MXene surface was found to increase its resistance. It was attributed to the dominance of -O and -OH surface functionalities of MXene. The sensor was found to possess the highest sensitivity towards NH<sub>3</sub> and theoretical LDL of 9.27 ppm toward C<sub>3</sub>H<sub>6</sub>O.

In this direction, Zhang et al.<sup>[99]</sup> predicted Ti<sub>3</sub>C<sub>2</sub>T<sub>x</sub> for effective recyclable capture of indoor formaldehyde (HCHO) using MD and DFT calculations. They predicted that the adsorption energy of HCHO to be 0.3 eV for single-molecule adsorption and 0.45 eV for monolayer coverage. Subsequently, Kim et al.<sup>[77]</sup> reported Ti<sub>3</sub>C<sub>2</sub>T<sub>x</sub> based metallic chemiresistor with an extraordinarily large signal-to-noise ratio to monitor various VOCs. The fabricated sensor possessed significant LDL towards VOCs (50–100 ppb) compared to conventional semiconducting chemiresistors. It was attributed to the complete termination of surface functionalities and excellent metallic conductivity of MXene. The experimental results were supported by DFT calculations, where Kim et al.<sup>[77]</sup> analyzed the contribution of surface functionalities on contaminant monitoring performance of Ti<sub>3</sub>C<sub>2</sub>T<sub>x</sub>. They confirmed their experimental results by estimating higher binding energies of NH<sub>3</sub> and C<sub>3</sub>H<sub>6</sub>O compared to that of other 2D materials (**Figure 17**).

This raised the need to develop advanced architectures of MXenes-based air contaminant chemiresistors by optimizing their structure, functionalization, and synthesis parameters. Hajian et al.<sup>[179]</sup> theoretically explored the effect of variation in -F groups present over Ti<sub>3</sub>C<sub>2</sub>T<sub>x</sub> MXene surface on its NH<sub>3</sub> detection performance. They evaluated Ti<sub>3</sub>C<sub>2</sub>T<sub>x</sub> MXene for two different fluorine ratios, including Ti<sub>3</sub>C<sub>2</sub>(OH)<sub>0.44</sub>F<sub>0.88</sub>O<sub>0.66</sub> and Ti<sub>3</sub>C<sub>2</sub>(OH)<sub>0.66</sub>F<sub>0.22</sub>O<sub>0.11</sub>, and proposed that lower -F ratio MXene showed better NH<sub>3</sub> adsorption. This was ascribed to smaller charge transfer among -F and NH<sub>3</sub> than other surface functionalities. This was followed by an experimental study performed by Yang et al.,<sup>[180]</sup> which proposed that the increment in surface O/F ratio and intercalation due to sodium ion enhances the sensing performance of Ti<sub>3</sub>C<sub>2</sub>T<sub>x</sub>. They intercalated synthesized Ti<sub>3</sub>C<sub>2</sub>T<sub>x</sub> using NaOH under constant magnetic stir at room temperature up to 2 h. This alkali-ion intercalated-MXene was found to show highly selective and two-fold enhanced sensitivity (28.87% at 200 ppm) toward NH<sub>3</sub> compared to that of pristine Ti<sub>3</sub>C<sub>2</sub>T<sub>x</sub>. It was attributed to alkali ion intercalation,

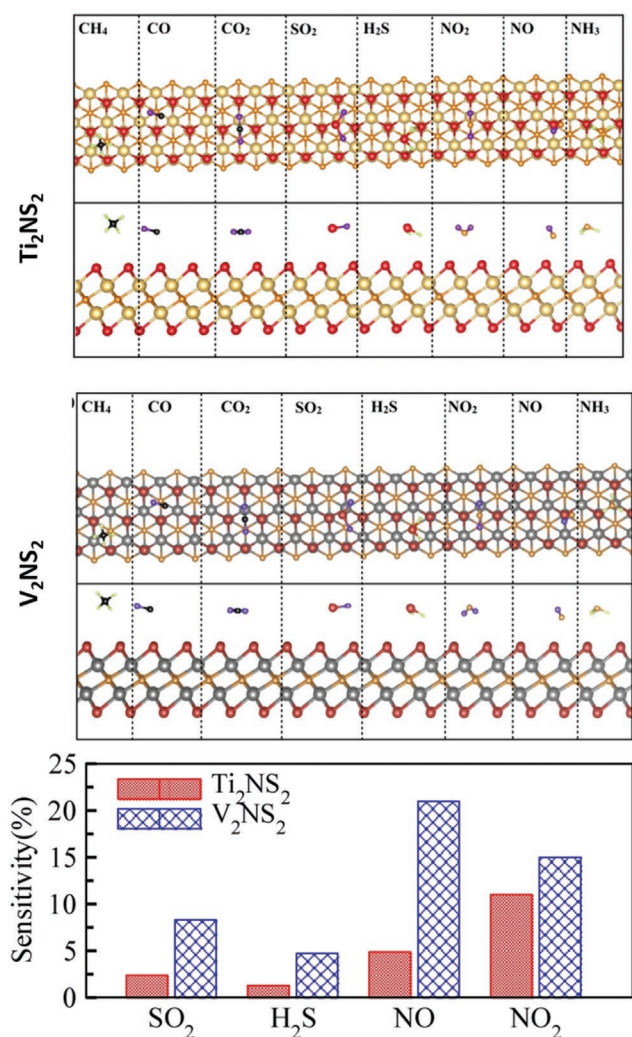


**Figure 17.** Schematic illustration of interaction of various air contaminant molecules with  $\text{Ti}_2\text{NS}_2$  and  $\text{V}_2\text{NS}_2$  MXenes revealing their gas sensing mechanism along with augmented formations and sensing response for various gaseous analytes on  $\text{V}_2\text{NS}_2$  and  $\text{Ti}_2\text{NS}_2$  MXenes. Reproduced with permission.<sup>[66]</sup> Copyright 2020, Elsevier.

which surges the surface oxygen-fluorine ratio resulting in better  $\text{NH}_3$  sensitivity. Other strategies to improve the surface oxygen-fluorine ratio were predicted by Khaledialidusti et al.,<sup>[181]</sup> which demonstrated the architecting of double transition metal MXenes. They examined surface-modified  $\text{Mo}_2\text{TiC}_2\text{T}_x$  for  $\text{CO}_2$  capture and revealed that specific functional group modified MXenes are more significant in  $\text{CO}_2$  capture than pristine MXene due to defect formation.

Further enhancement in MXene monitoring performance was reported by Koh et al.<sup>[182]</sup> experimentally and explained the effect of interlayer swelling of  $\text{Ti}_3\text{C}_2\text{T}_x$  on its contaminant sensing performance. Using a vacuum-assisted filtration strategy, this group fabricated a continuous film of  $\text{Ti}_3\text{C}_2\text{T}_x$  on anodized aluminum oxide (AAO) filter and moved it onto  $\text{SiO}_2/\text{Si}$  substrate. Subsequently, they performed intercalation by  $\text{NaOH}$  and deionized water, leading to the occupation of the interlayer space by  $\text{H}_2\text{O}$  molecules and alkali metal ions. The

interlayer spacing of intercalated  $\text{Ti}_3\text{C}_2\text{T}_x$  (4.3 Å) decreased by 0.84 Å on nitrogen purging.

However, interlayer spacing was found to increase on purging with  $\text{C}_2\text{H}_5\text{OH}$ , and there was no impact observed on  $\text{CO}_2$  purging. The degree of interlayer swelling was reported to correspond well with sensitivity towards contaminants.<sup>[182]</sup> It possessed the largest gas selectivity towards  $\text{C}_2\text{H}_5\text{OH}$  compared to other VOCs. Hence, the increase of interlayer distance and modifications in surface functionalities highly impacted air contaminants' selective and sensitive detection through MXenes. The typical outcome of all theoretical studies also indicated strong adsorption energies of air contaminants toward pristine MXenes, which resulted in their slow and incomplete recovery as observed experimentally.<sup>[53]</sup> Hence, optimizing adsorption energy is also crucial for the practical development of MXenes for contaminant monitoring. This suggested that the inclusion of foreign materials such as polymers in the form of HNCs may increase its interlayer spacing and modify the surface chemistries favorable to contaminant monitoring performances.

### 6.1.2. Vapor Monitoring Performance

Various DFT and MD studies predicted MXP HNCs to possess a specific affinity for VOCs depending upon the theory of adsorption energies.<sup>[46]</sup> It is attributed to the existence of multi interactions among surface terminals of MXP HNCs and specific contaminant molecules. Yuan et al.<sup>[8]</sup> fabricated a 3D MXP framework (3D-M) of  $\text{Ti}_3\text{C}_2\text{T}_x$ , PEI, and PVA (3TPP) and tested it for monitoring several VOCs, including  $\text{CH}_3\text{OH}$ ,  $\text{C}_2\text{H}_5\text{OH}$ , and  $\text{C}_3\text{H}_6\text{O}$ . MXene functionalized the surface of the 3D polymer framework through self-assembly due to electrostatic interactions among positively charged PEI components of the polymer framework and negatively charged MXene surface functionalities (Figure 18).

The 3D framework exhibited extremely porous interconnected morphology with a high specific surface area resulting in excellent sensitivity toward low ppb level ( $\approx 50$  ppb) of VOCs ( $\text{C}_3\text{H}_6\text{O}$ ,  $\text{CH}_3\text{OH}$ , and  $\text{C}_2\text{H}_5\text{OH}$ ). However, 3TPP chemiresistor showed negligible sensitivity toward hydrocarbons (cyclohexane and  $\text{C}_7\text{H}_8$ ) and very low sensitivity toward polar inorganic contaminants ( $\text{NH}_3$  and  $\text{NO}_x$ ). The surface functionalities on 3TPP surface ( $-\text{OH}$  and  $-\text{F}$ ) form H-bonds with VOCs and polar inorganic contaminants resulting in charge transfer. The magnitude of sensitivity was dependent on the strength of H-bonding among the contaminants and sensor surfaces.

The intriguing finding was that chemiresistor resistance increased regardless of the type of contaminated environment encountered. It was due to the dominance of metallic MXene during sensing phenomena. The reported chemiresistor possess a good detection range for  $\text{C}_3\text{H}_6\text{O}$  (50 ppb –  $3 \times 10^5$  ppm),  $\text{C}_2\text{H}_5\text{OH}$  (50 ppb –  $8 \times 10^4$  ppm), and  $\text{CH}_3\text{OH}$  (50 ppb –  $1.5 \times 10^5$  ppm), with the largest sensitivity toward  $\text{CH}_3\text{OH}$ . The chemiresistor was highly flexible as tested for 1000 bending cycles and works at room temperature. Interestingly, the sensitivity of MXene based 3TPP chemiresistor was found manifold higher than the widely used rGO based 3D polymer framework, especially for  $\text{C}_3\text{H}_6\text{O}$ ,  $\text{C}_2\text{H}_5\text{OH}$ , and  $\text{CH}_3\text{OH}$ .

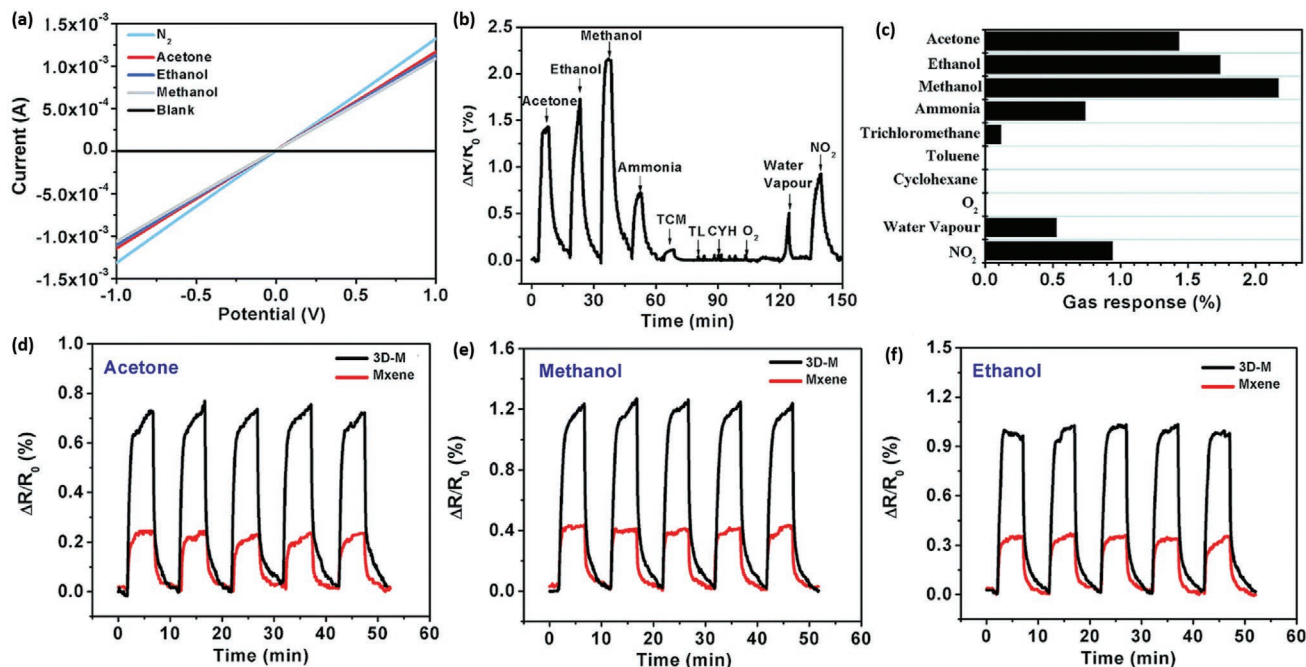


**Figure 18.** a) Variation in  $I$ - $V$  characteristics of 3TTP based chemiresistor on interacting with pure nitrogen,  $C_3H_6O$ ,  $CH_3OH$ , and  $C_2H_5OH$ . b) Sensitivity of 3TTP based chemiresistor in presence of different organic and inorganic VOCs and gases. c) Maximum sensitivity of 3TTP based chemiresistor toward different vapors. Sensitivity of MXene and 3TTP based chemiresistor for five successive exposure cycles of 5 ppm of d)  $C_3H_6O$ , e)  $CH_3OH$ , and f)  $C_2H_5OH$ . Reproduced with permission.<sup>[8]</sup> Copyright 2018, Royal Society of Chemistry.

The  $O_2$  terminations on the edge and basal plane of rGO are quite limited than that on MXene, which reduces the interaction between rGO and VOCs. The vicinity of oxygen terminals also favors the formation of hydrogen bonding among rGO and VOCs, limiting its recovery and sensitivity. However, the major bottleneck related to the 3TTP chemiresistor was their slower response and recovery time (in minutes).

Further, Zhao et al.<sup>[100]</sup> evaluated  $Ti_3C_2T_x$ -PAN synthesized at a very low temperature (0–5 °C) to monitor various VOCs. The low-temperature fabrication was reported to be advanced in terms of high yield and lesser damage to the  $Ti_3C_2T_x$  structure. The flexibility of chemiresistor was achieved using depositing a layer of synthesized  $Ti_3C_2T_x$ -PAN HNC over PET substrate. The HNC was revealed to possess fine accordion-like morphology, which is anticipated to form significant mass-transport pathways for rapid VOC diffusion, resulting in a prompt response at room temperature. The sensing performance was evaluated by recording variation in chemiresistor current in the presence of a contaminant environment. The chemiresistor was highly selective toward  $C_2H_5OH$  with sensitivity (1.56% at 1 ppm) compared to  $CH_3OH$ ,  $C_3H_6O$ , and  $NH_3$  ( $\approx 20\%$  for 200 ppm of  $CH_3OH$ ,  $C_3H_6O$ , and  $NH_3$ ). The chemiresistor was found to possess a good detection range (1–200 ppm), repeatable (140 cycles), rapid ( $\approx 0.5$  s as response and recovery time), and works at room temperature. The flexibility was significant as tested for various bend angles between (0–120)°. Researchers utilized DFT theory to evaluate the microscopic nature of recorded superior sensitivity and selectivity. It was performed by estimating contaminants' adsorption energy and bond length over the surface of OH-terminated  $Ti_3C_2T_x$ , O-terminated  $Ti_3C_2T_x$ , and F-terminated  $Ti_3C_2T_x$ , respectively. The OH-terminated

$Ti_3C_2T_x$  exhibited the smallest bond length and highest binding energies for  $C_2H_5OH$  compared to other contaminants, other terminated MXenes, and pristine precursors. It proposes highly selective, sensitive, and rapid detection of  $C_2H_5OH$  by OH-terminated  $Ti_3C_2T_x$ -PANI HNCs at room temperature. However, the studies related to stability were not incorporated, which can be further done for its practical applications.

Wang et al.<sup>[183]</sup> reported fabrication of a selective  $CH_3OH$  chemiresistor of  $Ti_3C_2T_x$ /PEDOT:PSS HNC using an ex situ route. This group studied the effect of precursor concentration and dominance over VOC monitoring by varying the PEDOT:PSS/ $Ti_3C_2T_x$  mass ratio in HNC, specifically of 10:1, 8:1, 4:1, 2:1, 1:1, and 1:2. It was investigated that the chemiresistor with the mass ratio 4:1 exhibited the utmost sensitivity for 300 ppm of VOCs. The variation in sensitivity with a concentration of MXene is due to the variable sensing mechanism for various chemiresistors. It is attributed to the predominance of particular precursor and variation in conductivity of HNC with change in MXene concentration. For instance, pristine PEDOT:PSS based chemiresistor exhibited p-type sensing behavior due to swelling, diffusion, and charge transfer, increasing its resistance in a contaminant environment.<sup>[183]</sup> The chemiresistor with mass ratios 10:1 and 8:1 also exhibited the same behavior due to the dominance of polymer precursors. However, the sensitivity for 10:1 and 8:1 HNC chemiresistors was less than that of the pristine polymer due to inclusion of MXene, resulting in less swelling of the polymer matrix. They proposed three conductive pathways in HNCs, including polymer–polymer, MXene–MXene, and polymer–MXene connections contributing to sensing phenomena. The highest sensitivity observed for 4:1 HNC was attributed to eliminating

the MXene–MXene connection due to PEDOT:PSS's presence among MXene layers. However, in other chemiresistors (2:1, 1:1, 1:2), the MXene–MXene connections were predominant, resulting in increased conductivity and reduced sensitivity. In addition, the response and recovery time were large compared to that of conventional sensors.<sup>[183]</sup> However, the 4:1 chemiresistor was found to be highly selective for CH<sub>3</sub>OH monitoring.

Other reports focused on M<sub>3</sub>X<sub>2</sub>T<sub>x</sub>–MXene hybrids with other materials, including graphene-based materials, metal oxides, and metal dichalcogenides for VOCs monitoring, have also been published.<sup>[53,184,185]</sup> However, the drawbacks associated with them have already been discussed in Section 2. The comparison among pristine MXenes, pristine polymers, MXP HNCs, and other hybrids of MXene and polymers-based VOC monitoring performance has been made in Table 4.

It is evident from Table 4 that M<sub>3</sub>X<sub>2</sub>T<sub>x</sub>-P exhibits enhanced sensing performance towards VOCs compared to their precursors and other hybrid materials and M<sub>4</sub>X<sub>3</sub>T<sub>x</sub>.<sup>[189]</sup> All the authors attributed the higher sensitivity of M<sub>3</sub>X<sub>2</sub>T<sub>x</sub>-P HNCs based chemiresistors toward VOCs to their excellent conductivity due to dominance of MXene, increasing the possibility of transfer of charge among VOC molecules and sensing material's surface. It increases the surface resistance of chemiresistors in the presence of every VOC, irrespective of their chemical nature. Moreover, all the reported M<sub>3</sub>X<sub>2</sub>T<sub>x</sub>-P HNCs based chemiresistors operate at room temperature, unlike conventional commercial sensors, which adds to a sustainable prospect in terms of energy consumption.

### 6.1.3. Gas Monitoring Performance

The slower response and incomplete recovery of MXene based chemiresistor to detect gaseous air contaminants, including NH<sub>3</sub>, NO<sub>x</sub>, SO<sub>2</sub>, CH<sub>4</sub>, and CO<sub>x</sub>, resulted in the quest to evaluate MXene hybrids as sensing materials.<sup>[53]</sup> However, most reports are dedicated to monitoring NH<sub>3</sub> through MXene hybrids, including MXP HNCs. Various DFT and MD studies have revealed that the MXenes and polymers possess a special affinity towards NH<sub>3</sub> in terms of adsorption energies, binding energies, and bond length.<sup>[53]</sup> Similar observations have been recorded for MXP HNCs, projecting them as a superior sensing material due to precursors' affinity and enhanced surface functionalities. Yuan et al.<sup>[8]</sup> evaluated 3TTP chemiresistor to detect gaseous air contaminants, including NH<sub>3</sub> and NO<sub>2</sub>, along with VOCs. The sensitivity of fabricated chemiresistor towards NH<sub>3</sub> (0.7% @ 10 ppm) and NO<sub>2</sub> (0.9% @ 10 ppm) was low compared to VOCs. Hence, the fabricated sensor exhibited high selectivity toward VOCs and was not further evaluated for gaseous contaminants. The reported selectivity was ascribed to the strength of H-bonding and interaction among air contaminants molecules and chemiresistor surface functionalities.

Zhao et al.<sup>[173]</sup> reported a flexible cross-linked CPAM/Ti<sub>3</sub>C<sub>2</sub>T<sub>x</sub> (CPAM-T<sub>x</sub>) HNCs for highly selective, sensitive, and rapid NH<sub>3</sub> detection. The interlayer spacing in HNC was estimated to be increased using spectroscopic outcomes compared to its pristine precursor, which is favorable during gas sensing. This group evaluated the *I*–*V* characteristics of fabricated chemiresistor in different contaminant environments. The estimated

sensitivity using signal-to-noise ratio of CPAM-T<sub>x</sub>-chemiresistor was threefold superior, with rapid response/recovery within 12.7/14.6 s than that of pristine precursor (14.2/19.5 s). The sensor was found to be repeatable for 10 consecutive cycles of contaminant exposure with rapid detection in low response and recovery time. The fabricated chemiresistor demonstrated excellent mechanical flexibility retaining its sensitivity as 45% for various bending angles (0 to 100) and bending cycles (three cycles), which was missing in pristine precursor-based devices. It is attributed to the gluing of Ti<sub>3</sub>C<sub>2</sub>T<sub>x</sub> stacks by CPAM, resulting in stronger bonding among precursors. The CPAM forms H-bonds with NH<sub>3</sub> enhancing NH<sub>3</sub> adsorption capacity in HNC, resulting in superior sensitivity. This group also reported an increment in relative humidity, which initially enhanced the NH<sub>3</sub> sensitivity of CPAM-T<sub>x</sub> (till 45% RH) and afterward decreased with RH rise.<sup>[173]</sup> It was ascribed to the blockage of NH<sub>3</sub> adsorption due to accumulation of water molecules layer over chemiresistor surface. The interaction of accumulated water molecules with the surface decreases the chemiresistor baseline resistance, which causes a decrease in sensitivity.

Li et al.<sup>[101]</sup> reported a similar type of observations in case of variation in sensitivity with RH estimated using PAN/Ti<sub>3</sub>C<sub>2</sub>T<sub>x</sub> chemiresistor. This research investigated the threshold value of RH as 40% RH, up to which sensitivity was found to be increased and afterward decreased. It is noteworthy that the chemiresistor exhibited LDL of 25 ppb, which is much lower compared to reported for pristine precursors and other hybrids reported so far in the literature. Moreover, the observed response was repeatable and sustainable, up to 88% of the initial response on the 35<sup>th</sup> day. Additionally, such fabricated chemiresistor exhibited excellent flexibility with negligible descent in sensing features on subjecting to different bending times (100, 300, and 500 times) and bending angles (20°, 30°, and 40°). Fascinatingly, their agricultural simulation experiment proved the practical viability of fabricated chemiresistor for accurate, human resource free, rapid, field-deployable, real-time, and intelligent agricultural operation. The LDL with significant sensitivity of fabricated chemiresistor (0.05% @ 25 ppb) was found to be significantly superior to that of reported systems based on pristine PAN (5 ppm), PNA-CeO<sub>2</sub> (10 ppm), PAN/Pd (10 ppm), PAN-TiO<sub>2</sub>-Au (10 ppm), PAN-GO (500 ppb), PAN-WS<sub>2</sub> (50 ppm), pristine Ti<sub>3</sub>C<sub>2</sub>T<sub>x</sub> (500 ppm), alkalinized Ti<sub>3</sub>C<sub>2</sub>T<sub>x</sub> (10 ppm), and TiO<sub>2</sub>/Ti<sub>3</sub>C<sub>2</sub>T<sub>x</sub> (2 ppm).<sup>[101]</sup>

On the contrary, Jin et al.<sup>[130]</sup> reported a negligible descent in NH<sub>3</sub> sensitivity of Ti<sub>3</sub>C<sub>2</sub>T<sub>x</sub>/PEDOT:PSS chemiresistor in varying humidity environments (RH: 20–90%). They reported an increment in NH<sub>3</sub> sensitivity with a surge in humidity and attributed it to enhanced charge carrier transfer due to a reduction in the average distance among accumulated water molecules. Moreover, they observed an increase in interlamellar spacing (*d*-spacing) of MXene sheets due to introduction of PEDOT:PSS in HNC using spectroscopic (XRD) and morphological (SEM) outcomes. The sensing performance of Ti<sub>3</sub>C<sub>2</sub>T<sub>x</sub>/PEDOT:PSS chemiresistor (9.6% @10 ppm with 116/40 s as response/recovery time) at room temperature is observed to be superior than pristine PAN (7.1% @ 92 ppm), graphene-PEDOT:PSS (0.9% @ 5 ppm), Pf-MWCNT/PANI (0.015% @ 20 ppm), CuTSPc@3D-(N)GF/PEDOTPSS (8% @ 50 ppm),

**Table 4.** Comparison of VOC monitoring performance of various sensing materials based on  $M_3X_2T_x$ -MXene and its hybrids at room temperature with different sensing parameters, including sensitivity, LDL, recovery and response period, and flexibility.

Sensing material	VOC	Sensitivity [%]	Concentration	Recovery/response time	LDL	Flexibility
$Ti_3C_2T_x$ <sup>[76]</sup>	C <sub>2</sub> H <sub>5</sub> OH	11.5	100 ppm	NR	100 ppm	NR
	C <sub>3</sub> H <sub>6</sub> O	7.5	100 ppm	≈4–6 min	9.27 ppm	NR
	CH <sub>3</sub> OH	14.3	100 ppm	NR	100 ppm	NR
Metallic $Ti_3C_2T_x$ <sup>[77]</sup>	C <sub>3</sub> H <sub>6</sub> O	0.97	100 ppm	≈5 min/10 min	50 ppb	NR
	C <sub>2</sub> H <sub>5</sub> OH	1.7	100 ppm	≈5 min/10 min	100 ppb	NR
	Propanol	0.88	100 ppm	≈5 min/10 min	100 ppb	NR
Graphite- $Ti_3C_2T_x$ <sup>[78]</sup>	C <sub>2</sub> H <sub>5</sub> OH	0.13	100 ppm	NR	NR	NR
	C <sub>3</sub> H <sub>6</sub> O	0.20	100 ppm	NR	NR	NR
TiC- $Ti_3C_2T_x$ <sup>[78]</sup>	C <sub>2</sub> H <sub>5</sub> OH	0.16	100 ppm	NR	NR	NR
	C <sub>3</sub> H <sub>6</sub> O	0.23	100 ppm	NR	NR	NR
Lampblack- $Ti_3C_2T_x$ <sup>[78]</sup>	C <sub>2</sub> H <sub>5</sub> OH	0.11	100 ppm	NR	NR	NR
	C <sub>3</sub> H <sub>6</sub> O	0.15	100 ppm	NR	NR	NR
Alkalized organ-like MXene <sup>[180]</sup>	C <sub>2</sub> H <sub>5</sub> OH	2	100 ppm	NR	NR	NR
	Acetaldehyde	3	100 ppm	NR	NR	NR
	HCHO	5	100 ppm	NR	NR	NR
	CH <sub>3</sub> OH	2	100 ppm	NR	NR	NR
Na <sup>+</sup> intercalated $Ti_3C_2T_x$ <sup>[182]</sup>	C <sub>2</sub> H <sub>5</sub> OH	9.995	0.1%	NR	NR	NR
3TTP <sup>[8]</sup>	CH <sub>3</sub> OH	2.7%	5 ppm	≈1.5/1.7 min	50 ppb	Flexible for 1000 bending cycles
	C <sub>2</sub> H <sub>5</sub> OH	4.4%	5 ppm	≈1.5/1.7 min	50ppb	Flexible for 1000 bending cycles
	C <sub>3</sub> H <sub>6</sub> O	0.08%	5 ppm	≈1.5/1.7 min	50 ppb	2% for 20 ppm for 1000 bending and unbending cycles
$Ti_3C_2T_x$ / PEDOT:PSS(4:1) <sup>[183]</sup>	CH <sub>3</sub> OH	0.4%	180 ppm	≈250 s/500 s	180 ppm	NR
	C <sub>2</sub> H <sub>5</sub> OH	0.1%	300 ppm	≈250 s/500 s	60 ppm	NR
	C <sub>3</sub> H <sub>6</sub> O	0.09%	300 ppm	≈250 s/500 s	NR	NR
$Ti_3C_2T_x$ - PANI sensor <sup>[100]</sup>	C <sub>2</sub> H <sub>5</sub> OH	1.56%	1 ppm	0.4s/0.5 s	1 ppm	≈25–27% for 150 ppm for bending angle (0–120)°
PANI/ $Ti_3C_2T_x$ <sup>[101]</sup>	HCHO	0.2%	25 ppm	NR	NR	Flexible
PEDOT:PSS/ $Ti_3C_2T_x$ <sup>[130]</sup>	C <sub>7</sub> H <sub>8</sub>	1.2%	100 ppm	NR	NR	Flexible
	C <sub>2</sub> H <sub>5</sub> OH	4.6%	100 ppm	NR	NR	Flexible
	CH <sub>3</sub> OH	14%	100 ppm	NR	NR	Flexible
	C <sub>3</sub> H <sub>6</sub> O	3.4%	100 ppm	NR	NR	Flexible
N- $Ti_3C_2T_x$ -PEI-rGO <sup>[175]</sup>	HCHO	0.3%	40 ppm	NR	NR	NR
CPAM/ $Ti_3C_2T_x$ <sup>[173]</sup>	CH <sub>3</sub> OH	15%	2000 ppm	NR	NR	Flexible
	C <sub>2</sub> H <sub>5</sub> OH	10%	2000 ppm	NR	NR	Flexible
	C <sub>3</sub> H <sub>6</sub> O	10%	2000 ppm	NR	NR	Flexible
RGO/ $Ti_3C_2T_x$ <sup>[85]</sup>	C <sub>2</sub> H <sub>5</sub> OH	1.8%	20 ppm	NR	NR	NR
$W_{18}O_{49}$ / $Ti_3C_2T_x$ <sup>[86]</sup>	C <sub>3</sub> H <sub>6</sub> O	11.6%	20 ppm	6 s to 170 ppb	NR	NR
	HCHO	1.2%	20 ppm	NR	NR	NR
$CuO$ / $Ti_3C_2T_x$ <sup>[87]</sup>	C <sub>7</sub> H <sub>8</sub>	11.4%	50 ppm	10 s to 50 ppm	320 ppb	NR
$WSe_2$ / $Ti_3C_2T_x$ <sup>[184]</sup>	C <sub>2</sub> H <sub>5</sub> OH	9.4%	40 ppm	6.6 s to 40 ppm	NR	NR
$\alpha$ - $Fe_2O_3$ / $Ti_3C_2T_x$ <sup>[187]</sup>	C <sub>3</sub> H <sub>6</sub> O	16.6%	5 ppm	5 s	5 ppm	NR
$\alpha$ - $\gamma$ - $Fe_2O_3$ / ex- $Ti_3C_2T_x$ -MoF <sup>[188]</sup>	C <sub>3</sub> H <sub>6</sub> O	215% (@255°C)	100 ppm	13 s/8 s	100 ppm	NR

palladium/polypyrrole (0.14% @ 20 ppm), SWCNTs/PEDOT:PSS (0.1% @ 2 ppm), PEDOT nanowire (2% @ 10 ppm), PEDOT nanotube (2.1% @ 5 ppm) and GO-CuFe<sub>2</sub>O<sub>4</sub> (2.35% @ 5 ppm).<sup>[130]</sup>

It's interesting to note that the MXene precursor is the same as Ti<sub>3</sub>C<sub>2</sub>T<sub>x</sub> in all of the MXP HNCs, and the variance in sensitivity was a function of RH. This is attributed to the dominance of CP precursors (PAN and CPAM) in respective HNCs, which exhibit a specific affinity for NH<sub>3</sub> adsorption. Jin et al.<sup>[128]</sup> further investigated variation in sensitivity, response time, and recovery span with weight percentage of Ti<sub>3</sub>C<sub>2</sub>T<sub>x</sub> (0%, 8%, 11%, 15%, 25%, 100%) in HNCs (Figure 10d–f). The optimum wt% of Ti<sub>3</sub>C<sub>2</sub>T<sub>x</sub> in HNCs was found to be 15 wt%, exhibiting maximum NH<sub>3</sub> sensing response. It was reported that till 15 wt% of Ti<sub>3</sub>C<sub>2</sub>T<sub>x</sub>, the conductivity and interlayer spacing of HNC increase and decrease afterward as a function of precursor concentration. An observed superior specific surface area, large porosity, and higher probability of oxidation of HNCs in an NH<sub>3</sub> environment resulting in superior sensing performance. Hence, this research described the requirement to optimize the precursor concentration in HNCs to maximize their air contaminant sensing performance. Moreover, this investigation observed the variation of RH (20–90%) on the NH<sub>3</sub> sensing performance of HNC. They reported the increase in NH<sub>3</sub> (100 ppm) sensing performance of the HNC chemiresistor with a surge in RH magnitude. It is ascribed to NH<sub>4</sub>OH formation due to the interaction of humidity with NH<sub>3</sub> leading to variation in resistance during the exposure and removal of chemiresistor to NH<sub>3</sub>. The surge in RH reduces the average distance between the moisture molecules, which increases the possibility of interactions due to charge transfer and the resulting sensitivity.

On the other hand, Li et al.<sup>[101]</sup> explored NH<sub>3</sub> sensing performance of PAN/Ti<sub>3</sub>C<sub>2</sub>T<sub>x</sub> with varying operating temperatures in the range of 0–40 °C. In this research, no variation was observed in sensitivity with variation in operational temperature indicating the stability of fabricated chemiresistor in a variable environment. This group<sup>[101]</sup> also evaluated the sensing performance of PAN/Ti<sub>3</sub>C<sub>2</sub>T<sub>x</sub> for CO and SO<sub>2</sub> and reported significant sensitivity values of approximately 8% for 10 ppm of both the contaminants. Although the sensing characteristics were not further evaluated for these contaminants, the sensitivity values are significant in the literature.

Zhou et al.<sup>[175]</sup> reported gaseous air contaminant performance of ternary MXP HNC of N-MXene, PEI, and rGO (NTPG). They correlated it with other precursors and their hybrids, including PEI, Ti<sub>3</sub>C<sub>2</sub>T<sub>x</sub>, rGO-PEI, Ti<sub>3</sub>C<sub>2</sub>T<sub>x</sub>-PEI, N-Ti<sub>3</sub>C<sub>2</sub>T<sub>x</sub>, and Ti<sub>3</sub>C<sub>2</sub>T<sub>x</sub>-rGO. The fabricated sensor exhibited superior sensitivity (1%) toward 8 ppm of CO<sub>2</sub> compared to that toward 8 ppm of H<sub>2</sub>S (No response), SO<sub>2</sub> (0.5%), and NH<sub>3</sub> (0.18%). The recorded sensitivity was suitable for monitoring indoor CO<sub>2</sub> as CO<sub>2</sub> beyond 1000 ppm is harmful in the indoor environment. However, the authors reported optimization of working temperature and relative humidity prior to recording sensing measurements. The threshold RH was found to be 62% as pristine rGO and N-MXene exhibit a negligible change in resistance at this RH level. Additionally, the change in resistance of PEI was not measurable below 36% due to its intrinsic insulating nature. However, with the surge in RH, the conductivity of PEI increases owing to the humidity-activated proton conduction

mechanism and achieves saturation at 62% RH.<sup>[175]</sup> Hence, the operating condition was chosen to 62% RH at 20 °C. Additionally, 4 NTPG chemiresistors were architected via changing PEI's concentration (0.0025, 0.005, 0.0075, and 0.01 mg mL<sup>-1</sup>) and superior sensing performance was observed for 0.01 mg mL<sup>-1</sup>. This is due to the dominance of PEI during sensing phenomena at this concentration. This group reported no recovery on purging dry air in the sensing chamber. However, on supplying wet air with 2.1% RH into the test chamber for removal of CO<sub>2</sub>, the sensitivity increases to 9% at 600 ppm of the gas. Furthermore, a recoverable response was also optimized. This outcome is ascribed to PEI's dominant proton-hopping conduction due to moisture in the supplied air. Although PEI was dominating the sensing mechanism and all the three precursors of sensing material contributed to the overall sensing performance of HNC. The presence of rGO provides conductive pathways for rapid charge transfer, and MXene contributes to the amplification of mobility of charge carriers and PEI producing charge carriers. Moreover, the sensing performance of CO<sub>2</sub> NTPG chemiresistor (≈1% for 8 ppm at 20 °C) was better than LaFeO<sub>3</sub> (119% for 2000 ppm at 300 °C), Ca/Al@ZnO (33% for 2500 ppm at 250 °C), Ag@CuO/BaTiO<sub>3</sub> (9% for 100 ppm at 120 °C), ZnO (20% for 200 ppm at 250 °C), PEEK/MWCNTs (10.5% for 500 ppm at 25 °C), Ru@WS<sub>2</sub> (≈1.8% for 20 ppm at 25 °C), and CeO<sub>2</sub> (1–10% for 150 ppm at 100 °C).<sup>[173]</sup> However, the operation of such ternary HNCs is complex due to the simultaneous optimization of many parameters, including the concentration of precursors and operation conditions.

Recently, Qiu et al.<sup>[144]</sup> reported an accordion-like N-doped Ti<sub>3</sub>C<sub>2</sub>T<sub>x</sub>/PEDOT:PSS HNC for molecular-level detection of NH<sub>3</sub> gaseous molecule. A downward shift in XRD peak at (002) confirmed the enlarged interlayer distance in HNC due to urea treatment and inclusion of PEDOT:PSS, which is highly favorable for molecular gas transport within the HNC. The chemiresistor exhibited enhanced room temperature sensitivity (13% for 10 ppm under 36% RH) of ammonia than pristine N-MXene/PEDOT:PSS precursors. Remarkably, this research explored the origin of n-type semiconducting behavior and sensing mechanism of N-MXene through UV-vis spectroscopic outcomes. The n-type semiconducting nature of N-Ti<sub>3</sub>C<sub>2</sub>T<sub>x</sub> was ascribed to the oxidation of a few Ti-sites into n-type TiO<sub>2</sub> nanoparticles along with N-doping substitution, which provides catalysis by serving as active electron donators. Further combination of n-type N-Ti<sub>3</sub>C<sub>2</sub>T<sub>x</sub> with p-type PEDOT:PSS results in synergistic effects favoring the interaction of HNC with gaseous analytes. The sensing mechanism was similar to the p–n type interfacial phenomenon as already discussed in Section 5 in terms of the formation of the depletion region and its modulation in the presence of contaminant molecules. A detailed comparative analysis of MXP HNCs evaluated for monitoring various contaminants is brief in **Table 5**.

It is clear from the analysis of Table 5 that M<sub>3</sub>X<sub>2</sub>T<sub>x</sub>-MXene HNCs based on PAN exhibit manifold superior sensitivity towards NH<sub>3</sub> compared to that of others. It is attributed to the redox behavior, tunable conductivity, and specific affinity of PAN towards NH<sub>3</sub>. However, these chemiresistors possess a bottleneck of slow recovery due to the slow desorption of NH<sub>3</sub> molecules from their surface. It is also evident that the M<sub>3</sub>X<sub>2</sub>T<sub>x</sub>-MXene HNCs sensors are more prone to NH<sub>3</sub> than

**Table 5.** Comparative analysis of gaseous contaminant monitoring performance of MXene based HNCs and their precursors at room temperature in terms of various sensing characteristics.

Sensing material	Gaseous contaminant	Sensitivity [%]	Concentration	Recovery/response time	LDL	Flexibility
Ti <sub>3</sub> C <sub>2</sub> T <sub>x</sub> <sup>[76]</sup>	NH <sub>3</sub>	21	100 ppm	NR	100 ppm	NR
Metallic Ti <sub>3</sub> C <sub>2</sub> T <sub>x</sub> <sup>[77]</sup>	NH <sub>3</sub>	0.8	100 ppm	NR	9.27 ppm	NR
	NO <sub>2</sub>	0.25	100 ppm	NR	100 ppm	NR
	SO <sub>2</sub>	0.2	100 ppm	NR	NR	NR
	CO <sub>2</sub>	0.1	10 000 ppm	NR	NR	NR
	Graphite-Ti <sub>3</sub> C <sub>2</sub> T <sub>x</sub> <sup>[78]</sup>	NH <sub>3</sub>	0.55	5 ppm	NR	5 ppm
TiCTi <sub>3</sub> C <sub>2</sub> T <sub>x</sub> <sup>[78]</sup>	NH <sub>3</sub>	0.62	5 ppm	NR	5 ppm	NR
Lampblack-Ti <sub>3</sub> C <sub>2</sub> T <sub>x</sub> <sup>[78]</sup>	NH <sub>3</sub>	0.38	5 ppm	NR	5 ppm	NR
Alkalized organ-like MXene <sup>[180]</sup>	NH <sub>3</sub>	28.87	100 ppm	NR	NR	NR
	NO <sub>2</sub>	10	100 ppm	NR	NR	NR
	CH <sub>4</sub>	4	100 ppm	NR	NR	NR
Na <sup>+</sup> intercalated Ti <sub>3</sub> C <sub>2</sub> T <sub>x</sub> <sup>[182]</sup>	CO <sub>2</sub>	0.53	1%	NR	NR	NR
3TTP sensor <sup>[8]</sup>	NH <sub>3</sub>	0.7	10 ppm	NR	NR	Flexible
	NO <sub>2</sub>	0.9	10 ppm	NR	NR	Flexible
Ti <sub>3</sub> C <sub>2</sub> T <sub>x</sub> - PANI sensor <sup>[100]</sup>	NH <sub>3</sub>	20	200 ppm	NR	NR	Flexible
PANI/Ti <sub>3</sub> C <sub>2</sub> T <sub>x</sub> <sup>[101]</sup>	H <sub>2</sub> S	1	25 ppm	NR	NR	Flexible
	NH <sub>3</sub>	0.05	25 ppb	≈600 s/1400 s for 25 ppb	25 ppb	≈22% at 10 ppm to bending angle (20, 30, 40)° and bending for 100, 200, and 500 times
	SO <sub>2</sub>	≈0.02	25 ppm	NR	NR	Flexible
	CO	≈0.05	25 ppm	NR	NR	Flexible
	CO <sub>2</sub>	≈0.01	10%	NR	NR	Flexible
PEDOT:PSS/Ti <sub>3</sub> C <sub>2</sub> T <sub>x</sub> <sup>[130]</sup>	NH <sub>3</sub>	36.6	100 ppm	40 s/116 s for 100 ppm	10 ppm	≈33% at 100 ppm for different bending angle (60°–240°)
CPAM/Ti <sub>3</sub> C <sub>2</sub> T <sub>x</sub> <sup>[171]</sup>	NH <sub>3</sub>	1.5	50 ppm	≈12–14 s for 150 ppm		≈45% for 2000 ppm of NH <sub>3</sub> for bending angles (0–100 °C) and bending cycles (3)
NTPG sensor <sup>[175]</sup>	CO <sub>2</sub>	1	8 ppm	NR	8 ppm	NR
	SO <sub>2</sub>	0.5	8 ppm	NR	NR	NR
	NH <sub>3</sub>	0.18	8 ppm	NR	NR	NR
RGO/Ti <sub>3</sub> C <sub>2</sub> T <sub>x</sub> <sup>[85]</sup>	NH <sub>3</sub>	6.8	50 ppm	NR	NR	NR
	H <sub>2</sub> S	0.5	50 ppm	NR	NR	NR
	SO <sub>2</sub>	0.59	50 ppm	NR	NR	NR
W <sub>18</sub> O <sub>49</sub> /Ti <sub>3</sub> C <sub>2</sub> T <sub>x</sub> <sup>[86]</sup>	NH <sub>3</sub>	2	20 ppm	NR	NR	NR
ZnTi-LDHs (LDHs/Ti <sub>3</sub> C <sub>2</sub> T <sub>x</sub> ) <sup>[191]</sup>	NH <sub>3</sub>	126%	100 ppb	9s/11s	100 ppb	NR
α-Fe <sub>2</sub> O <sub>3</sub> /Ti <sub>3</sub> C <sub>2</sub> T <sub>x</sub> <sup>[190]</sup>	NH <sub>3</sub>	18.3%	5 ppm	2.5s	5 ppm	NR
N-Ti <sub>3</sub> C <sub>2</sub> T <sub>x</sub> /PEDOT:PSS <sup>[144]</sup>	NH <sub>3</sub>	≈13%	10 ppm	280 s/393 s	10 ppm	Flexible
	H <sub>2</sub> S	≈3%	10 ppm	NR	10 ppm	Flexible
	SO <sub>2</sub>	≈2%	10 ppm	NR	10 ppm	Flexible
	NO <sub>x</sub>	≈1%	10 ppm	NR	NR	Flexible
	CO	≈0.5%	10 ppm	NR	NR	Flexible
Polysquaraine, poly-(1,4-diamino-2,5-dichlorobenzene-squaraine) (PDDS)/Ti <sub>3</sub> C <sub>2</sub> T <sub>x</sub> <sup>[192]</sup>	NH <sub>3</sub>	≈2.2%	1 ppm	NR	500 ppb	NR



other gaseous contaminants. It is due to the presence of surface functionalities on  $M_3X_2T_x$ -MXene HNCs, which act as specific adsorption sites for  $NH_3$  due to larger adsorption energies and bond length. In light of literature, these chemiresistors also possess to find significant sensing response toward  $SO_2$ . However, dedicated research is required for its practical applications as an  $SO_2$  sensor. The sensitivity of  $M_3X_2T_x$ -MXene HNCs chemiresistors is better than other materials owing to enlarged specific surface area and modified surface chemistries of HNC due to manifestation of polymer and improved charge transfer due to the presence of MXenes.

## 6.2. $M_2XT_x$ -P Based Chemiresistors for Air Contaminant Monitoring

### 6.2.1. Need for $M_2XT_x$ -P Based Chemiresistors

It is interesting to note that the first theoretical analysis of air pollutant molecule identification and monitoring used  $M_2XT_x$

MXenes. Yu et al.<sup>[82]</sup> first theoretically investigated the interaction among various air contaminants with  $Ti_2CO_2$  MXene. This research group demonstrated the successful adsorption of  $NH_3$  molecules over the MXene surface by forming an N-Ti bond by donating a large charge of magnitude 0.174e. Other contaminants were not observed to be adsorbed over the MXene surface due to their high adsorption energy than  $NH_3$  (-0.37 eV). The capture of  $NH_3$  molecules was reversible after removing the applied biaxial strain (3%) (Figure 19). MXene demonstrated superior sensitivity towards  $NH_3$  than  $MoS_2$  and phosphorene using current-voltage analysis.

Similarly, Xiao et al.<sup>[74]</sup> investigated the contaminants ( $N_2$ ,  $NO$ ,  $NH_3$ ,  $CO$ ,  $CO_2$ ,  $O_2$ ,  $H_2$ , and  $CH_4$ ), monitoring the performance of  $M_2CO_2$  ( $M = Zr, Ti, Sc, \text{ and } Hf$ ). The outcomes of this research suggested the physisorption of all tested contaminants over the MXene surface except  $NH_3$ . The  $NH_3$  was found to be chemisorbed on  $Zr_2CO_2$  surface by donating two electrons to two MXene. This phenomenon was attributed to high adsorption energy (-0.81 eV) and large charge transfer (0.188 e) of

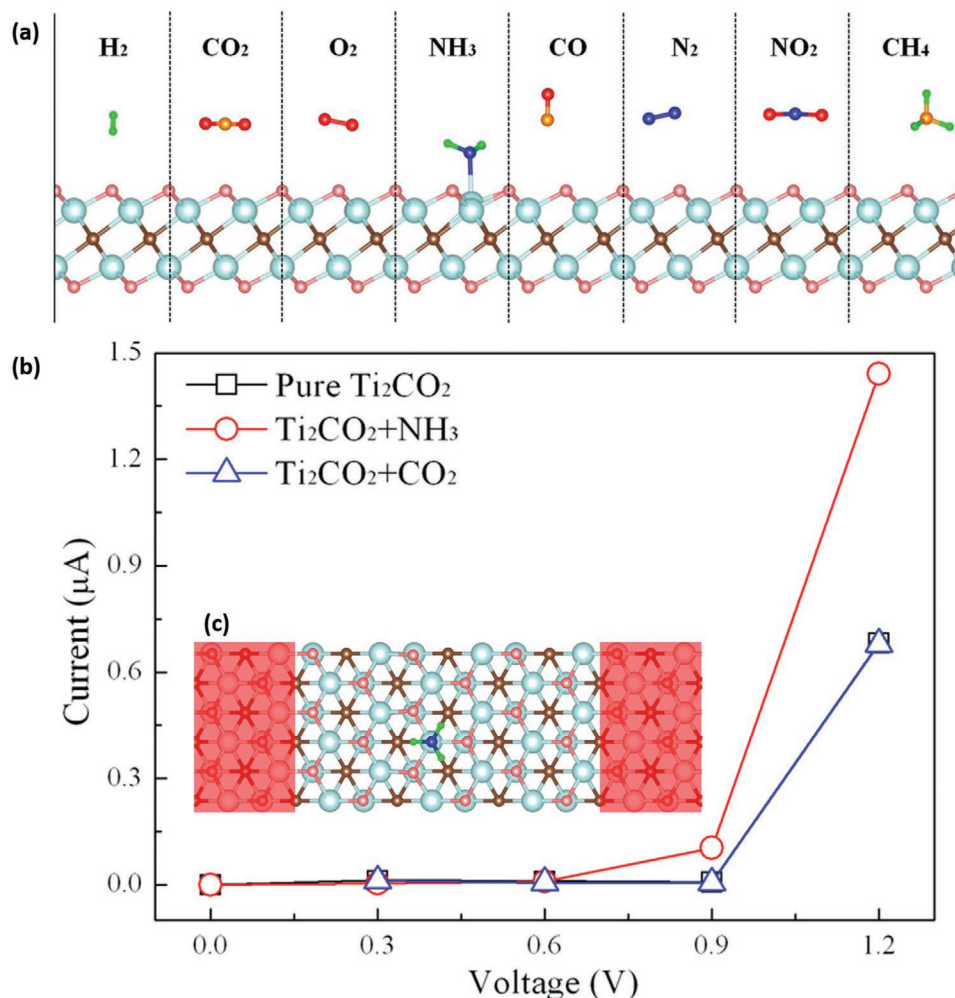


**Figure 19.** a) Schematic depiction of sideways outlook of the adsorption of various analytes including  $N_2$ ,  $NO$ ,  $NH_3$ ,  $CO$ ,  $CO_2$ ,  $O_2$ ,  $H_2$ , and  $CH_4$  over the monolayer of  $Ti_2CO_2$ -MXene. b) Estimated  $I$ - $V$  characteristics prior to and subsequent to the adsorption of  $NH_3$  molecules over  $Ti_2CO_2$ , phosphorene and  $MoS_2$ , c) schematic depiction of  $Ti_2CO_2$ -based chemiresistor to sense airborne  $NH_3$  molecules. Reproduced with permission.<sup>[82]</sup> Copyright 2015, American Chemical Society.

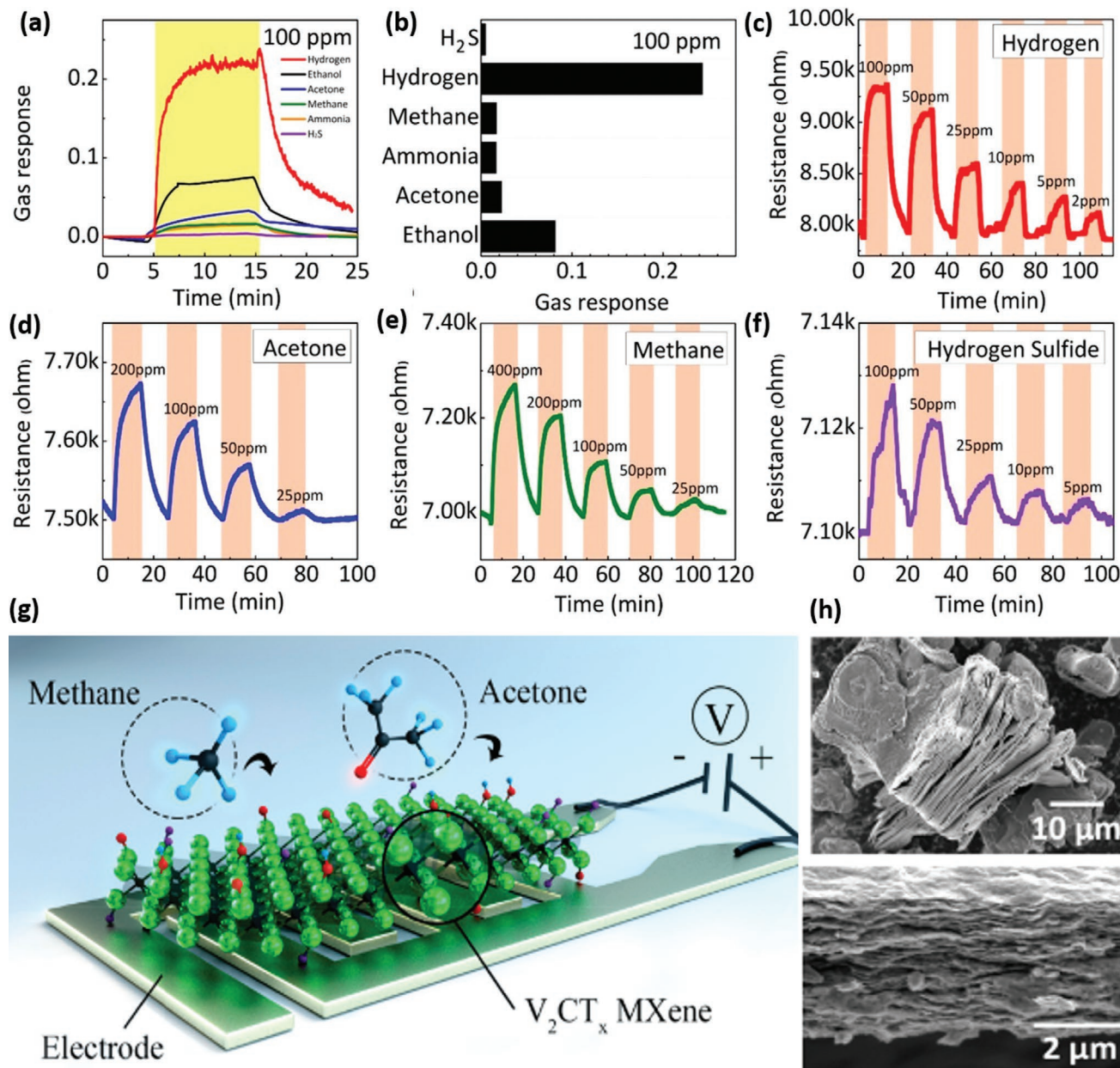


**Figure 20.** Air contaminant sensing performance of  $V_2CT_x$  based sensor in terms of a) net variation in resistance. b) Sensitivity towards 100 ppm of various air contaminants at room temperature. Real-time sensitivity values of  $V_2CT_x$  based sensor at various concentrations of c)  $H_2$ , d)  $C_3H_6O$ , e)  $CH_4$ , and f)  $H_2S$ . g) Schematic depiction of  $V_2CT_x$  based sensor performance. h) SEM micrographs of  $V_2CT_x$ . Reproduced with permission.<sup>[81]</sup> Copyright 2019, American Chemical Society.

$NH_3$  towards MXene. Further, Wang et al.<sup>[84]</sup> revealed that the inclusion of water molecules on the  $Hf_2CO_2$  surface increases its selective sensitivity towards  $NH_3$ . In addition, Ma et al.<sup>[83]</sup> reported the enormous potential of  $M_2CO_2$ -MXene for  $SO_2$  sensing. The  $SO_2$  molecules were physisorbed on  $Sc_2CO_2$  surface better than other tested contaminants. It was attributed to orbital hybridization of  $SO_2$  and MXene adjacent to the Fermi level in the anticipated DoSs resulting in metallic nature and enhanced charge transfer in the interaction system.

Moreover, Naqvi et al.<sup>[66]</sup> reported the potential of nitrides MXenes  $M_2NS_2$  ( $M = Ti, V$ ) for monitoring of  $H_2S$ ,  $NH_3$ ,  $CO$ ,

$SO_2$ ,  $NO_2$ ,  $CH_4$ ,  $CO_2$ , and  $NO$  gaseous molecules. A reversible adsorption behavior was observed for oxides of  $N_2$  over  $Ti_2NS_2$  and  $V_2NS_2$  MXenes, which can be developed as a high-performance sensing platform. However, experimental studies on  $M_2XT_x$  chemiresistors are limited owing to the lesser stability and complexity of processing. Lee et al.<sup>[81]</sup> reported monitoring of polar and non-polar gaseous contaminants using  $V_2CT_x$  based chemiresistor (Figure 20). It was observed that the surface groups  $-O$  and  $-OH$  persist much more compared to  $-F$  groups. It results in excellent room temperature sensitivity towards polar and nonpolar gaseous contaminants. However,

$V_2CT_x$  based chemiresistor was found to be more selective for  $H_2$  compared to other contaminants. Hence, the study indicated that selective detection of desirable air contaminants could be achieved by choosing appropriate transition metal.

Guo et al.<sup>[65]</sup> investigated  $Mo_2CT_x$  based chemiresistor for selective  $C_7H_8$  sensing at room temperature. However, the major outcome of this study is to optimize the concentration of MXene and sonication time to enhance the sensing performance. However, the various studies indicated the requirement of increasing interlayer distance for better sensing performances.<sup>[53]</sup> It was performed through intercalating or including foreign materials such as polymers or metal ions among the MXene layers. For instance, Zhang et al.<sup>[116]</sup> alkalized  $V_2CT_x$  for excellent selective and sensitive detection of  $NO_2$ . It was observed that the alkalization inserts a suitable amount of  $Na^+$  intercalants among MXene layers, which results in its swelling of interlayer distance. It resulted in 80 times better  $NO_2$  sensing (50 ppm) than the pristine MXene. Hence, intercalation increases specific surface area to achieve superior sensitivity and modifies surface functionalities to achieve stability. Henceforth, interlayer distance optimization and surface functionalities tuning were performed by fabricating  $M_2XT_x$  hybrids with materials such as polymers.

### 6.2.2. Air Contaminant Monitoring Performance

Various DFT and MD studies revealed that  $M_2XT_x$  MXenes possess greater affinity and binding energies for various air contaminants compared to  $M_3X_2T_x$  MXenes.<sup>[53]</sup> Such desired features are attributed to their fewer layers resulting in a large specific surface area. Hence, various hybrids of  $M_2XT_x$  MXenes were evaluated for various other technological applications. However, the reports on air contaminant sensing are limited and mainly dedicated to  $NH_3$ <sup>[10]</sup> due to excellent electrical conductivity resulting from faster charge transport in a few layered, low-dimensional materials. For instance, Wang et al.<sup>[79,80]</sup> performed two different studies to evaluate the air contaminant sensing performance of  $Nb_2CT_x/PANI$  HNCs. The differences in these two studies were majorly dedicated to the synthesis route adopted for HNC fabrication. This group fabricated  $Nb_2CT_x/PANI$  HNCs using ex situ (alternate spraying) and in situ (in situ polymerization) approaches. Using an ex situ approach, four different chemiresistors were designed by changing the concentration of  $Nb_2CT_x$  in spray volume (0.05 mL, 0.1 mL, 0.15 mL, and 0.2 mL). The optimum concentration of  $Nb_2CT_x$  in HNC for  $NH_3$  monitoring was observed as 0.1 mL, beyond which the room temperature sensitivity was decreased. It is ascribed to hindering of  $NH_3$  adsorption site beyond this MXene concentration. Hence, the 0.1 mL based chemiresistor was further evaluated for  $NH_3$  sensing performance and exhibited a sensitivity as 2.57% per ppm of  $NH_3$  with LDL as 1 ppm. The integration of a simple triboelectric nanogenerator (TENG) based on two Al electrodes, two triboelectric films (polytetrafluoroethylene (PTFE) film and nylon), and a flexible PET substrate resulted in an interesting self-operating chemiresistor. The sensitivity of the  $Nb_2CT_x/PANI/TENG$  (0.1 mL) chemiresistor (301.31%) toward 100 ppm of  $NH_3$  at room temperature under 87.1% RH is 2.34/36.93 fold

superior compared to that of pristine PANI (128.81%)/ $Nb_2CT_x$  (8.15%) chemiresistors. Additionally, the chemiresistor exhibited sustainable sensitivity under varying RH and temperature, highlighting its high stability for applications in harsh environments. This study gives preliminary research and prospects for potential MXP HNCs based on self-powered sustainable, intelligent chemiresistors to detect air contaminants.

In another study,<sup>[79]</sup> this research group fabricated  $Nb_2CT_x/PAN$  HNCs using in situ polymerization of PAN to manifest  $Nb_2CT_x$ . It exhibits a 14-fold enhanced sensitivity in the case of  $NH_3$  (29.95% sensitivity toward 1 ppm) compared to chemiresistor synthesized through the ex situ route (**Figure 21**). This is a result of heterojunction development between HNC precursors during in situ polymerization. Further, the chemiresistor exhibited superior sensing response (74.68% toward 10 ppm), repeatability (observed for three cycles), very low LDL (20 ppb), fast response (within 126 s), linear detection range (with  $R^2 = 0.9951$ ), long-term stability (stable for 35 consecutive days), stability in the varying humidity, but with slow recovery (in 640 s). The sensor also exhibited a significant sensing response toward 10 ppm of  $SO_2$  (9%) in the light of literature.<sup>[13–15,138]</sup> However, the study was dedicated to  $NH_3$  detection. A significant sensitivity of  $Nb_2CT_x/PANI$  HNCs towards  $SO_2$  does not cost its selectivity toward  $NH_3$ . It is because the nature of both the contaminants is opposite in nature, i.e.,  $NH_3$  as reducing and  $SO_2$  as oxidizing gas.

Hence, the sensing signal generated by each contaminant can be easily differentiated using appropriate electronic circuitry. Additionally, the reported LDL of 20 ppb for  $NH_3$  detection in exhaled human breath can substitute traditional time-consuming strategies for detecting renal disorders in humans. Chemiresistors with low LDL are also essential to detect early leakage or emission of contaminants for workplace safety to combat any probable accident. The sensitivity of both the  $Nb_2CT_x/PANI$  HNCs based chemiresistors was superior to their pristine precursors (**Table 6**),  $M_3XT_x-P$  (**Table 5**) and other prominent sensing materials including Ce-ZnO-PANI (40% @25 ppm), PANI-MWCNTs (92% @100 ppm), PANI- $WO_3$  (121% @100 ppm), PANI-rGO (13% @15 ppm), DPA-Ph-DBP-zDCN (72.7% @100 ppm), TFB (13% @100 ppb),  $TiO_2/Ti_3C_2T_x$  (1% @ 0.5 ppm) and PANI- $TiO_2-Au$  (17% @ 1ppm).<sup>[79,80]</sup> It is attributed to the presence of interfacial hetero-p-n-junctions and hydrogen bonding in MXP HNCs. Moreover,  $M_2XT_x-P$  based chemiresistor are found to be stable in a variable environment.

For instance, Wang et al.<sup>[79]</sup> estimated the stability of  $Nb_2CT_x/PAN$  chemiresistor for 35 consecutive days, maintaining a steady sensitivity for 10 ppm of  $NH_3$ . For variable surroundings, it is observed by measuring the sensitivity of a chemiresistor as a function of relative humidity and operational temperature. Li et al.<sup>[101]</sup> detected the sensing response of MXP HNC toward  $NH_3$  initially rises (0–40%RH) and then dropped (40–90%RH) with the proliferation in RH, and the threshold was at 40% RH (**Figure 22**). The formation of a thin coating of water molecules on the chemiresistor surface, inhibiting the  $NH_3$  adsorption sites, is thought to cause this threshold. Hence, there is a dynamic equilibrium between the magnitude of RH and  $NH_3$  sensitivity, which decides the particular threshold magnitude of RH. Further, it was observed that the sensitivity decreased

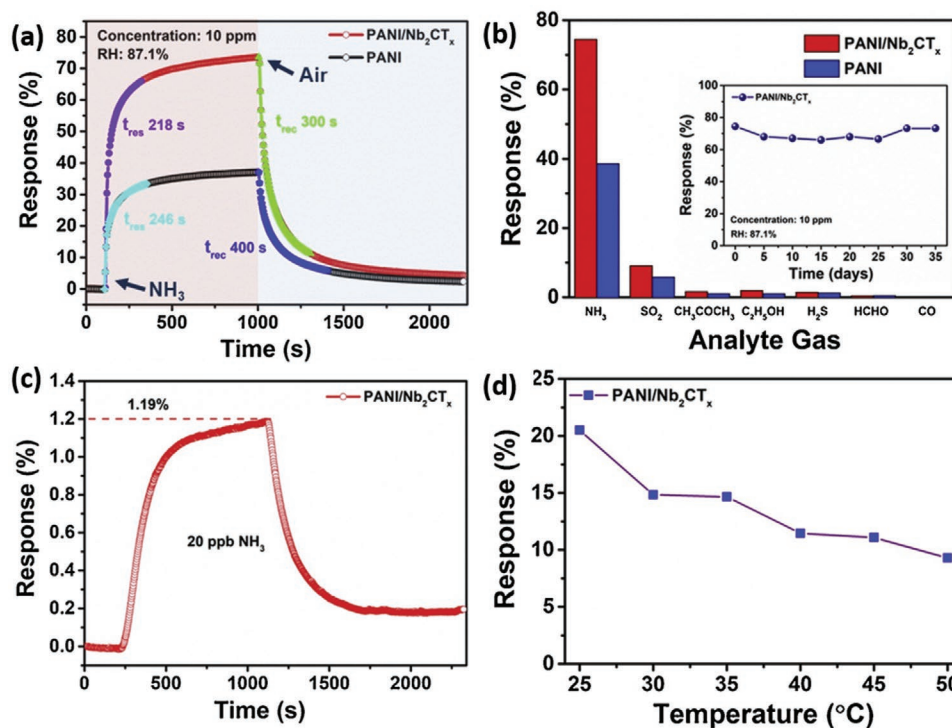


**Figure 21.** a) Dynamic sensitivity estimated for PAN and Nb<sub>2</sub>CT<sub>x</sub>/PAN chemiresistors towards 10 ppm of NH<sub>3</sub> under 87.1% RH at room temperature. b) Selectivity study of the fabricated chemiresistors with inset of (b) depicting the long-term stable behavior of Nb<sub>2</sub>CT<sub>x</sub>/PAN sensor for 10 ppm NH<sub>3</sub> within 35 d. c) Dynamic response of Nb<sub>2</sub>CT<sub>x</sub>/PAN chemiresistor for 20 ppb of NH<sub>3</sub>. d) Effect of variable working temperatures (25–50 °C) on the sensitivity of the Nb<sub>2</sub>CT<sub>x</sub>/PAN chemiresistor for 2 ppm of NH<sub>3</sub> under 87.1% RH. Reproduced with permission.<sup>[79]</sup> Copyright 2021, Elsevier.

with an increment in operational temperature for HNCs. This outcome is attributed to the desorption of H<sub>3</sub>O<sup>+</sup> ions from the HNC surface, reducing its sensitivity. A comparative summary of M<sub>2</sub>XT<sub>x</sub> MXenes based air contaminant monitoring is illustrated in Table 6.

It is evident that the M<sub>2</sub>XT<sub>x</sub>-P based chemiresistor exhibits superior sensitivity to air contaminants compared to M<sub>3</sub>X<sub>2</sub>T<sub>x</sub>-P, precursors, and other hybrids-based chemiresistors. However, these studies are limited and require more dedicated analysis in terms of all essential and advanced sensing parameters. It is worth noting that these chemiresistors also suffer from a prolonged response and recovery time, which can be optimized by controlling various fabrication parameters such as precursor concentration, film thickness, and nature of precursors.

Consequently, it is evident that MXP HNCs exhibit superior sensing behavior toward various air contaminants in terms of sensitivity, selectivity, stability, LDL, and flexibility compared to MXene-based chemiresistors. Moreover, all the reported MXP HNC-based sensors operate at room temperature and eliminate energy consumption requirements during contaminant monitoring, contributing to sustainable development goals related to the energy crisis and reducing the manufacturing cost.<sup>[44,172]</sup> Additionally, it averts the merging of grain boundaries of nanostructures at higher temperatures resulting in a more significant lifetime of chemiresistors. This feature also reduces the complexity and cost of chemiresistors by eliminating the requirement of automated micro-heating assemblages.

The most striking feature about MXP HNC-based chemiresistors is flexibility with persistent sensitivity, making them

more portable, compact, and easy to handle in every wear and tear situation of air contaminant monitoring measurements. It is ascribed to excellent conductivity and better conductive pathways in HNC due to the existence of MXenes. It also explained the superior specific surface area and pore volume due to intercalation of MXene layers through the inclusion of polymers preventing restacking and surging probability of interaction between contaminant molecules and chemiresistor. Additionally, the multi-interactions among precursors lead to stability of MXP HNCs chemiresistor in ambient and contaminant environment. The ease of processing, environmentally friendly nature, abundance of polymers, specific affinity and binding energies towards contaminant, and flexibility of polymers turns MXP HNCs into better sensing material than other MXene based HNCs for contaminant monitoring. However, MXP HNCs still require the dedicated attention of the sensing research community to develop practical environmental monitoring.

## 7. Challenges and Potential Alternative Solutions

The applications of MXP HNCs based chemiresistors for air contaminants detection necessitate imperative developments towards the precursor processing technologies, stoichiometric optimization, and device manufacture. The critical challenges for their practical applications are associated with fabrication strategies, precursor optimization, achieving advanced sensing features, scalable mass production, controlling environmental

**Table 6.** Room temperature air contaminant sensing behavior of materials based on  $M_2XT_x$  MXenes in terms of various sensing parameters.

Sensing material	Air contaminant	Sensitivity [%]	Concentration	Recovery/ response time	LDL	Flexibility
$V_2CT_x$ <sup>[20]</sup>	H <sub>2</sub> S	0.05	100 ppm	NR	NR	NR
	H <sub>2</sub>	24.5	100 ppm	≈7 min	100 ppm	NR
	CH <sub>4</sub>	1.67	100 ppm	≈4 min	100 ppm	NR
	NH <sub>3</sub>	1.66	100 ppm	NR	NR	NR
	C <sub>3</sub> H <sub>6</sub> O	2.66	100 ppm	NR	NR	NR
$Mo_2CT_x$ <sup>[65]</sup>	C <sub>2</sub> H <sub>5</sub> OH	8.16	100 ppm	NR	100 ppm	NR
	C <sub>7</sub> H <sub>8</sub>	2.81	140 ppm	NR	140 ppm	NR
	C <sub>6</sub> H <sub>6</sub>	0.97	140 ppm	NR	NR	NR
	C <sub>2</sub> H <sub>5</sub> OH	0.73	140 ppm	NR	NR	NR
	CH <sub>3</sub> OH	0.58	140 ppm	NR	NR	NR
Alkalized $V_2CT_x$ <sup>[116]</sup>	C <sub>3</sub> H <sub>6</sub> O	0.14	140 ppm	NR	NR	NR
	NO <sub>2</sub>	≈10	5 ppm	≈120 s	5 ppm	NR
$Nb_2CT_x/PANI-TENG$ <sup>[80]</sup>	NH <sub>3</sub>	9.33	1 ppm	105 s/143 s for 100 ppm	1 ppm	NR
	C <sub>2</sub> H <sub>5</sub> OH	3	10 ppm	NR	NR	NR
	C <sub>3</sub> H <sub>6</sub> O	2	10 ppm	NR	NR	NR
	SO <sub>2</sub>	6	10 ppm	NR	NR	NR
	H <sub>2</sub> S	2	10 ppm	NR	NR	NR
	HCHO	0.5	10ppm	NR	NR	NR
	CO	1	10 ppm	NR	NR	NR
	CH <sub>4</sub>	2.5	10 ppm	NR	NR	NR
$Nb_2CT_x/PANI$ <sup>[79]</sup>	NH <sub>3</sub>	1.19	20 ppp	218 s/300 s for 10 ppm	20 ppb	NR
	C <sub>2</sub> H <sub>5</sub> OH	2	10 ppm	NR	NR	NR
	C <sub>3</sub> H <sub>6</sub> O	2	10 ppm	NR	NR	NR
	SO <sub>2</sub>	9	10 ppm	NR	NR	NR
	H <sub>2</sub> S	1	10 ppm	NR	NR	NR
	HCHO	0.5	10 ppm	NR	NR	NR

contamination, and reducing nano-based/related waste production. Simultaneously optimizing different properties during machine processing to achieve high-performance chemiresistors is the major challenge associated with their commercial feasibility. Although various alternative strategies have been reported to address every challenge, strategically designing dedicated protocols is required. Hence, the state-of-the-art MXP HNC chemiresistors is concerned with developing safe, cost-effective, energy-efficient, and high-yielding strategies.

### 7.1. Safe and Scalable Processing Strategies

The current state-of-the-art MXene production involves harsh corrosive acid-based etching, adversely impacting the environment and humans. Even the advanced synthesis route involving the in situ formation of HF contaminates the environment up to a certain extent. The F-based synthesis strategies result in MXene with more fluorine terminals over its surface, unfavorable for air contaminant performance.<sup>[71]</sup> It has raised the pursuit of greener fabrication strategies such as CVD or salt-template growth.<sup>[193]</sup> However, the salt-template method is limited due to the dependence of the crystal structure of

MXene on lattice parameters and crystal symmetries of respective precursor salts.<sup>[72]</sup> On the other hand, CVD is feasible for synthesizing MXenes with a smaller number of layers (“n”) like  $M_2X$ . The synthesis of more layered (larger n values) MXenes through the CVD route is challenging due to its metamorphosis crystal structure and complex elemental compositions.<sup>[71]</sup> Various alternate physical fabrication routes like molecular beam epitaxy, CVD, and mechanical exfoliation have been proven for the high yield of nonterminated MXenes. However, using such nonterminated MXenes is not feasible for air contaminant monitoring. The storage and post-processing of MXenes are still challenging due to instability of MXenes like  $Ti_3C_2T_x$  in an oxygen environment. Hence, improved fabrication strategies are required for high yield MXenes with desired surface functionalities as per the application point of view.

### 7.2. Optimization of Precursors

The major obstacle in the scalable production of MXP HNCs is the concurrent optimization of different properties like mechanical strength, conductivity, mechanical flexibility, film thickness, and surface functionalities during machine processing. For

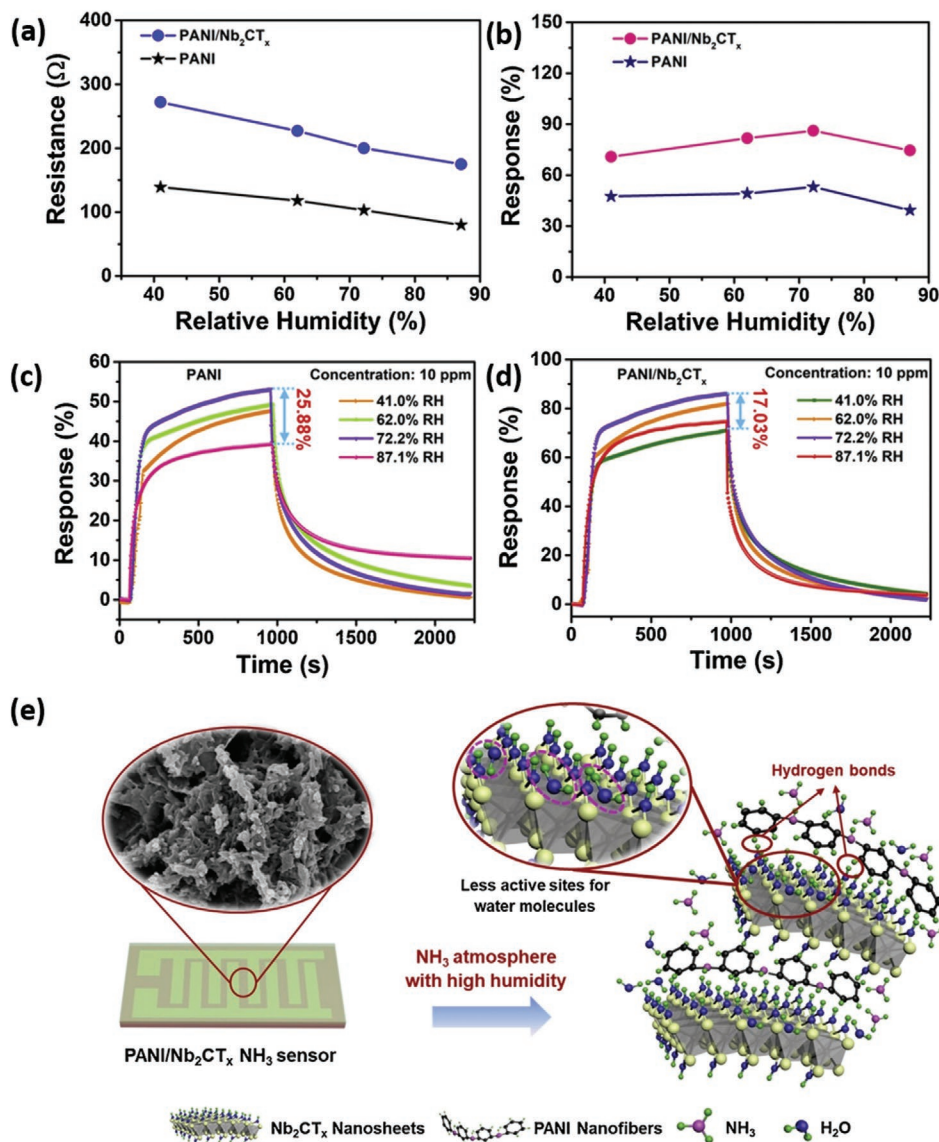


**Figure 22.** Humidity tolerance study on MXP HNCs sensing performance towards NH<sub>3</sub>. a) Variation in resistance of fabricated samples with different RH levels. b) Humidity tolerance study of fabricated chemiresistors. Sensing curves for c) pristine PAN precursor, d) Nb<sub>2</sub>CT<sub>x</sub>/PAN based chemiresistors at 10 ppm of NH<sub>3</sub> in varying RH. Reproduced with permission.<sup>[79]</sup> Copyright 2021, Elsevier.

instance, the high electroconductivity of HNC is achieved via including a significant amount of MXene precursor.<sup>[130]</sup> However, the presence of a large concentration of MXene may result in less mechanical flexibility and stretchability. Likewise, the simultaneous optimization of composition, surface functionalities, stability, and film thickness is challenging for processing. For example, an optimum concentration of MXene precursors is a prerequisite in HNC to obtain conductive pathways in the precursor polymer matrix.<sup>[79]</sup> The inclusion of polymers among MXene layers is also essential to increase interlayer separation. However, the increase in interlayer separation results in a particular strain range, which may break these conductive pathways. The inclusion of a high concentration of polymer precursor may result in a complete breakdown of conductive pathways on reaching a particular strain threshold. These

changes in conductive network distribution are established by a balanced reduction in the transient electrical current flowing through the chemiresistor and the magnitude of strain subjected to the chemiresistor. Nevertheless, the large concentration of MXenes causes high strains due to large conductivity resulting in no detectable change in resistance. Hence, there is a continuous equilibrium between different processing parameters and aspects. It requires numerous tribological evaluations to determine the threshold concentration of precursors in HNC with desired properties. These facts highlight the manifestation of trade-offs among physicochemical characteristics and precursor concentrations of MXP HNCs.

Interestingly, Shuck et al.<sup>[194]</sup> reported the massive and scalable synthesis of Ti<sub>3</sub>C<sub>2</sub>T<sub>x</sub> and alike MXenes utilizing an indigenous large size reactor with provisions for addressing most

safety and precursor optimization challenges. However, using HF during the fabrication is still a challenge considering environmental contamination and the origin of defects in fabricated MXene. It can be catered by either replacing HF with mild etchants in a large reactor reducing the chances of contamination and safety issues, and optimizing the reaction parameters such as chamber pressure and reaction temperature. Additionally, MXP HNCs can be directly obtained through this scalable technique by improvising the design by adding monomer/presynthesized polymer at the appropriate time in the reactor. Moreover, one-pot synthesis techniques are pretty famous for synthesizing inorganic–organic HNCs, in which both the precursors are fabricated at the same time.<sup>[13,144,170,174,195]</sup> It is advantageous as by-products resulting from the fabrication of one precursor act as reactant/dopant for another. Similarly, a monomer can be polymerized during the synthesis of MXene by optimizing the reaction parameters and conditions to obtain MXP HNCs from one-pot synthesis. By architecting such techniques and optimizing reaction parameters, MXP HNCs can be fabricated in less reaction or fabrication time, at a lesser cost, and with better physicochemical properties due to homogeneously distributed interfacial heterojunctions. It can be first predicted through advanced machine learning simulations by observing chemical reactions, parameters, and trade-offs, saving human resources and preventing environmental contamination caused by by-products. Hence, dedicated evaluation of reaction parameters, optimization of precursors, and engineering on stoichiometries are highly required to fabricate next-generation MXP HNCs. Moreover, green fabrication techniques and bio-derived routes to synthesize MXene and HNCs need to be part of future research.

### 7.3. Limited Practical Materials and Slow Recovery

Despite expeditious advances and significant theoretical predictions of MXene, very few of them have been successfully synthesized. However, there is a large gap between the sensing outcomes expected or estimated theoretically and experimentally. MXenes fabricated on nitrides are not extensively explored as that on carbides. The HNC of MXene is also limited to a few polymers like PAN, PEDOT:PSS, despite the large abundance of polymers. Hence, there are many options to fabricate HNCs using different MXenes and polymer precursors. It will help in meeting advanced sensing requirements. For instance, vanadium based MXenes have been recently reported to be highly selective in detecting nitrous oxides. The choice of appropriate transition metal in MXenes induces selectivity for specific contaminant detection. Thus, the gap between theoretical predictions, in-laboratory observation, and practical applicability of MXP HNCs can be achieved using the appropriate choice of their stoichiometric and structural composition, scalable production, and regulated machine processability.

MXP HNC chemiresistors exhibit a slower response and recovery time with reference to targeted air contaminants, limiting their realistic prospects. This is due to higher binding energies of some contaminants with sensing materials surface. The outcomes analyzed based on various DFT and MD suggested that several contaminants' gaseous molecules possess

specific affinity, which varies according to precursors, MXene, and polymer counterparts due to a difference in the surface energies of contaminants and MXP HNC surface. It results in adsorption of the analyte to a deeper level, which increases the diffusion length. As a result, the chemiresistor takes longer to recover to its initial conducting state. However, the key solution to this serious problem is optimizing stoichiometry, concentration of precursors, and engineering desired surface terminals in accordance with specific air contaminants.

Moreover, engineering a next-generation chemiresistor with a response and recovery time of a few seconds is a prerequisite. It can also be achieved by engineering various architects of chemiresistor such as employing interdigitated electrodes instead of conventional parallel conducting electrodes, reducing the noise due to the electrode-material-wire interface via optimizing appropriate choice of fabrication components. For example, the surface modifications of MXenes, such as, N-based functionalization, and the use of metallic nanoparticles based surface enhancement in MXenes, contribute to rapid response owing to the catalytic action of additives. Moreover, the proper choice of stoichiometry of sensing material by examining its surface interactions and bondings with target analyte using advanced machine learning approaches is an economic way to improve response and recovery period. Other governing factors which can be tuned for prompt response/recovery include optimization of sensing film thickness for faster desorption, introducing desired surface functionalization to avoid strong absorption/bonding, and integrating rapid data acquisition technologies. Additionally, the utilization of secondary nanomaterials in the form of ternary hybrids/nanocomposites is another prominent way to optimize and enhance response and recovery characteristics.

### 7.4. Alternate Approaches

These crucial challenges are manageable by adopting various alternative and acceptable strategies. Surface functionalization and modification are the primary tasks and need alternative approaches to meet commercial sensing requirements. For example, the –OH terminals over the MXene surface enhance reactivity and sustain different surface functionalization processes.<sup>[196]</sup> Moreover, the H-bonding among polymer and MXene precursors results in a longer lifetime and stability of HNCs. It also forms a well-ordered MXene network in the HNC chemiresistor resulting in the reduction of the percolation threshold of MXene. In this direction, Guo et al.<sup>[197]</sup> reported a reduction in the percolation threshold of MXene precursor in the polymer matrix from 40 to 6% owing to the development of H-bonds on surface functionalizations. These generated H-bonds act as stress transfer channels among the precursors of HNCs resulting in their improved mechanical flexibility. Hence, surface functionalization of MXenes aids as an alternate method for concurrent optimization of mechanical flexibility and electrical conductivity during machine processing.

The utilization of secondary nanostructures for the surface functionalization of MXenes in HNCs serves as another alternative approach to meet practical requirements. The inclusion of secondary NPs of different dimensions, including 0D (like

metal QDs), 1D (like CNTs), 2D (like graphene), and 3D (like metal oxide NPs) into HNCs result in the fabrication of mixed-dimensional HNCs.<sup>[34]</sup> For instance, silane-modified secondary NPs provide a positive charge at the surface resulting in strong electrostatic interactions among precursors.<sup>[198]</sup> It results in the formation of ternary HNCs with enhanced properties. Zhou et al.<sup>[173]</sup> reported superior sensing performance of ternary HNC of rGO, N-MXene, and PEI compared to precursors and HNCs. The inclusion of rGO as a secondary NPs enhances conductive pathways contributing to superior sensing performance.<sup>[173]</sup> Moreover, the N-surface treatment of MXene results in reinforced HNC due to strong H-bonding. The issue of selectivity can be addressed by selecting appropriate transition metal for the fabrication of MXene and its harsh toxic fabrication by adopting green synthesis approaches.<sup>[193,199]</sup> Hence, adopting alternate approaches more reliably by optimizing synthesis parameters is essential to meet commercial requirements for MXP HNC-based chemiresistors detecting air contaminants.

## 8. Toward Fifth Generation Sensing; Integrating IoTs, 5G, and AI

The advanced sensing systems using sensor arrays, such as designing electrical nose from MXP HNCs sensors, can also be achieved via incorporating recent technologies like machine learning (ML), artificial intelligence (AI), and pattern recognition (Figure 23). Moreover, integrating IoTs, 5G communication networks, and AI with chemiresistors can revolutionize the state-of-the-art MXP HNC chemiresistor based air contaminant monitoring. The chemiresistors with the feature to connect with the internet, Bluetooth, and each other are essential for real-time detection of diversified air contaminants. These

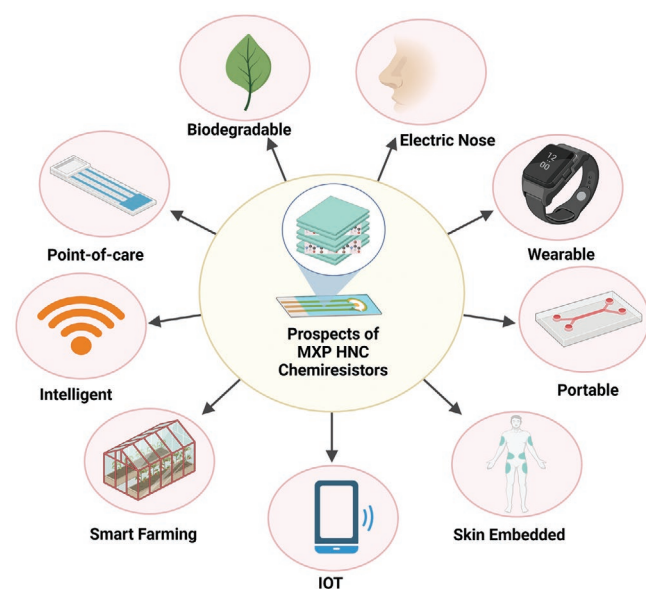


**Figure 23.** Prospects of MXP HNCs chemiresistor in designing next-generation intelligent portable electronic devices for diversified applications including personalized healthcare, point-of-care detection, smart farming, wearable and skin-embedded electronics, artificial sense organ with advanced features [Created with BioRender.com].

chemiresistors possess excellent durability to withstand the extreme variations of the environment in terms of pressure, humidity, and temperature.

Toward intelligent sensing, the chemiresistor integrated with IoT can be installed at every probable emission/leakage site. The small design of essential structural components assists in recording data and monitoring contaminants more effectively and accurately than conventional IoT devices. The next-generation IoT integrated chemiresistors can detect air contaminants and share output signals wirelessly to monitoring and analyzing devices/centers for situation analysis. Automated sensing and informatics processing supported by IoTs supports the aspects of “point-of-detection” modules. They possess latent to transform traditional public management and health systems with lesser human resources and time consumption. For instance, installing IoT chemiresistor near active/probable volcanoes can save thousands of lives by timely prediction/detection of eruption using pre-integrated machine algorithms.

Moreover, IoT integrated smart chemiresistors using modern machine algorithms can be developed as a “solution-on-chip” solution for numerous complex problems. For instance, IoT-ethylene chemiresistors can be installed in food storage and warehouses to detect the degradation of stored vegetables. On detection can instruct the ethylene-absorption pump to suction generated ethylene molecules automatically and initiate an audio/visual alarm. Such intelligent and intelligent strategies can revolutionize food storage and the supply chain.

The MXP HNCs can also be utilized for better and more intelligent farming practices using internet-of-things and artificial intelligence. For instance, Li et al.<sup>[99]</sup> demonstrated the potential of flexible PAN/Ti<sub>3</sub>C<sub>2</sub>T<sub>x</sub> HNC for monitoring NH<sub>3</sub> volatilization in agricultural fields. In the context of air contaminants, modern materials can be integrated on a single chemiresistor chip for scavenging the detected contaminants, which helps attain sustainability in modern “point-of-solution” sensing strategies. Thus, the state-of-the-art chemiresistor requires the fast development of modern machine algorithms to pre-process and analyze the observed information to convey big data-based forecasts such as early-stage diagnosis of chronic diseases, early monitoring of epidemic outbreaks, or early detection of contaminant emission/leakages contributing towards human and environmental welfare.

## 9. Cutting-Edge Prospects

The MXP HNCs have also been reported for excellent humidity sensing, resulting in food packaging, storage, and transport application. It reduces the human workforce, time, and efforts resulting in intelligent and sustainable agricultural practices. However, the scope of MXP HNC chemiresistors is not limited to air contaminant monitoring and detection. It extends to the application as point-of-care biomarkers with the potential to replace sophisticated, time-consuming strategies. For instance, an NH<sub>3</sub> sensor with LDL less than 0.8 ppm can be used as a biomarker for renal failure and gastric ulcer patients.<sup>[11]</sup> A C<sub>3</sub>H<sub>6</sub>O chemiresistor with a detecting range of 300–1800 ppb can be utilized to detect diabetes.<sup>[7]</sup> However, the analysis of clinical data is crucially required to observe their exact detecting



potential. Additionally, the potential of MXP HNCs can also be explored in the monitoring of low trace aromatic VOCs like  $C_6H_6$ , toluene etc., as they have already been detected using pristine MXenes and polymer precursors. For example, Guo et al.<sup>[65]</sup> reported the selective room temperature detection of the low trace of toluene (220 ppb) with ultrahigh sensitivity (0.0366  $\Omega$  per ppm) utilizing  $Mo_2CT_x$ -MXene over Si/SiO<sub>2</sub> substrate using photolithography. Moreover, Hermawan et al.<sup>[87]</sup> explored copper oxide (CuO) NPs/Ti<sub>3</sub>C<sub>2</sub>T<sub>x</sub> MXene for toluene detection with an ultrafast recovery time of 10 s. The fabricated sensor exhibits an LDL of 50 ppm, which can be further improved by utilizing MXP HNCs based chemiresistors.

The MXP HNCs possess potent to achieve sustainable aspects suggested for chemiresistors. These prospects include energy efficiency, eco-friendly, recyclable, biodegradable, self-operation, biocompatibility, and greener fabrication. A chemiresistor is an assembly of different electronic components, including wires, electrodes, substrate, PCB board, and sensing material, which can be made eco-friendly and biocompatible. They must be designed and developed using biodegradable/biocompatible/recyclable/bioderived materials using green approaches, or the fabricating component must be environmentally friendly. Moreover, the waste produced during the fabrication process can be repurposed, avoiding secondary contaminations. In this direction, the residue produced during the delamination of MXenes has been utilized to manufacture ink used for screen printing. This approach is toward the waste-to-wealth model and reduces secondary contamination produced in the form of by-products.<sup>[200]</sup> Furthermore, the inclusion of nanotriboelectric generators in chemiresistor circuitry results in their self-operation without using any external power source. For instance, Sardana et al.<sup>[201]</sup> reported self-driven room temperature ammonia detecting chemiresistor based on MXene/TiO<sub>2</sub>/Cellulose nanofiber heterojunction driven using electrospun-based triboelectric nanogenerators. The chemiresistor demonstrated high sensitivity, selectivity and reproducibility with rapid response and recovery within 76 and 32 s. The work opened a new window to architect intelligent and real-time gas leakage detection by self-driven and sustainable chemiresistor powered by human motion. Additionally, MXP HNCs owing to their metallic and flexible nature, are used to fabricate triboelectric generators.<sup>[202]</sup> With the integration of a triboelectric generator, MXP HNC chemiresistor embedded in wearable gadgets can be powered on energy generated through the motion of body parts based on fundamentals of triboelectricity.

It also suggests that the entire sensing set-up can be powered using various renewable or clean energy sources such as wind energy, solar energy, geothermal energy, and tidal energy. For example, NH<sub>3</sub> detecting chemiresistors employed in agricultural fields can be run on solar energy powered modules under smart agricultural practices. Additionally, MXP HNC layers have also been employed as joule heaters for the selective and sensitive operation of chemiresistors based on other sensing materials.<sup>[203]</sup> MXP HNCs are also reported to be either biodegradable<sup>[204]</sup> or degradable<sup>[205]</sup> in specific solutions, which reduces the probability of solid-waste generation due to the anticipated massive application of MXP HNCs. For instance, Zhang et al.<sup>[205]</sup> fabricated a pressure sensor utilizing cross-linked collagen fibers and MXene aerogel. They showed

the sensor degrades on soaking in an alkaline solution within forty days, indicating that the inclusion of natural fibers in the aerosol aid in biodegradability. In totality, the integration of sustainable aspects in chemiresistors possesses enormous potential to address the global challenges by helping in attaining sustainable development goals.

Therefore, MXP HNCs open new prospects for intelligent detection of air contaminants through energy-efficient, cost-effective, portable, compact, flexible, and rapid chemiresistors with high sensitivity, selectivity, stability, and providing sustainable development prospects. They are near future to devise intelligent and smart modules and technologies to architect smart green connected societies.

## 10. Conclusions

The recent extensive development in MXene and hybrid science during the last several years has opened a new domain for detecting and monitoring air contaminants based on chemiresistors technology. It is ascribed to synergetic effects among the merits of precursors. For example, MXP HNCs exhibit simultaneous mechanical flexibility and strength due to the presence of polymer and MXene, respectively. To facilitate better understanding, this review focuses on advancements in synthesis strategies, distinctive morphologies, surface chemistries, and unique properties of MXP HNCs. The reported air contaminant monitoring performance of MXP HNC chemiresistors has been comparatively analyzed and discussed. According to the reports, MXP HNCs have tremendous potential for air contaminant monitoring, and their sensing performance is better than reported sensing materials. For instance, metal oxide-based chemiresistors have dominated the air contaminant detecting chemiresistor market for ages. However, their operation at elevated temperatures increases cost and energy requirement, complexity, hazards and decreases their lifetime and stability.

On the contrary, MXP HNCs based chemiresistors are cost-effective, energy-efficient, stable, and less hazardous due to their room-temperature operation. Additionally, their operation in chemiresistive mode makes them portable, compact, user friendly and enables them to be utilized at every emission site, unlike spectroscopic or electrochemical sensors. The advanced sensing characteristics of MXP HNCs are attributed to their exceptional physicochemical, structural, and functional characteristics like tunable conductivity, sizeable interlayer distance, rich surface chemistries, presence of heterojunctions at precursor interfaces, enhanced charge transport channels, high mechanical and thermal endurance, flexibility, stretchability, improved porosity, high effective surface area, and synergistic effects. Nevertheless, the research dedicated to MXP HNCs chemiresistors is in its infancy, and there are still numerous challenges before revealing the commercial prospects of these chemiresistors.

There is a vast scope for exploring sensing mechanisms for specific air contaminants through advanced spectroscopic technologies like in situ Raman and FTIR spectroscopy along with Kelvin probe force microscopy during the detection of the contaminant. However, the colossal possibilities of MXP HNC in less explored application sectors, including food engineering

and defense strategies, are yet to be evaluated. In the near future, MXP HNCs are anticipated to expand and evolve in every prospect for developing next-generation intelligent devices for the betterment of humanity.

## Acknowledgements

V.C. thanks the Vice-Chancellor, University of Delhi and Department of Science & Technology, Government of India, India, for providing e-resources. Y.K.M. thanks funding from Interreg Deutschland-Denmark with money from the European Regional Development Fund, project number 096-1-1-18 (Access and Acceleration) and also to Mads Clausen Institute, SDU Denmark. M.K. acknowledges Sunway University's International Research Network Grant Scheme (STR-IRNGS-SET-GAMRG-01-2022).

## Conflict of Interest

The authors declare no conflict of interest.

## Keywords

air contamination, chemiresistor, intelligent sensors, MXene-polymer hybrid nanocomposites, synergistic effects

Received: December 16, 2021

Revised: May 13, 2022

Published online:

- [1] I. Manisalidis, E. Stavropoulou, A. Stavropoulos, E. Bezirtzoglou, *Front. Public Health* **2020**, *8*, 14.
- [2] S. Aranda, *Ten threats to global health in 2019* **2019**, pp. 1, <https://www.who.int/news-room/spotlight/ten-threats-to-global-health-in-2019> (accessed: June 2022).
- [3] WHO, Ambient (outdoor) air pollution, **2018**, [https://www.who.int/news-room/fact-sheets/detail/ambient-\(outdoor\)-air-quality-and-health](https://www.who.int/news-room/fact-sheets/detail/ambient-(outdoor)-air-quality-and-health) (accessed: September 2021).
- [4] Q. Li, Y. Li, W. Zeng, *Chemosensors* **2021**, *9*, 225.
- [5] J. Wang, Q. Zhou, S. Peng, L. Xu, W. Zeng, *Front. Chem.* **2020**, *8*.
- [6] D. Li, G. Liu, Q. Zhang, M. Qu, Y. Q. Fu, Q. Liu, J. Xie, *Sens. Actuators, B* **2021**, *331*, 129414.
- [7] V. Saasa, T. Malwela, M. Beukes, M. Mokgotho, C.-P. Liu, B. Mwakikunga, *Diagnostics* **2018**, *8*, 12.
- [8] W. Yuan, K. Yang, H. Peng, F. Li, F. Yin, *J. Mater. Chem. A* **2018**, *6*, 18116.
- [9] S. Dhall, B. R. Mehta, A. K. Tyagi, K. Sood, *Sens. Int.* **2021**, *2*, 100116.
- [10] V. Chaudhary, A. Gautam, Y. K. Mishra, A. Kaushik, *Nanomaterials* **2021**, *11*, 2496.
- [11] P. P. Ricci, O. J. Gregory, *Sci. Rep.* **2021**, *11*, 7185.
- [12] S. Mulmi, V. Thangadurai, *J. Electrochem. Soc.* **2020**, *167*, 037567.
- [13] V. Chaudhary, A. Kaur, *RSC Adv.* **2015**, *5*, 73535.
- [14] V. Chaudhary, H. Singh, A. Kaur, *Polym. Int.* **2017**, *66*, 699.
- [15] V. Chaudhary, *Polym.-Plast. Technol. Mater.* **2022**, *61*, 107.
- [16] S. Mahajan, S. Jagtap, *Appl. Mater. Today* **2020**, *18*, 100483.
- [17] D. E. Schraufnagel, J. R. Balmes, C. T. Cowl, S. De Matteis, S.-H. Jung, K. Mortimer, R. Perez-Padilla, M. B. Rice, H. Riojas-Rodriguez, A. Sood, G. D. Thurston, T. To, A. Vanker, D. J. Wuebbles, *Chest* **2019**, *155*, 417.
- [18] T. Suzuki, T. Hidaka, Y. Kumagai, M. Yamamoto, *Nat. Immunol.* **2020**, *21*, 1486.
- [19] S. Lolli, Y.-C. Chen, S.-H. Wang, G. Vivone, *Sci. Rep.* **2020**, *10*, 16213.
- [20] A. Bag, N.-E. Lee, *J. Mater. Chem. C* **2019**, *7*, 13367.
- [21] A. Gage, K. Brunson, K. Morris, S. L. Wallen, J. Dhau, H. Gohel, A. Kaushik, *Front. Nanotechnol.* **2021**, *3*, 700888.
- [22] N. Kaur, A. Khunger, S. L. Wallen, A. Kaushik, G. R. Chaudhary, R. S. Varma, *Curr. Opin. Green Sustainable Chem.* **2021**, *30*, 100488.
- [23] M. A. Ali, L. Dong, J. Dhau, A. Khosla, A. Kaushik, *J. Electrochem. Soc.* **2020**, *167*, 037550.
- [24] V. K. Tomer, R. Malik, V. Chaudhary, Y. K. Mishra, L. Kienle, R. Ahuja, L. Lin, *Appl. Mater. Today* **2019**, *16*, 193.
- [25] M. González-Garnica, A. Galdámez-Martínez, F. Malagón, C. D. Ramos, G. Santana, R. Abolhassani, P. Kumar Panda, A. Kaushik, Y. K. Mishra, T. V. K. Karthik, A. Dutt, *Sens. Actuators, B* **2021**, *337*, 129765.
- [26] K. R. Singh, V. Nayak, J. Singh, R. P. Singh, *Mater. Lett.* **2021**, *304*, 130614.
- [27] J. Chen, K. Chen, D. Tong, Y. Huang, J. Zhang, J. Xue, Q. Huang, T. Chen, *Chem. Commun.* **2015**, *51*, 314.
- [28] M. Swan, *J. Sens. Actuator Networks* **2012**, *1*, 217.
- [29] D. W. Kim, J. H. Lee, J. K. Kim, U. Jeong, *NPG Asia Mater.* **2020**, *12*, 6.
- [30] Y. C. Wong, B. C. Ang, A. S. M. A. Haseeb, A. A. Baharuddin, Y. H. Wong, *J. Electrochem. Soc.* **2020**, *167*, 037503.
- [31] P. Kumar Sharma, A. Ruotolo, R. Khan, Y. K. Mishra, N. Kumar Kaushik, N.-Y. Kim, A. K. Kaushik, *Mater. Lett.* **2022**, *308*, 131089.
- [32] B. Ortiz-Casas, A. Galdámez-Martínez, J. Gutiérrez-Flores, A. Baca Ibañez, P. Kumar Panda, G. Santana, H. A. de la Vega, M. Suar, C. Gutiérrez Rodelo, A. Kaushik, Y. Kumar Mishra, A. Dutt, *Mater. Today* **2021**, *50*, 533.
- [33] U. Chakraborty, G. Bhanjana, J. Adam, Y. K. Mishra, G. Kaur, G. R. Chaudhary, A. Kaushik, *RSC Adv.* **2020**, *10*, 27764.
- [34] R. Malik, V. K. Tomer, Y. K. Mishra, L. Lin, *Appl. Phys. Rev.* **2020**, *7*, 021301.
- [35] S.-J. Choi, I.-D. Kim, *Electron. Mater. Lett.* **2018**, *14*, 221.
- [36] S. Park, C. Park, H. Yoon, *Polymers* **2017**, *9*, 155.
- [37] V. Chaudhary, M. Chavali, *J. Appl. Polym. Sci.* **2021**, *138*, 51288.
- [38] W. Huang, L. Hu, Y. Tang, Z. Xie, H. Zhang, *Adv. Funct. Mater.* **2020**, *30*, 2005223.
- [39] E. S. Agudosi, E. C. Abdullah, N. M. Mubarak, M. Khalid, in *Pure and Functionalized Carbon Based Nanomaterials: Analytical, Biomedical, Civil and Environmental Engineering Applications*, (Ed: P. K. Zarzycki), CRC Press, Boca Raton, FL **2020**, pp. 147–174.
- [40] A. P. F. Turner, *ECS Sens. Plus* **2022**, *1*, 011601.
- [41] T. Ueda, N. Oide, K. Kamada, T. Hyodo, Y. Shimizu, *ECS Sens. Plus* **2022**, *1*, 013604.
- [42] F. Da Silva Santos, L. Vitor da Silva, P. V. S. Campos, C. de Medeiros Strunkis, C. M. G. Ribeiro, M. O. Salles, *ECS Sens. Plus* **2022**, *1*, 013603.
- [43] B. K. S. Reddy, P. H. Borse, *J. Electrochem. Soc.* **2021**, *168*, 057521.
- [44] T. Zhou, T. Zhang, *Small Methods* **2021**, *5*, 2100515.
- [45] A. Huang, Y. He, Y. Zhou, Y. Zhou, Y. Yang, J. Zhang, L. Luo, Q. Mao, D. Hou, J. Yang, *J. Mater. Sci.* **2019**, *54*, 949.
- [46] E. Lee, D.-J. Kim, *J. Electrochem. Soc.* **2020**, *167*, 037515.
- [47] C. Anichini, W. Czepa, D. Pakulski, A. Aliprandi, A. Ciesielski, P. Samorì, *Chem. Soc. Rev.* **2018**, *47*, 4860.
- [48] S. Yang, C. Jiang, S. Wei, *Appl. Phys. Rev.* **2017**, *4*, 021304.
- [49] S. Kumar, V. Pavelyev, P. Mishra, N. Tripathi, P. Sharma, F. Calle, *Mater. Sci. Semicond. Process.* **2020**, *107*, 104865.
- [50] L. Wang, M. Zhang, B. Yang, J. Tan, X. Ding, W. Li, *Small Methods* **2021**, *5*, 2100409.
- [51] D. H. Ho, Y. Y. Choi, S. B. Jo, J. Myoung, J. H. Cho, *Adv. Mater.* **2021**, *33*, 2005846.
- [52] Y. Jian, D. Qu, L. Guo, Y. Zhu, C. Su, H. Feng, G. Zhang, J. Zhang, W. Wu, M. S. Yao, *Front. Chem. Sci. Eng.* **2021**, *15*, 505.

- [53] S. Mehdi Aghaei, A. Aasi, B. Panchapakesan, *ACS Omega* **2021**, 6, 2450.
- [54] M. M. Hasan, M. M. Hossain, H. K. Chowdhury, *J. Mater. Chem. A* **2021**, 9, 3231.
- [55] V. Chaudhary, A. Kaushik, H. Furukawa, A. Khosla, *ECS Sens. Plus* **2022**, 1, 013601.
- [56] M. Khazaei, A. Ranjbar, M. Arai, T. Sasaki, S. Yunoki, *J. Mater. Chem. C* **2017**, 5, 2488.
- [57] H. Bai, G. Shi, *Sensors* **2007**, 7, 267.
- [58] H. Riazi, G. Taghizadeh, M. Soroush, *ACS Omega* **2021**, 6, 11103.
- [59] X. Chen, Y. Zhao, L. Li, Y. Wang, J. Wang, J. Xiong, S. Du, P. Zhang, X. Shi, J. Yu, *Polym. Rev.* **2021**, 61, 80.
- [60] Z. Ren, J. Yang, D. Qi, P. Sonar, L. Liu, Z. Lou, G. Shen, Z. Wei, *Adv. Mater. Technol.* **2021**, 6, 2000889.
- [61] Y. Wen, G. Wang, X. Jiang, X. Ye, W. Li, G. Xu, *Angew. Chem.* **2021**, 133, 19862.
- [62] V. Chaudhary, A. Kaur, *J. Ind. Eng. Chem.* **2015**, 26, 143.
- [63] G. S. Gund, J. H. Park, R. Harpalsinh, M. Kota, J. H. Shin, T. il Kim, Y. Gogotsi, H. S. Park, *Joule* **2019**, 3, 164.
- [64] B. Anasori, M. R. Lukatskaya, Y. Gogotsi, *Nat. Rev. Mater.* **2017**, 2, 16098.
- [65] W. Guo, S. G. Surya, V. Babar, F. Ming, S. Sharma, H. N. Alshareef, U. Schwingenschlöggl, K. N. Salama, *ACS Appl. Mater. Interfaces* **2020**, 12, 57218.
- [66] S. R. Naqvi, V. Shukla, N. K. Jena, W. Luo, R. Ahuja, *Appl. Mater. Today* **2020**, 19, 100574.
- [67] H. Riazi, S. K. Nemani, M. C. Grady, B. Anasori, M. Soroush, *J. Mater. Chem. A* **2021**, 9, 8051.
- [68] A. Kausar, *Polym.-Plast. Technol. Mater.* **2021**, 60, 1377.
- [69] H. Aghamohammadi, N. Amousa, R. Eslami-Farsani, *Synth. Met.* **2021**, 273, 116695.
- [70] X. Jiang, A. V. Kuklin, A. Baev, Y. Ge, H. Ågren, H. Zhang, P. N. Prasad, *Phys. Rep.* **2020**, 848, 1.
- [71] Y. Wei, P. Zhang, R. A. Soomro, Q. Zhu, B. Xu, *Adv. Mater.* **2021**, 33, 2103148.
- [72] M. Naguib, M. W. Barsoum, Y. Gogotsi, *Adv. Mater.* **2021**, 33, 2103393.
- [73] H. Kim, Z. Wang, H. N. Alshareef, *Nano Energy* **2019**, 60, 179.
- [74] B. Xiao, Y. Li, X. Yu, J. Cheng, *Sens. Actuators, B* **2016**, 235, 103.
- [75] C. Ma, M. Ma, C. Si, X. Ji, P. Wan, *Adv. Funct. Mater.* **2021**, 31, 2009524.
- [76] E. Lee, A. VahidMohammadi, B. C. Prorok, Y. S. Yoon, M. Beidaghi, D.-J. Kim, *ACS Appl. Mater. Interfaces* **2017**, 9, 37184.
- [77] S. J. Kim, H.-J. Koh, C. E. Ren, O. Kwon, K. Maleski, S.-Y. Cho, B. Anasori, C.-K. Kim, Y.-K. Choi, J. Kim, Y. Gogotsi, H.-T. Jung, *ACS Nano* **2018**, 12, 986.
- [78] C. E. Shuck, M. Han, K. Maleski, K. Hantanasirisakul, S. J. Kim, J. Choi, W. E. B. Reil, Y. Gogotsi, *ACS Appl. Nano Mater.* **2019**, 2, 3368.
- [79] S. Wang, Y. Jiang, B. Liu, Z. Duan, H. Pan, Z. Yuan, G. Xie, J. Wang, Z. Fang, H. Tai, *Sens. Actuators, B* **2021**, 343, 130069.
- [80] S. Wang, B. Liu, Z. Duan, Q. Zhao, Y. Zhang, G. Xie, Y. Jiang, S. Li, H. Tai, *Sens. Actuators, B* **2021**, 327, 128923.
- [81] E. Lee, A. VahidMohammadi, Y. S. Yoon, M. Beidaghi, D.-J. Kim, *ACS Sens.* **2019**, 4, 1603.
- [82] X. Yu, Y. Li, J. Cheng, Z. Liu, Q. Li, W. Li, X. Yang, B. Xiao, *ACS Appl. Mater. Interfaces* **2015**, 7, 13707.
- [83] S. Ma, D. Yuan, Z. Jiao, T. Wang, X. Dai, *J. Phys. Chem. C* **2017**, 121, 24077.
- [84] Y. Wang, S. Ma, L. Wang, Z. Jiao, *Appl. Surf. Sci.* **2019**, 492, 116.
- [85] S. H. Lee, W. Eom, H. Shin, R. B. Ambade, J. H. Bang, H. W. Kim, T. H. Han, *ACS Appl. Mater. Interfaces* **2020**, 12, 10434.
- [86] S. Sun, M. Wang, X. Chang, Y. Jiang, D. Zhang, D. Wang, Y. Zhang, Y. Lei, *Sens. Actuators, B* **2020**, 304, 127274.
- [87] A. Hermawan, B. Zhang, A. Taufik, Y. Asakura, T. Hasegawa, J. Zhu, P. Shi, S. Yin, *ACS Appl. Nano Mater.* **2020**, 3, 4755.
- [88] Z. Ling, C. E. Ren, M.-Q. Zhao, J. Yang, J. M. Giammarco, J. Qiu, M. W. Barsoum, Y. Gogotsi, *Proc. Natl. Acad. Sci.* **2014**, 111, 16676.
- [89] H. Zhang, L. Wang, Q. Chen, P. Li, A. Zhou, X. Cao, Q. Hu, *Mater. Des.* **2016**, 92, 682.
- [90] M. H. Tran, R. Brilmayer, L. Liu, H. Zhuang, C. Hess, A. Andrieu-Brunsen, C. S. Birkel, *ACS Appl. Nano Mater.* **2020**, 3, 4069.
- [91] S. Kohli, G. Rathee, S. Hooda, R. Chandra, *Dalt. Trans.* **2021**, 50, 7750.
- [92] S. A. Bansal, S. Singh, A. Srivastava, A. P. Singh, S. Kumar, *Polymer (Guildf).* **2021**, 213, 123195.
- [93] Y. Wang, X. Gao, L. Zhang, X. Wu, Q. Wang, C. Luo, G. Wu, *Appl. Surf. Sci.* **2019**, 480, 830.
- [94] J. Fu, J. Yun, S. Wu, L. Li, L. Yu, K. H. Kim, *ACS Appl. Mater. Interfaces* **2018**, 10, 34212.
- [95] C. Chen, M. Boota, X. Xie, M. Zhao, B. Anasori, C. E. Ren, L. Miao, J. Jiang, Y. Gogotsi, *J. Mater. Chem. A* **2017**, 5, 5260.
- [96] M. Zhu, Y. Huang, Q. Deng, J. Zhou, Z. Pei, Q. Xue, Y. Huang, Z. Wang, H. Li, Q. Huang, C. Zhi, *Adv. Energy Mater.* **2016**, 6, 1600969.
- [97] P. Zhang, X.-J. Yang, P. Li, Y. Zhao, Q. J. Niu, *Soft Matter* **2020**, 16, 162.
- [98] X. Sheng, Y. Zhao, L. Zhang, X. Lu, *Compos. Sci. Technol.* **2019**, 181, 107710.
- [99] Y. Zhang, Z. Zhou, J. Lan, P. Zhang, *Appl. Surf. Sci.* **2019**, 469, 770.
- [100] L. Zhao, K. Wang, W. Wei, L. Wang, W. Han, *InfoMat* **2019**, 1, 407.
- [101] X. Li, J. Xu, Y. Jiang, Z. He, B. Liu, H. Xie, H. Li, Z. Li, Y. Wang, H. Tai, *Sens. Actuators, B* **2020**, 316, 128144.
- [102] Y. Gogotsi, B. Anasori, *ACS Nano* **2019**, 13, 8491.
- [103] M. Naguib, M. Kurtoglu, V. Presser, J. Lu, J. Niu, M. Heon, L. Hultman, Y. Gogotsi, M. W. Barsoum, *Adv. Mater.* **2011**, 23, 4248.
- [104] M. Naguib, M. Kurtoglu, V. Presser, J. Lu, J. Niu, M. Heon, L. Hultman, Y. Gogotsi, M. W. Barsoum, *Adv. Mater.* **2011**, 23, 4207.
- [105] M. A. Hope, A. C. Forse, K. J. Griffith, M. R. Lukatskaya, M. Ghidui, Y. Gogotsi, C. P. Grey, *Phys. Chem. Chem. Phys.* **2016**, 18, 5099.
- [106] M. Kurtoglu, M. Naguib, Y. Gogotsi, M. W. Barsoum, *MRS Commun.* **2012**, 2, 133.
- [107] M. Naguib, J. Halim, J. Lu, K. M. Cook, L. Hultman, Y. Gogotsi, M. W. Barsoum, *J. Am. Chem. Soc.* **2013**, 135, 15966.
- [108] R. Meshkian, M. Dahlqvist, J. Lu, B. Wickman, J. Halim, J. Thörnberg, Q. Tao, S. Li, S. Intikhab, J. Snyder, M. W. Barsoum, M. Yildizhan, J. Palisaitis, L. Hultman, P. O. Å. Persson, J. Rosen, *Adv. Mater.* **2018**, 30, 1706409.
- [109] B. Anasori, Y. Xie, M. Beidaghi, J. Lu, B. C. Hosler, L. Hultman, P. R. C. Kent, Y. Gogotsi, M. W. Barsoum, *ACS Nano* **2015**, 9, 9507.
- [110] M. Ghidui, M. Naguib, C. Shi, O. Mashtalir, L. M. Pan, B. Zhang, J. Yang, Y. Gogotsi, S. J. L. Billinge, M. W. Barsoum, *Chem. Commun.* **2014**, 50, 9517.
- [111] P. Urbankowski, B. Anasori, T. Makaryan, D. Er, S. Kota, P. L. Walsh, M. Zhao, V. B. Shenoy, M. W. Barsoum, Y. Gogotsi, *Nanoscale* **2016**, 8, 11385.
- [112] X. Sang, Y. Xie, M.-W. Lin, M. Alhabeb, K. L. Van Aken, Y. Gogotsi, P. R. C. Kent, K. Xiao, R. R. Unocic, *ACS Nano* **2016**, 10, 9193.
- [113] L. H. Karlsson, J. Birch, J. Halim, M. W. Barsoum, P. O. Å. Persson, *Nano Lett.* **2015**, 15, 4955.
- [114] M. Khazaei, M. Arai, T. Sasaki, A. Ranjbar, Y. Liang, S. Yunoki, *Phys. Rev. B:Condens. Matter Mater. Phys.* **2015**, 92, 075411.
- [115] J. Peng, X. Chen, W. J. Ong, X. Zhao, N. Li, *Chem* **2019**, 5, 18.
- [116] Y. Zhang, Y. Jiang, Z. Duan, Q. Huang, Y. Wu, B. Liu, Q. Zhao, S. Wang, Z. Yuan, H. Tai, *Sens. Actuators, B* **2021**, 344, 130150.
- [117] M. Alhabeb, K. Maleski, B. Anasori, P. Lelyukh, L. Clark, S. Sin, Y. Gogotsi, *Chem. Mater.* **2017**, 29, 7633.
- [118] X.-H. Zha, J. Zhou, P. Eklund, X. Bai, S. Du, Q. Huang, *in 2D Metal Carbides and Nitrides (MXenes): Structure, Properties and*

- Applications, (Eds: B. Anasori, Y. Gogotsi), Springer International Publishing, Cham, Switzerland **2019**, pp. 53–68.
- [119] Y.-C. Zhou, L.-F. He, Z.-J. Lin, J.-Y. Wang, *J. Eur. Ceram. Soc.* **2013**, *33*, 2831.
- [120] G. Gao, G. Ding, J. Li, K. Yao, M. Wu, M. Qian, *Nanoscale* **2016**, *8*, 8986.
- [121] J. Zhou, X. Zha, F. Y. Chen, Q. Ye, P. Eklund, S. Du, Q. Huang, *Angew. Chem., Int. Ed.* **2016**, *55*, 5008.
- [122] X. H. Zha, J. Zhou, K. Luo, J. Lang, Q. Huang, X. Zhou, J. S. Francisco, J. He, S. Du, *J. Phys.: Condens. Matter* **2017**, *29*, 165701.
- [123] C.-C. Lai, R. Meshkian, M. Dahlqvist, J. Lu, L.-Å. Näslund, O. Rivin, E. N. Caspi, O. Ozeri, L. Hultman, P. Eklund, M. W. Barsoum, J. Rosen, *Acta Mater.* **2015**, *99*, 157.
- [124] D. Xiong, X. Li, Z. Bai, S. Lu, *Small* **2018**, *14*, 1703419.
- [125] Y. Gogotsi, *Nat. Mater.* **2015**, *14*, 1079.
- [126] C.-F. Du, X. Zhao, Z. Wang, H. Yu, Q. Ye, *Nanomaterials* **2021**, *11*, 166.
- [127] M. Naguib, T. Saito, S. Lai, M. S. Rager, T. Aytug, M. Parans Paranthaman, M.-Q. Zhao, Y. Gogotsi, *RSC Adv.* **2016**, *6*, 72069.
- [128] X. Zhan, C. Si, J. Zhou, Z. Sun, *Nanoscale Horiz.* **2020**, *5*, 235.
- [129] B. Yu, B. Tawiah, L.-Q. Wang, A. C. Yin Yuen, Z.-C. Zhang, L.-L. Shen, B. Lin, B. Fei, W. Yang, A. Li, S.-E. Zhu, E.-Z. Hu, H.-D. Lu, G. H. Yeoh, *J. Hazard. Mater.* **2019**, *374*, 110.
- [130] L. Jin, C. Wu, K. Wei, L. He, H. Gao, H. Zhang, K. Zhang, A. M. Asiri, K. A. Alamry, L. Yang, X. Chu, *ACS Appl. Nano Mater.* **2020**, *3*, 12071.
- [131] L. Qin, Q. Tao, X. Liu, M. Fahlman, J. Halim, P. O. Å. Persson, J. Rosen, F. Zhang, *Nano Energy* **2019**, *60*, 734.
- [132] M. Carey, Z. Hinton, M. Sokol, N. J. Alvarez, M. W. Barsoum, *ACS Appl. Mater. Interfaces* **2019**, *11*, 20425.
- [133] C. Si, K.-H. Jin, J. Zhou, Z. Sun, F. Liu, *Nano Lett.* **2016**, *16*, 6584.
- [134] W. Zhi, S. Xiang, R. Bian, R. Lin, K. Wu, T. Wang, D. Cai, *Compos. Sci. Technol.* **2018**, *168*, 404.
- [135] M. Ghidui, M. R. Lukatskaya, M. Q. Zhao, Y. Gogotsi, M. W. Barsoum, *Nature* **2015**, *516*, 78.
- [136] A. Ajnsztajn, S. Ferguson, J. O. Thostenson, E. Ngaboyamahina, C. B. Parker, J. T. Glass, A. D. Stiff-Roberts, *Crystals* **2020**, *10*, 152.
- [137] M. F. Mabrook, C. Pearson, M. C. Petty, *Sens. Actuators, B* **2006**, *115*, 547.
- [138] P. Sobolčiak, A. Ali, M. K. Hassan, M. I. Helal, A. Tanvir, A. Popelka, M. A. Al-Maadeed, I. Krupa, K. A. Mahmoud, *PLoS One* **2017**, *12*, e0183705.
- [139] L. Kumar, I. Rawal, A. Kaur, S. Annapoorni, *Sens. Actuators, B* **2017**, *240*, 408.
- [140] V. Chaudhary, A. Kaur, *RSC Adv.* **2016**, *6*, 95349.
- [141] V. Chaudhary, A. Kaur, *Polym. Int.* **2015**, *64*, 1475.
- [142] Z. Chen, Y. Wang, J. Han, T. Wang, Y. Leng, Y. Wang, T. Li, Y. Han, *ACS Appl. Energy Mater.* **2020**, *3*, 9326.
- [143] Y. Sheth, S. Dharaskar, V. Chaudhary, M. Khalid, R. Walvekar, *Chemosphere* **2022**, *293*, 133563.
- [144] J. Qiu, X. Xia, Z. Hu, S. Zhou, Y. Wang, Y. Wang, R. Zhang, J. Li, Y. Zhou, *Nanotechnology* **2022**, *33*, 065501.
- [145] M. Boota, B. Anasori, C. Voigt, M.-Q. Zhao, M. W. Barsoum, Y. Gogotsi, *Adv. Mater.* **2016**, *28*, 1517.
- [146] V. Chaudhary, *Appl. Phys. A* **2021**, *127*, 536.
- [147] R. B. Rakhi, P. Nayak, C. Xia, H. N. Alshareef, *Sci. Rep.* **2016**, *6*, 36422.
- [148] A. Khunger, N. Kaur, Y. K. Mishra, G. Ram Chaudhary, A. Kaushik, *Mater. Lett.* **2021**, *304*, 130656.
- [149] S. Zheng, C. Zhang, F. Zhou, Y. Dong, X. Shi, V. Nicolosi, Z. S. Wu, X. Bao, *J. Mater. Chem. A* **2019**, *7*, 9478.
- [150] J. H. Ciou, S. Li, P. S. Lee, *Small* **2019**, *15*, 1903281.
- [151] J. Halim, I. Persson, E. J. Moon, P. Kühne, V. Darakchieva, P. O. Å. Persson, P. Eklund, J. Rosen, M. W. Barsoum, *J. Phys.: Condens. Matter* **2019**, *31*, 165301.
- [152] M. Khazaei, M. Arai, T. Sasaki, C.-Y. Chung, N. S. Venkataraman, M. Estili, Y. Sakka, Y. Kawazoe, *Adv. Funct. Mater.* **2013**, *23*, 2185.
- [153] R. Li, W. Sun, C. Zhan, P. R. C. Kent, D. Jiang, *Phys. Rev. B* **2019**, *99*, 085429.
- [154] X.-H. Li, S.-S. Li, X.-H. Cui, R.-Z. Zhang, H.-L. Cui, *Appl. Surf. Sci.* **2021**, *563*, 150264.
- [155] Y. Yang, C. S. Ting, *J. Phys. D.: Appl. Phys.* **2020**, *53*, 485301.
- [156] H. Kim, H. N. Alshareef, *ACS Mater. Lett.* **2020**, *2*, 55.
- [157] A. D. Dillon, M. J. Ghidui, A. L. Krick, J. Griggs, S. J. May, Y. Gogotsi, M. W. Barsoum, A. T. Fafarman, *Adv. Funct. Mater.* **2016**, *26*, 4162.
- [158] H. Weng, A. Ranjbar, Y. Liang, Z. Song, M. Khazaei, S. Yunoki, M. Arai, Y. Kawazoe, Z. Fang, X. Dai, *Phys. Rev. B* **2015**, *92*, 075436.
- [159] K. Hantanasirisakul, Y. Gogotsi, *Adv. Mater.* **2018**, *30*, 1804779.
- [160] E. A. Mayerberger, O. Urbanek, R. M. McDaniel, R. M. Street, M. W. Barsoum, C. L. Schauer, *J. Appl. Polym. Sci.* **2017**, *134*, 45295.
- [161] S. Ansari, E. P. Giannelis, *J. Polym. Sci., Part B: Polym. Phys.* **2009**, *47*, 888.
- [162] W.-T. Cao, F.-F. Chen, Y.-J. Zhu, Y.-G. Zhang, Y.-Y. Jiang, M.-G. Ma, F. Chen, *ACS Nano* **2018**, *12*, 4583.
- [163] J.-Q. Luo, S. Zhao, H.-B. Zhang, Z. Deng, L. Li, Z.-Z. Yu, *Compos. Sci. Technol.* **2019**, *182*, 107754.
- [164] J. Shao, J. W. Wang, D. N. Liu, L. Wei, S. Q. Wu, H. Ren, *Polymer* **2019**, *174*, 86.
- [165] X. H. Zha, J. Zhou, Y. Zhou, Q. Huang, J. He, J. S. Francisco, K. Luo, S. Du, *Nanoscale* **2016**, *8*, 6110.
- [166] Y. Cao, Q. Deng, Z. Liu, D. Shen, T. Wang, Q. Huang, S. Du, N. Jiang, C. Te Lin, J. Yu, *RSC Adv.* **2017**, *7*, 20494.
- [167] R. Kang, Z. Zhang, L. Guo, J. Cui, Y. Chen, X. Hou, B. Wang, C.-T. Lin, N. Jiang, J. Yu, *Sci. Rep.* **2019**, *9*, 9135.
- [168] X. Cao, M. Wu, A. Zhou, Y. Wang, X. He, L. Wang, *e-Polym.* **2017**, *17*, 373.
- [169] V. N. Borysiuk, V. N. Mochalin, Y. Gogotsi, *Comput. Mater. Sci.* **2018**, *143*, 418.
- [170] X. Tong, W. Shen, X. Chen, J. P. Corriou, *Ceram. Int.* **2017**, *43*, 14200.
- [171] C. S. Rout, M. Hegde, A. Govindaraj, C. N. R. Rao, *Nanotechnology* **2007**, *18*, 205504.
- [172] A. Kaushik, R. Kumar, S. K. Arya, M. Nair, B. D. Malhotra, S. Bhansali, *Chem. Rev.* **2015**, *115*, 4571.
- [173] L. Zhao, Y. Zheng, K. Wang, C. Lv, W. Wei, L. Wang, W. Han, *Adv. Mater. Technol.* **2020**, *5*, 2000248.
- [174] J. Choi, Y. Kim, S. Cho, K. Park, H. Kang, S. J. Kim, H. Jung, *Adv. Funct. Mater.* **2020**, *30*, 2003998.
- [175] Y. Zhou, Y. Wang, Y. Wang, X. Li, *Anal. Chem.* **2020**, *92*, 16033.
- [176] V. Chaudhary, *Polym. Technol. Mater.* **2021**, *60*, 1547.
- [177] J. A. Kumar, P. Prakash, T. Krithiga, D. J. Amarnath, J. Premkumar, N. Rajamohan, Y. Vasseghian, P. Saravanan, M. Rajasimman, *Chemosphere* **2022**, *286*, 131607.
- [178] S. Abdulla, T. L. Mathew, B. Pullithadathil, *Sens. Actuators, B* **2015**, *221*, 1523.
- [179] S. Hajian, P. Khakbaz, M. Moshayedi, D. Maddipatla, B. B. Narakathu, V. S. Turkani, B. J. Bazuin, M. Pourfath, M. Z. Atashbar, *IEEE Sensors* **2018**, *1*, <https://doi.org/10.1109/ICSENS.2018.8589699>.
- [180] Z. Yang, A. Liu, C. Wang, F. Liu, J. He, S. Li, J. Wang, R. You, X. Yan, P. Sun, Y. Duan, G. Lu, *ACS Sens.* **2019**, *4*, 1261.
- [181] R. Khaledialidusti, A. K. Mishra, A. Barnoush, *J. Mater. Chem. C* **2020**, *8*, 4771.
- [182] H.-J. Koh, S. J. Kim, K. Maleski, S.-Y. Cho, Y.-J. Kim, C. W. Ahn, Y. Gogotsi, H.-T. Jung, *ACS Sens.* **2019**, *4*, 1365.
- [183] X. Wang, K. Sun, K. Li, X. Li, Y. Gogotsi, *Chin. Chem. Lett.* **2020**, *31*, 1018.
- [184] Y. Li, Z. Peng, N. J. Holl, M. R. Hassan, J. M. Pappas, C. Wei, O. H. Izadi, Y. Wang, X. Dong, C. Wang, Y.-W. Huang, D. Kim, C. Wu, *ACS Omega* **2021**, *6*, 6643.

- [185] G. P. Neupane, T. Yildirim, L. Zhang, Y. Lu, *Adv. Funct. Mater.* **2020**, *30*, 2005238.
- [186] W. Y. Chen, X. Jiang, S.-N. Lai, D. Peroulis, L. Stanciu, *Nat. Commun.* **2020**, *11*, 1302.
- [187] M. Liu, J. Ji, P. Song, M. Liu, Q. Wang, *Sens. Actuators, B* **2021**, *349*, 130782.
- [188] D. Huang, H. Li, Y. Wang, X. Wang, L. Cai, W. Fan, Y. Chen, W. Wang, Y. Song, G. Han, B. Zheng, G. Liu, *Chem. Eng. J.* **2022**, *428*, 131377.
- [189] W. N. Zhao, N. Yun, Z. H. Dai, Y. F. Li, *RSC Adv.* **2020**, *10*, 1261.
- [190] Y. Qin, H. Gui, Y. Bai, S. Liu, *Sens. Actuators, B* **2022**, *352*, 131077.
- [191] M. Liu, J. Ji, P. Song, J. Wang, Q. Wang, *J. Alloys Compd.* **2022**, *898*, 162812.
- [192] J. Zhou, S. H. Hosseini Shokouh, H. Komsa, L. Rieppo, L. Cui, Z. Lv, K. Kordas, *Adv. Mater. Technol.* **2022**, 2101565, <https://doi.org/10.1002/admt.202101565>.
- [193] A. Rozmysłowska-Wojciechowska, A. Szuplewska, T. Wojciechowski, S. Pożniak, J. Mitrzak, M. Chudy, W. Ziemkowska, L. Chlubny, A. Olszyna, A. M. Jastrzębska, *Mater. Sci. Eng. C* **2020**, *111*, 110790.
- [194] C. E. Shuck, A. Sarycheva, M. Anayee, A. Levitt, Y. Zhu, S. Uzun, V. Balitskiy, V. Zahorodna, O. Gogotsi, Y. Gogotsi, *Adv. Eng. Mater.* **2020**, *22*, 1901241.
- [195] A. A. Ansari, B. D. Malhotra, *Coord. Chem. Rev.* **2022**, *452*, 214282.
- [196] W. Y. Chen, S. N. Lai, C. C. Yen, X. Jiang, D. Peroulis, L. A. Stanciu, *ACS Nano* **2020**, *14*, 11490.
- [197] Q. Guo, X. Zhang, F. Zhao, Q. Song, G. Su, Y. Tan, Q. Tao, T. Zhou, Y. Yu, Z. Zhou, C. Lu, *ACS Nano* **2020**, *14*, 2788.
- [198] K. Zhang, J. Sun, J. Song, C. Gao, Z. Wang, C. Song, Y. Wu, Y. Liu, *ACS Appl. Mater. Interfaces* **2020**, *12*, 45306.
- [199] T. B. Limbu, B. Chitara, J. D. Orlando, M. Y. Garcia Cervantes, S. Kumari, Q. Li, Y. Tang, F. Yan, *J. Mater. Chem. C* **2020**, *8*, 4722.
- [200] S. Abdolhosseinzadeh, R. Schneider, A. Verma, J. Heier, F. Nüesch, C. J. Zhang, *Adv. Mater.* **2020**, *32*, 2000716.
- [201] S. Sardana, H. Kaur, B. Arora, D. K. Aswal, A. Mahajan, *ACS Sens.* **2022**, *7*, 312.
- [202] Y. Dong, S. S. K. Mallineni, K. Maleski, H. Behlow, V. N. Mochalin, A. M. Rao, Y. Gogotsi, R. Podila, *Nano Energy* **2018**, *44*, 103.
- [203] K. Hassan, N. Stanley, T. T. Tung, P. L. Yap, H. Rastin, L. Yu, D. Losic, *Adv. Mater. Interfaces* **2021**, *8*, 2101175.
- [204] M. H. Abbasi Geravand, E. Saljoughi, S. M. Mousavi, S. Kiani, *J. Taiwan Inst. Chem. Eng.* **2021**, *128*, 124.
- [205] W. Zhang, Z. Pan, J. Ma, L. Wei, Z. Chen, J. Wang, *ACS Sustainable Chem. Eng.* **2022**, *10*, 1408.



**Vishal Chaudhary** is assistant professor of Physics at Bhagini Nivedita College, University of Delhi, India for 6 years. Dr. Chaudhary received Ph.D. in Physics from Department of Physics & Astrophysics, DU, New Delhi, India. He has expertise in engineering the physicochemical characteristics of nanostructures/nanocomposites through optimizing the reaction parameters for gas/vapor monitoring. He introduced the interlink of VRH-based charge carrier conduction in nanosystems of macromolecules and their gas-sensing phenomenon, and indigenously designed in situ FTIR strategy to explore gas/vapor detection mechanism. He has published >20 articles dedicated to the architect of controllable nanosystems to monitor air contaminants and received SDG service award (2021).



**Mohammad Khalid** is a professor and head of Graphene and Advanced 2D Materials Research Group (GAMRG) at Sunway University, Malaysia. His research interests lie primarily in advanced nanomaterial synthesis for energy harvesting, storage and conversion applications. He has authored over 200 peer-reviewed scientific articles, edited 6 books and filed 5 patents, including a recent patent filing for rapid and efficient MXene synthesis.



**Ajeet Kaushik**, Fellow-ICS, is working as assistant professor of Chemistry at Florida Polytechnic University and exploring nanobiotechnology for health wellness. Ajeet is an accomplished scientist (supported by publication, journal editor, edited books, patents, and international collaborations) and recipient of several international awards in support of his credentials. Dr. Kaushik is open for collaborative research as his research interest include nano-biotechnology, analytical systems, design & develop nanostructures, nanocarriers for drug delivery, nanotherapeutics for CNS diseases, on-demand site-specific release of therapeutic agents, exploring personalized nano- medicines, biosensors, point-of-care sensing devices, and related areas of health care monitoring.



**Yogendra Kumar Mishra** is professor MSO at Mads Clausen Institute University of Southern Denmark, Sønderborg. Previously, he was leading a group at Kiel University, Germany where he did Habilitation (2015) in Materials Science. He received Ph.D. (2008) in Physics from JNU, New Delhi, India. He introduced the flame process for tetrapod-nanostructuring and their 3D networks which found many applications in different technologies including using them as novel templates to create hybrid and/or new 3D materials. Smart Materials Lab is developing tetrapod-based spongy materials for advanced technologies. He has published >250 papers which are cited over 12 100 times with H-index of 61.